TAILORING ONCOLYTIC VIRUSES FOR THE TREATMENT OF PANCREATIC CANCER

MARIE-ÈVE WEDGE

Thesis submitted to the University of Ottawa in partial fulfillment of the requirements for the Masters of Science degree in the program of Cellular and Molecular Medicine

Department of Cellular and Molecular Medicine

Faculty of Medicine

Univeristy of Ottawa

ABSTRACT

Pancreatic cancer (PC) is a highly aggressive disease with unmet therapeutic needs. Recent advances in the use of oncolytic viruses (OVs) as cancer therapeutic agents bring new hope to fight the notorious disease that is PC. Although OVs have shown promising results in certain cancers, some tumors remain resistant to OV therapy due to their inherent residual antiviral mechanisms. We hypothesized that the use of OV-encoded artificial microRNAs (amiRNAs) could help target the cellular antiviral components associated with the observed OV resistance and could also sensitize neighboring tumor cells to OV therapy and small molecule inhibitors through the secretion of amiRNA-containing extracellular vesicles (EVs) from infected cells. To find such amiRNAs, a viral surrogate library encoding ~16,000 unique amiRNAs was passaged in pancreatic cancer cell lines to enrich for sequences that could enhance OV replication. An amiRNA that improves PC cell killing when expressed from an OV was identified. Target identification of this amiRNA (amiR-4) revealed ARID1A as a key player in resistance to OV therapy in pancreatic cancers. This target is of particular interest, since its downregulation acts in a synthetic lethal fashion with inhibition of the EZH2 methyltransferase. Combining VSVΔ51-amiR-4 with a small molecule inhibitor of EZH2 enhances PC cell death. Moreover, amiR-4 is packaged in cancer cell-secreted EVs which can reach neighboring naïve cells to sensitize them to EZH2 inhibition-mediated cell death and to spread the OV-mediated tumor killing effect throughout the tumor. This data translates into tumor debulking and survival in animal models of highly aggressive PC. This work not only broadens our knowledge on the resistance of select tumors to oncolytic virotherapy and the EV-mediated bystander killing effect in OV-infected tumors, but it also establishes OVs as a

novel tool to produce anti-cancer therapeutic EVs *in situ* to improve therapeutic gain. Ultimately, our work provides new hope for a cure to the grim disease that is PC.

TABLE OF CONTENTS

LIST OF TABLES

LIST OF FIGURES

ABBREVIATIONS

amiR/amiRNA – Artificial microRNA

ARID1A – AT-Rich Interaction Domain 1A

BiTE – Bi-specific T-cell engager

c-pri-miRNA – Cytoplasmic primary miRNA

CAF – Cancer-associated fibroblast

GFP – Green fluorescent protein

CMC – Carboxymethyl cellulose

CRISPR – Clustered Regularly Interspaced Short Palindromic Repeats

Ctrl – Control

DAMP – Damage associated molecular pattern

DIP – Defective interfering particle

DMEM – Dulbecco's Modified Eagle Medium

DMSO – Dimethyl sulfoxide

DOX – Doxycycline

EM – Electron microscopy

EMT – Epithelial to mesenchymal transition

EUS-FNA – Endoscopic ultrasound-guided fine-needle aspiration

EV – Extracellular vesicle

FBS – Fetal bovine serum

GAPDH – g

GO – Gene ontology

gRNA – Guide RNA

HDAC-4 – Histone deacetylase 4

hEGF – Human epidermal growth factor

hpi – Hours post-infection

HSV-1 – Herpes simplex virus 1

ICI – Immune checkpoint inhibitor

IFN – Interferon

IHC – Immunohistochemistry

IP – Intraperitoneal/Intraperitoneally

IRF – Interferon regulatory factor

IT – Intratumoral/Intratumorally

ITG – Integrin

IV – Intravenous/Intravenously

KO – Knockout

lncRNA – Long non-coding RNA

MCM2 – Minichromosome Maintenance Complex Component 2

MDSC – Myeloid-derived suppressor cell

miRNA – MicroRNA

MOI – Multiplicity of infection

MRB – Maraba virus

MRBΔG – Maraba virus with deletion of the glycoprotein (G) gene

mRNA – Messenger RNA

MSC – Mesenchymal stem cell

NGS – Next generation sequencing

NOD/SCID – Nonobese diabetic/severe combined immunodeficiency

NTA – Nanoparticle tracking analysis

NTC – Non-targeting control

oHSV-1 – Oncolytic Herpes simplex virus 1

OV – Oncolytic virus

PAMPs – Pathogen associated molecular patterns

PBS – Phosphate buffered saline

PC – Pancreatic cancer

PDAC – Pancreatic ductal adenocarcinoma

PFU – Plaque forming unit

piRNA – Piwi-interacting RNA

PLEC – Plectin

pre-miR – Precursor microRNA

PRR – Pathogen recognition receptor

PVDF – Polyvinylidene fluoride

RdRp – RNA-dependant RNA polymerase

RNAi – RNA interference

RPN – Ribonucleocapsid

RPMI – Roswell Park Memorial Institute

RT-qPCR – Quantitative real time PCR

SC – Subcutaneous

SEV – Small extracellular vesicle

ssRNA – single stranded RNA

SV – Sindbis virus

TAA – Tumor associated antigen

TLR – Toll-like receptor

Treg – Regulatory T cell

VSe – Viral sensitizer

VSV – Vesicular stomatitis virus

VSVΔ51 – Oncolytic Vesicular stomatitis virus with deletion of methionine 51

VV TK^- VGF^- – Vaccinia virus with deletion of the thymidine kinase (TK) and virus growth factor (VGF) genes

WT – Wild-type

ACKNOWLEDGEMENTS

I would first like to thank my supervisors Drs. Carolina Ilkow and John Bell for their mentorship, support and for allowing me to work in an environment where countless and diverse opportunities were offered to me. I would also like to thank my TAC members Drs. Jean-Simon Diallo, Derrick Gibbings and Christina Addison for their guidance and support. I wish to extend a very special thank you to Christiano Tanese de Souza for his extensive technical support and for his friendship. I thank all authors of the 'amiR-4 paper', especially Brian Laight, Hayley McKay, Adrian Pelin, Larissa Pikor, Elaine Rose and Sarwat Khan, without whom the completion of this project would not have been possible. In addition, I would equally like to thank all current and past members of the Ilkow and Bell labs for their valuable input, help and encouragement. Most importantly, I thank my parents, Myriam and Amine for their constant love and support and for reminding me to always stay true to myself.

1. INTRODUCTION

1.1 Pancreatic cancer

1.1.1 Epidemiology

Pancreatic cancer (PC) currently ranks as the fourth leading cause of cancer-related deaths in both sexes in Canada and other developed countries and is the seventh most lethal cancer worldwide[1–3]. The disease is the third cause of cancer-related deaths in the United States and is estimated to reach the same ranking in Canada in 2019[4] and to climb to the second rank of cancer-related deaths by 2030[5]. This trend can be explained by the advances in early detection and treatment of other cancers, notably breast cancers. Meanwhile, the prevention, early detection and treatment of PC remains a challenge to tackle. Therefore, its mortality rate has remained virtually unchanged for the past decades[1,5]. Moreover, once diagnosed, less than half of patients survive past four months and the disease is associated with a staggeringly low 5-year relative survival ratio of 7%[1]. In 2019, it is estimated that 5,800 Canadians will be diagnosed with PC and 5,200 will die from the disease[6]. Major risk factors associated to the disease are age, tobacco, alcohol, diet and excessive body weight, most of which can be targeted for prevention of the disease. Aside from making healthy lifestyle choices to prevent the disease, the early detection of PC could help achieve durable cures. However, early detection is made difficult by the late onset of symptoms which tend to be unspecific, like nausea, weight loss and jaundice[1].

1.1.2 Current standard-of-care

The poor prognosis associated to PC is in part due to the late diagnosis of the disease and the lack of treatment options available. In fact, since the onset of PC is associated with few early symptoms and is quite aggressive, most PCs are diagnosed at stage III or IV, where patients are usually not eligible for the therapeutic option associated with the best prognosis; curative surgery[7–9]. This can be attributed to the metastatic nature of PC as well as the location and size of the tumor, which makes for a complicated surgical procedure[10]. Indeed, PCs located in the pancreatic head can be surgically removed using the Whipple procedure (partial pancreatico-duodenectomy) and tumors located in the tail of the pancreas can be excised by performing a distal pancreatectomy. However, tumors are deemed unresectable if they involve important veins or arteries, like the superior mesenteric artery[11]. Thus, only a small fraction of patients (~10-20%) are eligible for surgery and among those, a mere 20-30% will survive beyond 5 years with adjuvant chemotherapy despite improvement of surgical techniques and perioperative measures over the years[11–14].

When surgery is not a viable option, patients are treated with the standard-of-care combination chemotherapy regimens. These chemotherapy regimens consist of gemcitabine in combination with erlotinib[15] or albumin-bound paclitaxel[16] as well as the FOLIFIRNOX combination therapy[17]. These treatments generally offer poor to moderate response rates due to high rates of chemotherapy resistance in pancreatic cancers. In the event of their failure, the only second-line therapy available is an attempt to use a combination regimen not previously used on the patient[18].

1.1.3 Pathology

The pancreas is an organ found in the abdomen and is composed of two different subtypes of cells: exocrine and endocrine cells. The majority of PCs arise in exocrine cells and are more aggressive than PCs that arise from endocrine cells[19]. Pancreatic ductal adenocarcinoma (PDAC) is the most prevalent type of PC as it accounts for approximately 90% of diagnoses[20]. Other rarer types of PC include neuroendocrine, colloid and medullary carcinomas that tend to be associated with better prognosis than PDAC as well as adenosquamous carcinomas which tend to have much worse prognosis[21].

1.1.4 Carcinogenesis

It is now well established that KRAS activating mutations culminate in the establishment of pancreatic intraepithelial neoplasia (PanIN) in the pancreas which leads to PDAC after a succession of additional mutations[19]. Aberrant activation of several signaling pathways have been shown to lead to PC carcinogenesis. Besides KRAS mutations, other key protein mutations have been found to participate in the culmination of PC, like CDKN2A, TP53 and SMAD4[22]. Altered pathways in PC also include embryonic development signaling pathways, like mutations responsible for the activation of the Hedgehog (Hh) and Wtn-β-catenin pathways, as well as the EGFR, mTOR, PI3K/Akt and angiogenesis pathways[19,23]. It is also important to note that more than one of these genetic events usually acts synergistically to culminate in the establishment of the disease.

1.1.5 Resistance to treatments

Drug resistance in PC is generally associated to genetic changes in signaling pathways which can be influenced by different components of the influence of the tumor microenvironment (TME), the presence of cancer stem cells in tumors and the activity of several non-coding RNAs, like microRNAs (miRNAs) and long non-coding RNAs (lncRNAs)[24,25]. For example, miRNA profiles have been shown to differ significantly between gemcitabine sensitive or resistant tumors and some miRNAs have been shown to participate in oncogene expression inhibition[26–28]. Moreover, many tumors are refractory to treatment due to the inherent biology of PCs which are highly composed of cancer-associated fibroblasts (CAFs), an important stromal component of the PC TME. These tumors tend to be very poorly vascularized and under immense hydrostatic pressure which is believed to impede the delivery of chemotherapeutic agents to the cancer cells hidden by the desmoplasia[29].

1.1.6 The tumor microenvironment

In addition to tumor cells, solid tumors harbour many other cell types, like immune cells and stromal cells. The PC TME is composed notably of tumor cells, cancer stem cells, immune cells, stromal cells, endothelial cells and extracellular matrix (ECM). The invasion of stromal components (mostly CAFs) in the PC TME can be described as tumor desmoplasia. In addition to its contribution to the creation of a physical barrier to treatment, CAFs play a pro-tumorigenic role in the TME. They are involved in ECM remodeling by secreting several molecules, like collagen, they play a role in metastasis and they secrete protumorigenic factors like cytokines and growth factors[30]. In addition, the immune landscape of pancreatic tumors is generally composed of immunosuppressive cells, like regulatory T cells (Tregs), myeloid-

derived suppressor cells (MDSCs) as well as M2 polarized tumor-associated macrophages which creates "cold tumors"[31]. This phenomenon explains why attempts at using immune checkpoint blockade strategies have failed[32].

1.1.7 Emerging treatments

Several attempts have been made at targeting the main PC gene mutations like KRAS, CDKN2A, TP53 and SMAD4 or their downstream effectors. However, this has proven ineffective, since some of those genes are undruggable, but also because of the heterogeneous mutational landscape of PCs[33]. Moreover, the important cross-talk between tumor cells and other components of the TME further complicates treatment. Thus, efforts are now mainly focused on targeting not only cancer cells, but also other components of the TME. Emerging evidence points towards the therapeutic benefit of CAF depletion[34–36]. Novel antifibrotic therapies (e.g. monoclonal antibodies and enzymatic inhibitors) have thus been developed in an attempt to clear this barrier to treatment, but these have shown limited efficacy in clinical trials[37–39].

1.1.8 Disease models

Although there has been a large increase in PC knowledge in the past decade, this increase in knowledge has translated into very limited clinical benefit. This can, in part, be attributed to the fact that some models used to study the disease or to test novel therapeutics are not clinically relevant. Indeed, most studies do not account for the broad inter- and intra-patient tumor heterogeneity[40]. Efforts are now geared towards establishment of animal models that account for this diversity.

Emerging sampling methods like endoscopic ultrasound-guided fine needle aspirate (EUS-FNA) offer sampling access to a wider variety of tumor samples, as this method is less invasive than surgery. Although mainly used for diagnostic purposes, samples obtained by EUS-FNA can also be implanted in mice to establish patient-derived xenografts (PDXs) to study PC[41–43]. Several studies have shown that PDXs recapitulate accurately human disease in mice[44–46]. In the case of pancreatic cancers, this method is especially beneficial since it gives access to tumors normally not accessible via surgery, thus accounting for virtually all subsets of the disease. Validating the efficacy of novel preclinical therapeutics in these models will ensure their effectiveness in a wide range of tumor samples, thus enhancing the confidence that these will show clinical success.

Thus, despite advances in chemotherapy regimens, surgical procedures, novel treatments, attempts at early disease diagnosis and establishment of suitable models to study the disease and test novel therapies, disease prognosis remains grim. Novel approaches to treat PC are therefore urgently needed.

1.2 Oncolytic virotherapy

A promising new approach in the treatment of PC is the use of oncolytic or "cancer lysing" viruses (OVs), a novel class of immunotherapeutics aimed at tumor clearing.

1.2.1 History and rationale

Since its infancy, cancer therapy has consisted of surgery, chemotherapy and radiation. After the establishment of surgery as a viable option for cancer treatment, other therapeutic options came into the spotlight. These included the use of chemotherapeutic drugs as well as radiation after the discovery of x-rays. In addition to these therapies, the use of viruses also emerged as a potential therapeutic option to treat patients, even prior to viruses being described and characterized as biological entities[47]. The first accounts of case reports describing tumor shrinkage or even cures in cancer patients naturally infected by viruses, like influenza, prompted attempts at using these pathogens to treat cancer[48–51]. Early clinical trials consisted of transferred sera or tissues from individuals suffering from viral infections to cancer patients[52,53]. Although this proved to be more detrimental than therapeutic in some patients, others benefited from this strategy. Later, a more sophisticated, but still primitive, rationale for using these pathogens to treat cancer came about; viruses became known as obligate parasitic entities with lethal lytic properties, which could lead to cancer cell killing upon their infection. Over the next few decades, a quest to find suitable OV candidates was undertaken and with the onset of the sophistication of scientific techniques and knowledge, a few candidates emerged as potential viable therapies. This pursuit culminated in the clinical approval of select oncolytic viruses, notably the H101 adenovirus in China in 2005[54] and a Herpes simplex virus (T-VEC) approved by the FDA in the United States in 2015[55].

1.2.2 Mechanisms of action

OVs are multimodal therapeutic platforms that can 1) directly kill cancer cells since viral infection culminates in cell lysis, 2) replicate within and kill other cells in the TME and 3) stimulate a potent anti-tumor immune response which prevents cancer relapse in patients.

1.2.2.1 Cancer cell lysis

OVs have the ability to specifically replicate in cancer cells, since the physiological processes that favor antiviral activity are often defective in cancer cells[56]. Indeed, to enhance tumor growth and progression and to avoid clearance or transformed cells by the immune system, antiviral pathways are commonly deregulated in tumors. While providing an advantage to the tumor, common immune dysfunction of cancer cells render them more susceptible to infection and this very vulnerability of the tumor is exploited by virotherapies. More specifically, cancer cells commonly have defects in their interferon (IFN) induction or response pathways. IFNs constitute key players in antiviral immunity. The IFN response is generally initiated upon recognition of pathogen-associated molecular patterns (PAMPs) (e.g. viral DNA or RNA) by pathogen recognition receptors (PRRs), like toll-like receptors (TLRs). This activation launches a cascade of signaling events using factors such as interferon regulatory factors (IRFs) which culminates in the production and secretion of IFN from infected cells to alert neighboring cells of an imminent infection[57]. In cancer cells, this signaling cascade can malfunction due to the disruption of different key players involved[58,59]. Thus, although OVs can enter both malignant and healthy cells, the intact antiviral response of healthy cells is able to fend off the OV infection, leaving them unharmed. Conversely, the disrupted antiviral response of cancer cells leaves them more susceptible to viral infections[58–60].

1.2.2.2 Tumor microenvironment cell targeting

Moreover, OVs have been shown to have the ability to not only replicate within and kill cancer cells, but can also be lethal to other cells of the TME. This broad tropism of OVs for various tumor compartments offers an interesting means of tumor biostructure destruction. Indeed

OVs can invade vascular tissues, notably vascular endothelial cells, which often promotes vascular shutdown[61,62]. OVs can also infect stromal cells, like CAFs[63,64]. This is particularly interesting for the treatment of PC tumors, since these can be composed of more CAFs than cancer cells, which impede the delivery of systemically administered treatments[39,65]. Destruction of this stroma component could therefore be of importance to sensitize these tumors to chemotherapy or other treatments administered via the systemic route.

1.2.2.3 Anti-tumor immunity

In addition, the promise of OV therapy not only lies in direct tumor cell lysis, but also in generating a robust and long lasting antitumor immune response by exposing tumor associated antigens (TAAs) in the TME upon cell lysis, a process known as the *in situ* vaccine effect[66–69]. Cancer immunotherapy has grown into an effective form of cancer treatment. Its premise of stimulating one's immune system to fight cancer allows tumor clearance and the generation of an antitumor immune response able to prevent tumor recurrence. OVs have emerged as an important class of cancer immunotherapy drug. They have the advantage of being able to turn non-inflamed "cold" tumors into inflamed "hot" tumors[68,70]. This potent immunomodulatory benefit is conferred by their direct cell lysis abilities which promotes a pro-inflammatory state in the TME. Indeed, the release of damage-associated molecular patterns (DAMPs), PAMPs and pro-inflammatory cytokines following OV infection of tumor cells facilitate the recruitment of dendritic cells to the tumor which enables cross-presentation of tumor-associated antigens (TAAs) to CD8+ T cells. This cascade of events culminates in the generation of an antitumor immune response orchestrated by effector and memory T cell

populations[68,70]. This facet of oncolytic virotherapy is especially attractive for the treatment of PC tumors, since it could render tumors susceptible to checkpoint blockade therapy.

1.2.3 Current use in clinical settings

The field of OV therapy is currently gaining traction largely as a result of clinical successes. The first FDA approved OV-based therapy, Talimogene laherparepvec (T-VEC), has shown promising results in melanoma patients[71]. Following success in clinical trials, the oncolytic herpesvirus (oHSV-1) T-VEC, was approved for use as monotherapy or in combination with immune checkpoint inhibitors (ICIs)[72]. In addition, a large number of OV platforms are currently being tested in preclinical and clinical settings and are showing promising results for multiple types of cancers[72,73]. As for PC, clinical trials using different viruses, like the HF10 oHSV, the ONYX-015 adenovirus and the pelareorep oncolytic reovirus, in combination with gemcitabine or erlotinib have been undertaken. Phase I clinical trials generally show a good safety profile, but phase II trials show limited efficacy of these combination treatments[74–76]. Thus, further investigation of novel OVs for the treatment of PC is needed and other clinical trials are currently underway (NCT02705196, NCT03252808, NCT02045589).

1.2.4 Viral platforms

Some OVs used and studied are naturally occurring viruses, like reovirus[77], but most are engineered with desired properties to exclusively replicate within cancer cells. Indeed, the genome of OVs can be readily engineered to favor their replication specifically within tumor cells to enhance their safety profile by removing viral genes allowing their replication within normal cells. On the other hand, they also offer interesting platforms for transgene expression

of factors improving their killing abilities in cancer cells. Engineered OV platforms include, but are not limited to, T-VEC, Pexa-Vec and LOAd703; modified herpes, vaccinia and adenoviruses, respectively. Today, the selection of viruses possessing good therapeutic indexes is also turning to less known viruses. For example, the Maraba virus (MRB) isolated from Brazilian sand flies was selected as a potent OV following the screening of several rhabdoviruses in the NCI-60 panel[78,79]. That virus was nevertheless engineered to have superior cancer-specific properties[79] and is now being tested in the clinic.

1.2.5 Rhabdoviruses

1.2.5.1 Virion and genomic structure of Rhabdoviridae

The Rhabdoviridae family of viruses consists of RNA viruses with a single-stranded genome of negative polarity. Their virions are characterized by their bullet-shaped enveloped helical nucleocapsid. Their genomes (~11 kb in size for VSV) are composed generally of five genes, coding for the nucleocapsid protein (N), phosphoprotein (P), matrix protein (M), glycoprotein (G) and large polymerase (L). The two archetypal rhabdoviruses, the rabies virus and the vesicular stomatitis virus (VSV) are extensively studied[80].

1.2.5.2 VSV replication cycle

The replication cycle of VSV begins when the glycoprotein on the surface of virions attaches to the target cell membrane via the LDL receptor[81]. The virion then enters the cell by endocytosis via actin- and clathrin-dependent mechanisms[82,83]. Upon acidification of the endosome, the ribonucleocapsid (RNP) is released in the cytoplasm after fusion of the viral and endosomal membranes[84]. The RNA-dependent RNA polymerase (RdRp) then proceeds to

synthesize the genomic RNA and mRNAs in the cytoplasm[85]. Cellular ribosomes then translate the mRNAs to create the viral proteins that assemble to form virions upon budding of the particles from the plasma membrane[85].

1.2.5.3 Oncolytic rhabdoviruses

The two most common rhabdoviruses studied and employed as virotherapies are VSV and MRB. Their cytoplasmic replication cycle makes for relatively safe OVs and the low or even absent pre-existing immunity associated to these platforms in human populations makes them ideal candidates for use as therapeutics. In mammalian cells, these viruses have a rapid replication cycle and will multiply to high titers, making them relatively easy to produce and also confer them natural biotherapeutic advantages. Their genome, although quite small, allows for genetic manipulations and addition of transgenes useful for tracking the virus or for enhancing its cancer-killing abilities[79]. In order to enhance their replication within cancer cells and enhance their safety profile, VSV and MRB have been engineered. **VSVΔ51**: In the oncolytic VSV candidate (VSVΔ51), the methionine 51 in the M protein is deleted to enhance the safety profile of VSV wild-type (WT)[86]. This mutation renders the virus unable to block the IFN response in infected cells, thus allowing its clearance from normal cells with intact IFN responsiveness. IFN-deficient cancer cells are thus targeted selectively. The WT VSV virus has also been engineered to express IFNβ to limit the infection of normal, non-malignant cells, thus enhancing its safety profile. The VSV-IFNβ clinical candidate was deemed safe in a clinical trial in patients with solid tumors (NCT02923466) and is now being tested alone (NCT03017820, NCT01628640) or in combination with an anti-PD1 checkpoint inhibitor (Pembrolizumab) (NCT03647163) in other cancers. **MRB MG1**: The oncolytic MRB virus

candidate (MRB MG1) harbors M protein L123W and L protein Q242R mutations[79]. These mutations enhance the safety profile of the virus in normal cells and also enhance the lytic ability of the virus in cancer cells compared to MRB WT[79]. This virus is currently undergoing clinical evaluation in solid tumors in a prime-boost regimen consisting of two viral platforms expressing the tumor antigen MAGE-3, MG1MA3 with AdMA3 (NCT02285816) and in combination with Pembrolizumab in patients with non-small cell lung cancers (NCT02879760).

1.2.6 Challenges to overcome

Despite their mild side effects, OVs are generally considered less toxic than other standard-of-care cancer treatments[87]. They are also generally considered a more affordable and sustainable class of immunotherapy, compared to adoptive cell therapy or CAR-T cell therapy. However, despite preclinical and clinical success, challenges associated with OV therapy include viral delivery to tumor tissues following systemic administration, virus neutralization by the host's pre-existing immunity against the OV platform, viral spread within the tumor and sufficient transgene expression within the tumor bed[88–91]. Indeed, the self-amplifying nature of OVs makes them optimal therapeutic vectors for transgene expression. However, efficient and proficient viral replication is needed in tumor cells in order for this strategy to be effective. Thus, in addition to these above-mentioned challenges in need of careful attention, the intrinsic properties of some tumor cells that impede viral replication need to be scrutinized. While most cancer cells display deregulated antiviral immunity[60], some cancer cells retain systems responsible for the detection of virus infections. The efficacy of OV therapy will thus depend upon the extent of antiviral program loss within cancer cells. It is now well established that

cancer cells generally display impaired IFN responsiveness and OV therapy takes advantage of this property to selectively infect these malignant cells. However, due to the heterogeneous nature of most tumors and their ease of adaptability to treatment, not all cells will be susceptible to viral infection. Some tumors may harbor cells with residual antiviral immunity. It is also known that cancer cells are not equally susceptible to VSVΔ51 infection, and this can be attributed to the fact that not all tumors bear IFN defects[86,92–94]. Novel strategies to overcome or bypass these residual antiviral mechanisms to enhance OV-derived transgene expression within the tumor bed are therefore needed.

1.3 Overcoming resistance to oncolytic virotherapy using high-throughput bioselection screens

In order to identify mechanisms involved in OV resistance, bioselection screens can be put to use. These screens apply various pressures to OV-infected cancer cells in the form of drugs or even genome editing and gene expression manipulation. They can shed light on previously unsuspected interactions between tumor cells and OVs. In order to build better OVs or to find better therapeutic targets, these interactions need to be understood. These screens thus provide insight on which molecules can be targeted within cancer cells in order to modulate cellular responses to OV therapy and thus enhance OV activity.

1.3.1 Pharmaceutical screens

Since the deregulated antiviral pathways in cancer cells can be affected at different junctions of important signaling pathways, pharmacoviral screens offer an approach to select for compounds that can be effective on multiple target proteins in the pathway. The first high-

throughput oncolytic pharmacoviral screen interrogated the effects of a chemical library composed of ~12,000 drugs in OV-resistant 4T1 cancer cells and identified an array of viral sensitizer (VSe) compounds. The most promising, VSe1, was shown to synergize with VSVΔ51 to enhance OV replication by disrupting IFN signaling[95]. This screen also identified microtubule-destabilizing agents, such as colchicine, as potent enhancers of VSVΔ51 and MRB MG1 replication[96]. Similarly, a different high-throughput screen of 73 compounds was able to identify multiple drug candidates that enhance the Myxoma OV efficacy in stem-like glioma cells[97].

1.3.2 Genome editing screens

First described as a bacterial antiviral defense mechanism, the CRISPR-Cas9 system is now widely used as a powerful genome editing tool. In addition to offering the possibility to selectively knock out genes from a given cell line or organism with impressive precision, this system can be used as a screening tool in a high-throughput fashion. CRISPR "dropout" or loss-of-function negative selection screens allow the identification of lethal phenotypes in cells by using a genome-wide targeting approach to find genetic vulnerabilities that can then be targeted for therapeutic purposes[98]. Such a screen was performed on acute myeloid leukemia cells and found novel therapeutic targets for this cancer, but also confirmed known targets using this method[99]. More recently, a similar screen was performed on acute lymphoblastic leukemia cells infected with a MRB MG1 virus, identifying several genes involved in OV resistance that enhanced OV efficacy once targeted[100].

1.3.3 Genome-wide RNA interference screens

RNA interference (RNAi) is an endogenous process used by a variety of eukaryotic organisms to regulate gene expression at the mRNA level by degrading transcripts or blocking their translation. Since its discovery by Fire and Melo in *Caenorhabditis elegans* in the late 1990s[101], RNAi has become not only important to understand several biological processes, but was also established as an essential biomolecular tool.

Endogenous small RNAi effector molecules include miRNAs and small interfering RNAs (siRNAs). miRNAs are the most studied of all small regulatory RNAs. These non-coding RNA molecules are made up of a sequence containing two complementary ~22 nucleotide sequences which encourage the formation of a hairpin structure by folding in on itself once transcribed from the genome to form a primary miRNA. In the canonical miRNA processing pathway, the hairpin is then recognized by the nuclear DGCR8/Drosha complex which cleaves the RNA at the base of the hairpin, creating the precursor miRNA (pre-miRNA) which is then exported to the cytoplasm by the Exportin-5 protein for further processing[102,103]. The Dicer endonuclease then recognizes the pre-miRNA and cuts the loop of the hairpin, yielding the miRNA:miRNA duplex[104]. Although both strands of this duplex can act as a mature effector miRNA, only one is kept in this complex to act in downstream mRNA targeting, the other degraded[105]. Other proteins, namely Argonaute proteins, then come into play and interact with the Dicer-miRNA complex to form the RNA-induced silencing complex (RISC)[106]. In mammals, miRNAs use a short "seed sequence" of 6-8 nucleotides at their 5' end to target the 3' UTR region of mRNAs. This prevents mRNA translation, thus repressing protein expression[107]. However, the seed sequence is not sufficient to cleave the target mRNA. This partial target mRNA recognition also offers the advantage of multitargeting. Indeed, a single miRNA can target several mRNAs

and a single mRNA transcript can be targeted by multiple miRNAs. Like miRNAs, eukaryotic endogenous siRNAs are similarly processed by the cellular RNAi machinery. However, these usually come from longer RNA hairpins or from other double-stranded RNAs (dsRNA) and they exhibit perfect complementarity to their target, allowing cleavage and degradation of the mRNA transcript, so are thus more specific[108,109]. The concept of endogenous RNAi has now become a popular tool for exogenous genetic manipulation. To this end, miRNAs, siRNAs and short hairpin RNAs (shRNAs) are currently used in biomedical research to downregulate gene expression.

These molecules have been utilized in several bioselection screens to enhance OV replication or cytotoxicity. In order to enhance adenovirus replication within PC cells, Rovira-Rigau and colleagues generated a library of adenoviruses encoding over 200 endogenous human miRNAs. This allowed for the identification of hsa-miR-99b and hsa-miR-485, two miRNAs with the ability to enhance oncolytic adenovirus-mediated PC cell death[110]. Varble and colleagues have also made use of an SV library encoding ~16,000 artificial miRNAs (amiRNAs) passaged *in vivo* to identify cellular factors involved in antiviral immunity[111]. Another screen made use of a library constituted of siRNAs targeting some 18,000 genes which uncovered a strategy to sensitize tumors to oncolytic rhabdovirus therapy by inhibiting the ER stress response[112]. Moreover, shRNAs screens have been useful, notably in identifying the SRSF2 splicing factor as a barrier to oHSV-1 cytotoxicity[113].

1.4 Oncolytic virotherapy-enabled synthetic sensitization

Since their discovery as oncolytic therapeutics, viruses have been combined with various other treatment options in the hopes of enhancing therapeutic gain, either by encoding transgenes in the viruses themselves, or by co-administering molecules. They have notably been tested in combination with cytokines, checkpoint inhibitors, bi-specific T-cell engagers (BiTEs), chemotherapeutics, small molecule inhibitors, siRNAs, shRNAs, miRNAs and lncRNAs[114–117]. These studies have inspired the use of *synthetic sensitization* strategies to modulate OV efficacy.

Synthetic lethality occurs when the simultaneous perturbation of two target genes results in cell death, whereas the sole targeting of one of the two leaves cells unharmed. With the rise of genomics and the ever-increasing availability of tools to study the genome, it has become easier to identify such interactions within cancer cells and to target these vulnerabilities. Synthetic lethal approaches are also useful in circumventing drug resistance in cancers, which are notoriously known for their high genetic and epigenetic adaptability that translates into quickly acquired resistance to treatment. However, since its debut over 20 years ago in the cancer research field[118], synthetic lethality has made very little progress in the clinic. Today, the unique treatment making use of this strategy in the clinic is poly(ADP-ribose) polymerase (PARP) inhibition in BRCA-mutated cancers[119]. Due to their many benefits, OVs offer a promising platform to enable the use of synthetic lethality for cancer treatment. Ning and colleagues have described a synthetic-like interaction that sensitizes oHSV-infected cells to PARPi, whether they were PARP-resistant or -sensitive. In this treatment, oHSV naturally renders PARP-resistant cancer cells sensitive to PARPi by selectively targeting elements of the DNA damage response, culminating in enhanced cell death of glioblastoma tumors[120].

Moreover, it will also be interesting to engineer OVs as expression vectors of molecules targeting the expression of one gene in combination with the administration of drugs targeting the expression of a second gene, thus enabling a synthetic sensitization phenomenon within tumors. Using an OV as a synthetic lethality tool would provide a substantial advantage over current regimens, since the expression of one of the payloads would depend on viral replication, which prominently occurs successfully in cancer cells.

1.5 Extracellular vesicles

Extracellular vesicles (EVs) comprise another novel up-and-coming promising cancer therapeutic. EVs are cell-derived membrane nanovesicles secreted by all cell types to facilitate intercellular communication via their cargoes, which can include small proteins, lipids, small DNA sequences and RNA sequences (e.g. mRNAs, miRNAs, lncRNAs)[121–126]. EVs are generally subdivided into three main categories according to their size; exosomes (50-150 nm), microvesicles (100 nm - 1 μm) and apoptotic bodies (100 nm - 5 μm)[127], the most extensively studied being the smallest vesicles. Since these populations share markers and that *bona fide* markers for these subpopulations have yet to be identified[123,128], the International Society for Extracellular Vesicles advises to use the umbrella term "*extracellular vesicles*", unless the cellular origin of the vesicle can be confirmed[129]. Moreover, the term "*small extracellular vesicle*" (SEV) has been coined to refer to small particles (~100 nm) isolated together with a given technique, like differential ultracentrifugation. These can include exosomes and small microvesicles or apoptotic bodies. SEVs are found in all biological fluids and have been shown to play several roles in normal and pathological conditions[130]. They thus consist in interesting biological entities with biomarker and therapeutic potential.

1.5.1 Extracellular vesicles in intercellular communication networks

In order to maintain a homeostatic state, cells make use of several information transmission networks in response to internal or external stimuli. These can include the production and response to cytokines and hormones. In humans, cell-cell communication is indispensable to the optimal functioning of multiple bodily processes. Since these signal transduction pathways are so important, research has shed light on many different pathways used by cells to communicate to other cells within a given organism. When they were first discovered, the secretion of EVs was viewed as a means of shedding unwanted cellular components. Now, EVs are being investigated as carriers of information with roles in intercellular communication in physiological and pathological processes[131–133]. We now know that EV composition is changed and their production is often upregulated as a result of cellular stress, and thus must have important biological functions[134,135]. This was hypothesized to work in similar ways as the upregulation of cytokine production to alert neighboring cells of an imminent threat. This type of communication, where one compromised cell can send out messages to neighboring cells, is referred to as the bystander effect. The bystander effect can work to protect surrounding cells, or can also be hijacked in the case of diseases to sabotage the host. EVs can cause bystander effects in multiples biological processes, including tumor formation, metastasis and viral infections[136,137].

1.5.1.1 Extracellular vesicles in cancer

Accumulating evidence indicate an important role of EVs in tumor establishment, progression and metastasis. They have been shown to do so by promoting the expansion of cancer cells, remodeling cancer metabolism, upregulating angiogenesis, modulating immune responses

within the TME, inducing epithelial to mesenchymal transition (EMT) and promoting metastasis[136]. For example, the oncogenic EGFRvIII protein can be horizontally transferred between cells. This promotes activation of oncogenic EGFR pathways that lead to cell transformation and enhanced growth[138,139]. In addition, cancer cells can secrete EVs containing several EMT-inducing molecules, like TGF-β, HIF-1α and several miRNAs[140]. These EVs can thus prime neighboring cells for invasion and metastasis. Similarly, cancer cells have also been shown to secrete EVs harboring specific integrins (ITGs) in their membrane that allow for organ-specific priming of the pre-metastatic tumor niche. For example, PC-derived EVs can display ITGαvβ5 with selective tropism to liver Kupffer cells. This effect is abrogated when the cancer cells of the primary tumor do not express the ITGαvβ5 protein[141,142]. Novel strategies to circumvent the effects of such EVs are currently being investigated.

1.5.1.2 Extracellular vesicles in viral infections

EVs are known to share a few characteristics with some viruses. Indeed, their physical characteristics, biochemical composition and even their uptake and secretion mechanisms can be very similar[143]. They do differ, however, in their function. Viruses are pathogens that can cause infection by hijacking the cellular machinery to replicate and generate progeny virions with the ability to propagate within an organism or spread to other organisms. EVs, however, do not have the ability to replicate within cells and they are not infectious *per se*. These two distinct types of nano-entities can nonetheless collaborate in biological processes. Indeed, viruses have the ability to hijack cellular EV production mechanisms for their own gain. EVs have been shown to usurp cellular pathways to transfer molecules between cells to perpetuate viral spread. A prime example is the use of EVs by the HIV virus that can transfer several

factors to neighboring cells that have the ability to render uninfected neighboring cells more sensitive to an incoming viral infection, like cellular CCR5 and CXCR4 receptors, its gp120 envelope protein as well as its Nef non-structural protein[144]. On the flip side, EV-mediated bystander effects can be used by the host to subvert viral infections. For example, HIV-infected cells can package APOBEC3G, a cellular antiviral protein, into EVs. The uptake in neighboring cells of these EVs can thus alert them of an incoming viral infection and prepare them to restrict HIV replication[145]. Thus, EVs can be reprogrammed upon viral infection of the cell to either interrupt or promote viral infection depending on the situation.

1.5.2 Therapeutics

EVs have gained much attention from the scientific community in the past decade due to their ability to serve as disease-related biomarkers and to their thrilling therapeutic potential. Recent preclinical and clinical studies have shown that small EVs produced from fibroblasts, mesenchymal stem cells (MSCs) or patient-derived cells can be used as drug-, gene- or RNAi-delivering devices for the treatment of cancer and other diseases[126,146]. To this end, first-generation therapeutic EVs were produced *ex vivo* from patient-derived dendritic cells and loaded with their cargo by electroporation, chemical-based transfection of EVs or simply by incubating EVs with the therapeutic cargo[147]. Now, cell lines are manipulated *in vitro* to secrete EVs that contain therapeutic cargoes and display specific surface proteins[148,149]. A plethora of pre-clinical studies demonstrating therapeutic benefits of therapeutic EVs for several diseases have led to the launch of a few clinical trials to test their safety and efficacy including three making use of SEVs to treat cancer[150]. These include a trial using dendritic cell-derived SEVs containing TAAs to treat non-small cell lung cancer (NCT01159288) and

plant-derived SEVs containing curcumin for colon cancer treatment (NCT01294072). In addition, for the treatment of PC, the delivery of an siRNA targeting oncogenic $Kras^{G12D}$ via MSC-derived SEVs was investigated and displayed promising pre-clinical results in several models of PC[151] and this therapy will shortly be tested in a phase I clinical trial (NCT03608631).

2. HYPOTHESIS AND OBJECTIVES

2.1 Hypothesis

We hypothesized that the use of OV-encoded amiRNAs could help target the residual cellular antiviral components associated with resistance to OV therapy in pancreatic cancers. We also hypothesized that these amiRNAs, once transcribed in cells, could be packaged by infected cell-secreted EVs and could sensitize naïve neighboring tumor cells to OV therapy and small molecule inhibitors.

2.2 Objectives

1) Find novel amiRNA sequences that enhance oncolytic viral replication and cytotoxicity in pancreatic cancer cells.

2) Encode these amiRNAs in our oncolytic virus platform of choice, VSVΔ51, and validate the efficacy of this strategy in cancer cells and tumors highly resistant to oncolytic virotherapy.

3) Describe the effects of amiRNA-targeting of a novel antiviral factor.

4) Evaluate the combinatorial effects of our amiR-encoding oncolytic virus with a small molecule inhibitor

5) Explore the bystander killing effect generated by amiRNA-containing extracellular vesicles derived from infected cancer cells.

3. MATERIAL AND METHODS

3.1 Cells and cell culture

MIA PaCa-2, 786-0, Vero, BxPC-3, PANC1, HPAF-II, HPAC, 4T1 and B16-F10 cells were purchased from the American Type Culture Collection (ATCC, Manassas, VA). Normal human GM00038 skin fibroblasts (abbreviated herein as GM38), human fetal pancreatic fibroblasts (PCa-CAF) and T-Rex™-293 cells were obtained from the Coriell Cell Repositories (Camden, NJ), Vitro Biopharma (Golden, CO) and Invitrogen, respectively. The murine pancreatic adenocarcinoma cell line Panc02 of C57BL/6 origin was developed by Corbett *et al*[152]. Mel888 cells were a gift from Dr. Melcher at the Institute of Cancer Research, London, UK. 786-0 and PANC1 CRISPR-Cas9 mediated ARID1A knockout and 4T1 Rab27a knockout cell lines were generated using the lentiCRISPRv2 protocol. The P025 cell line was derived from a pancreatic cancer patient-derived xenograft as previously described[43]. The murine TH04 PC cell line was derived from spontaneous pancreatic tumors of $Kras^{G12D}$ and $Trp53^{R172H}$ C57BL/6 mice and were a gift from Dr. Juliana Candido at the Barts Cancer Institute, Queen Mary University of London, UK. MIA PaCa-2, 786-0, Vero, BxPC-3, PANC1, Panc02, HPAF-II, 4T1, B16-F10, PCa-CAF, TH04 and Mel888 cells were cultured in Dulbecco's minimal essential medium (DMEM; Corning) containing 10% fetal bovine serum (FBS; Hyclone). 786-0 $ARID1A^{-/-}$, PANC1 $ARID1A^{-/-}$, 4T1 $Rab27a^{-/-}$ were cultured in DMEM containing 10% FBS and puromycin (3.5 μg/ml for 786-0 $ARID1A^{-/-}$, 4 μg/ml for PANC1 $ARID1A^{-/-}$, 1 μg/ml for 4T1 $Rab27a^{-/-}$; Cayman Chemical). GM38 fibroblasts were cultured in DMEM containing 2% FBS. T-Rex™-293 cells were cultured in DMEM containing 10% FBS, zeocin (300 μg/ml; Gibco) and blasticidin (5 μg/ml; Invivogen). HPAC cells were grown in RPMI-1640 medium (Corning), 10% FBS, 15 mM HEPES, 0.5 mM

sodium pyruvate, 2 µg/mL insulin, 5 µg/mL transferrin, 40 mg/mL hydrocortisone, 10 mg/mL human epidermal growth factor (hEGF). P025 cells were grown in RPMI-1640 medium, 10% FBS, 15 mM HEPES, 0.5 mM sodium pyruvate, 2 µg/mL insulin, 5 µg/mL transferrin, 40 mg/mL hydrocortisone, 10 mg/mL hEGF, 100 µg/mL Gentamicin, 0.1 mg/mL Normocin™ (InvivoGen) and 1 x Antibiotic-Antimycotic (Gibco). All cell lines were cultured under 5% CO_2 at 37 ºC and were routinely tested for mycoplasma contamination using Hoechst stain (Invitrogen) and the e-Myco VALiD Myco PCR detection kit (FroggaBio). All cell lines have tested negative for mycoplasma contamination.

3.2 Generation of CRISPR knockout cell lines

The lentiCRISPRv2 plasmid was digested with FastDigest BbsI (NEB) and gel purified using the QIAquick Gel Extraction kit (Qiagen). Forward and reverse gRNA oligonucleotides for *ARID1A* or *Rab27a* were phosphorylated and annealed according to the Zhang lab lentiCRSPRv2 and lentiGuide oligo cloning protocol (Addgene). LentiCRISPR v2 was a gift from Feng Zhang (Addgene plasmid # 52961; http://n2t.net/addgene:52961; RRID:Addgene_52961)[153]. Annealed oligonucleotides were diluted 1:200 and ligated into BbsI digested lentiCRISPRv2 at room temperature with Quick Ligase (NEB) and then transformed in Stbl3 cells (Invitrogen). DNA was extracted using the Qiagen MiniPrep kit (Qiagen) and verified by Sanger sequencing. gRNA targets were chosen from the GeCKO Lentiviral sgRNA v2 libraries; hARID1A: 5'-GATGCATGATGCTGTCCGAC-3', mRab27a: 5'-GTTTCCTCAATGTCCGAAAC-3'. Lentivirus encoding the individual gRNAs was produced as previously described using 3rd generation packaging plasmids[154]. Cells seeded in 6-well plates were transduced with 1 mL of lentivirus and 24 hours post transduction,

were placed in selective media containing puromycin (4 μg/mL for PANC1 ARID1A$^{-/-}$, 3.5 μg/mL for 786-0 ARID1A$^{-/-}$ and 1 μg/mL for 4T1 Rab27a$^{-/-}$). Once selection was complete, limiting dilution plating was performed in order to obtain single cell colonies. Clonal cell lines were expanded such that lysates and DNA could be harvested to assess target gene knockout. Targeted knockout was confirmed using immunoblotting analysis, T7 endonuclease assay and Sanger sequencing. T7 endonuclease assay to confirm gRNA cleavage was performed using DNA from clonally derived cell lines was extracted using the DNeasy Blood & Tissue kit (Qiagen). Genomic DNA was used as the template to amplify the targeted locus of interest using Q5 Hot Start High-Fidelity 2x Master Mix (NEB) following the manufacturer's protocol and using these primer pairs: hARID1A-F 5'- TGTGTGTGATACTGGGAGGT-3'; hARID1A-R 5'- CACAATTTGCTGCTGGGTCT-3'; mRab27a-F 5'-CTTAGCTCCTCCTT TTGTGC-3'; mRab27a-R 5'- TTCCTGAGAGGATGAGGAAG-3'. PCR products were purified using the PureLink PCR Purification kit (Thermo Fisher). 200 ng of purified DNA was mixed with 10x NEBuffer 2 and dH_2O to a final volume of 19 μl. Samples were heated to 95 °C for 5 minutes, followed by slow ramp-down to room temperature to enable heteroduplex formation. 1ul of T7 endonuclease I (NEB) was added to each sample and incubated at 37 °C for 15 minutes. Following digestion, samples were resolved on a 2% agarose gel to assess for the presence of indels. Clonally derived PANC1, 786-0 and 4T1 cell lines with a positive T7 result were sent for Sanger sequencing to confirm T7 results and determine indel size and location. All sequencing was completed at the StemCore Laboratories (Ottawa, ON) using the primers listed here: hARID1A-F 5'-GCCTCTTCATGAGCCATTTC-3'; hARID1A-R 5'-AATTTGCTGCAGGGATTGTC-3'; mRab27a-F 5'-CTCTTCCACCATACTTGGAG-3'; mRab27a-R 5'- TAGTAGCCTCGACACTGAGC -3'.

3.3 Viruses

The oncolytic VSVΔ51[86], Maraba[79], oHSV-1[155] and VV TK$^-$ VGF^{-156} virus backbones and propagation protocols have previously been described. To construct and rescue the replication competent amiRNA-expressing VSVΔ51 viruses, plasmids containing the amiR-1-5 sequences or the non-targeting control (NTC; sequence targeting the GFP mRNA) (**Table 3.1**) encoded in pre-miR-30-based short hairpin cassette (Figure 3.1) flanked with XhoI and NheI restriction sites were purchased from GenScript. Both amiR-encoding plasmids and VSVΔ51-GFP encoding plasmids were digested using XhoI and NheI (NEB) and amiRNA inserts were ligated individually into the VSVΔ51 empty vector at the gene junction between G and L proteins as previously described[63]. Single cycle MRBΔG viruses (replication-defective) were generated using a similar strategy by PCR amplifying the corresponding pre-amiR sequences from GenScript plasmids or the NTC (sequence targeting the firefly luciferase mRNA) using specific primers containing the BsrD1 and KpnI restriction enzyme sites (Forward: 5'-GCAATGACGAGTTTGTTTGAATGAGGCTTC-3'; Reverse: 5'-GGTACCAAAGTGA TTTAATTTATACCATTTTA-3'). A plasmid containing the Maraba virus genome where the glycoprotein (G) gene was replaced by the GFP sequence was then used to insert the desired pre-miR cassette. Briefly, the pBR-MRBΔG vector was digested with BsrD1 and KpnI to remove the GFP gene, and then the digested vector and PCR-amplified pre-miR cassettes were ligated. The resulting plasmid contains the MRBΔG genome and the amiR sequences, which were inserted between the M and L genes. All constructs were verified by sequencing (StemCore Laboratories, Ottawa, ON). All viruses were rescued using an infection-transfection method as previously described[63]. In the case of single cycle viruses, MRBΔG, viruses were rescued and titrated in T-Rex™-293 cells expressing the MRB G protein. T-

Rex™-293 cells containing a plasmid with doxycycline-inducible MRB G protein expression were used to produce the MRBΔG viruses. G protein expression was first induced with 800 μM doxycycline (DOX) and cells were immediately infected at MOI 0.05 in serum-free DMEM. After 2 hours, the inoculum was removed and fresh DMEM with 10% FBS was added. After 48 hours, media was harvested and large cellular debris was removed using a 1500 rpm spin for 15 minutes at 4 °C. The media was further cleared by filtering on a 0.22 μm Steritop™ filter unit (Millipore). Virus was pelleted at 12,000 rpm for 2 hours (Beckman Coulter Avanti J-E centrifuge).

3.4 Sindbis virus amiRNA library passaging

A replicating Sindbis virus amiRNA library (SV-amiRNA library) encoding approximately 16,000 unique amiRNA sequences was used in our studies. The targeting amiRNA sequences in our library were designed using the Hannon and Elledge algorithm (http://www.ncbi.nlm.nih.gov/projects/genome/probe/doc/DistrOpenBiosystems.shtml). Essentially, a pre-miR-30 cassette is used to house the shRNA and approximately 16,000 unique amiRNAs were originally cloned into a SV expression vector as previously described[111]. To serially passage the library in malignant and healthy cells, we first infected PANC1, MIA PaCa-2, Panc02, PCa-CAF and GM38 normal fibroblasts with the original pooled SV-amiRNA library at a MOI of 0.1. 24 hpi, virus outputs were collected and saved for subsequent infection cycles. A fraction of the sample was saved separately and tittered by plaque assay in Vero cells. Four consecutive serial passages of the SV-library were conducted using five parallel biological replicates (a schematic representation of our screening pipeline can be found in Figure 3.2).

3.5 Small RNA sequencing of the passaged SV-amiRNA library

Small RNA sequencing from both the unpassaged (input) and passaged library samples was performed from total RNA collected using an RNeasy Kit (Qiagen), as previously described[111]. Input samples were collected 18 hpi and passaged samples were collected 18 hours following fourth passage. Briefly, to monitor SV-amiRNA populations (diversity) upon passaging in selected healthy and malignant cells, total RNA was converted to cDNA using a SuperScript III reverse transcriptase (Invitrogen) and random hexamers. Specific primers for the pre-miR-30 cassette (**Table 3.1**) with added Illumina-specific overhang adapter sequences compatible with high-throughput (HT) sequencing were used to amplify the amiRNA hairpin region. Deep sequencing analysis was performed using a MiSeq instrument (Illumina; SeqMatic LLC, CA). Using custom shell and Python scripts, the data was stripped of adapters and barcodes and matched against the full list of 16,000 amiRNAs in the original library, generating observed counts for each amiRNA in each replicate. To control for sequencing errors or variations, the sequences were aligned and grouped in "families of sequences". Enrichment of specific amiRNA hairpins was calculated by comparing the frequency of each amiRNA in the input original library and in the passaged samples.

3.6 RNA sequencing of PANC1 ARID1A wild-type and knockout clones

PANC1 cells (5E5) were seeded into 6-well plates. 18 hours later, cells were infected with VSVΔ51 at MOI 3 or mock-infected with serum-free media. 1 hour after infection, media was aspirated and replaced with fresh media containing 10% FBS. 18 hpi, RNA was harvested in Trizol (Thermo Fisher). RNA was extracted using the manufacturer's protocol and quantified. PANC1 wild-type or ARID1A knockout total RNA was sequenced by The Centre for Applied

Table 3.1 Artificial microRNA sequences

Artifical microRNA	**Sense sequence (5'-3')**	**Antisense sequence (5'-3')**
amiR-1	TTGTCTTACTCTTCAATAACAT	ATGTTATTGAAGAGTAAGACAA
amiR-2	ATAGTGATAACTCACTAGTACC	GGTACTAGTGAGTTATCACTAT
amiR-3	TTTAGTGATAACTCATAGTACA	TGTACTATGAGTTATCACTAAA
amiR-4	ACCGTCATGTCTGTTACGTTAA	TTAACGTAACAGACATGACGGT
amiR-5	TGCAGAGAGTGTTATATTGCAT	ATGCAATATAACACTCTCTGCA
amiR-NTC (GFP)	ACAAGCTGACCCTGAAGTTCAT	ATGAACTTCAGGGTCAGCTTGC
amiR-NTC (Fluc)	GTTGGCCACCGAAGCAGCGCAC	GTGCGCTGCTTCGGTGGCCAAC

Genomics (TCAG) at The Hospital for Sick Children (Toronto, Canada) using the Illumina HiSeq2500 platform to generate single-end 100 bp reads. Adapters were trimmed using Trimmomatic[157] and adapter-free reads were mapped to the human genome (hg19) using TopHat2[158]. Transcript abundance and differential expression analysis were performed using cufflinks and cuffdiff[159] as part of a previously described pipeline[160]. Genes with an FDR value smaller than 0.05 and with a fold change greater or smaller than 4 were considered for pathway analysis using gProfiler[161]. Heat maps were generated using Package 'pheatmap' - R Project version 1.0.8.

3.7 Bioinformatics predication of amiR-4 targets

Bioinformatic prediction of amiR-4 targets carried out by TargetS based on Total Delta Energy of Duplex or by BLAST complementarity revealed nine potential amiR-4 targets. *ARID1A*, *PLEC*, *HDAC4* and *MCM2* were selected for further validation based on their high targeting prediction values. From the initial nine targets predicted, three were significantly downregulated by amiR-4 (*ARID1A*, *PLEC* and *HDAC4*). Although *MCM2* was a predicted target, its downregulation was not observed in our *in vitro* systems and was thus used as a negative control. The remaining five targets were not significantly downregulated by amiR-4 in our *in vitro* systems.

3.8 Quantitative real time PCR

Quantitative RT-PCR (RT-qPCR) was performed on non-pooled replicate samples. RNA extractions were performed using TRIzol™ reagent as per manufacturer protocol (Invitrogen). Cellular RNA was converted to cDNA by Superscript RT II (Invitrogen) or iScript™ cDNA

synthesis kit (Bio-Rad) and EV miRNA was converted to cDNA using the miRNA cDNA synthesis kit (Quanta Bioscience). RT-qPCR was carried out using SYBR Green (Invitrogen) according to the manufacturer instructions. Analysis was performed on a Rotor-Gene RG-3000A machine (Corbett Research) or a 7500 Fast Real-Time PCR System (Applied Biosystems) according to the manufacturers recommended protocols. Primer pairs specific for various gene products or miRNA sequences used are provided in **Table 3.2**. qRT-PCR measurements were normalized to the human *Rplp0* gene or Let7f-1 miRNA using the $2^{-\Delta\Delta Ct}$ method[162]. Copy number per reaction in Appendix 1 was calculated using the diluted sample in a three-point standard curve.

3.9 Immunoblotting analysis

Cells or SEVs were harvested and lysed in NP-40 buffer (1% NP-40, 150 mM NaCl, 2 mM EDTA, 50 mM Tris, pH 7.4) containing Complete™ EDTA-free protease inhibitors (Roche). Cell lysates were clarified by centrifugation at 12,000 x g for 20 minutes at 4 °C. Proteins were separated on Nupage® 4–12% Bis-Tris Protein Gels (Invitrogen) and transferred on polyvinylidene fluoride (PVDF) membranes (Immobilon-P Millipore, Bedford, MA) for two hours or overnight at 4 °C. Blocked membranes were incubated overnight at 4 °C with the following diluted antibodies: ALIX (1:2000; sc-53538), CD9 (1:1000; ab92726), TSG101 (1:1000; ab125011), Calreticulin (1:1000; BioVision #3076), ARID1A (1:500; Cell signaling technology #12354), HDAC4 (1:500; ab12172), PLEC (Plectin-1) (1:500; Cell signaling technology #2863), MCM2 (1:2000; ab4461), GAPDH (1:1000; ab37168 or 1:1000; Cell signaling technology #2118), β-tubulin (1:1000; Cell signaling technology #2146), VSV

Table 3.2 Primers used in RT-qPCR assays

Gene or miRNA	Forward primer (5'-3')	Reverse primer (5'-3')
ARID1A	GAAGTGACTCCACATTCCAG	ACTCCCTGGAGCTTTCC
PLEC	CTGCACTTCCAGATCTCAG	CTGGAGGTGAAGTTGTCG
HDAC4	GACCTGACCGCCATTTGC	GGGAGAGGATCAAGCTCGTTT
MCM2	ATCAGAACTACCAGCGTATC	TCAGCTCTATCTCGTCTCC
ICAM-I	GGCTGACGTGTGCAGTAATA	CCTCTGGCTTCGTCAGAATC
CXC3L1	TGTAGCTTTGCTCATCCACTATC	CCTTGACCCATTGCTCCTT
IFITM1	ATCAACATCCACAGCGAGAC	GGAGTAGGCGAATGCTATGAAG
IFITM2	CCTGTTCAACACCCTCTTCAT	AACCATCTTCCTGTCCCTAGA
PARP9	GTACCTTGGGAGAAAGGAACAT	CGGGCTCCTTCAATCTCTAAC
CCL2	CTCAGCCAGATGCAATCAATG	TGCTGCTGGTGATTCTTCTAT
CLDN1	AAGTGCTTGGAAGACGATGAG	TACCATGCTGTGGCAACTAAA
Rplp0	TTAAACCCTGCGTGGCAATCC	CCACATTCCCCCGGATATGA
hsa-let-7f-1 5p	TGAGGTAGTAGATTGTATAGTT	PerfeCTa® Universal PCR Primer (QuantaBio qScript® MicroRNA cDNA Synthesis kit)

(1:1000)[62] and Rab27a (1:500; ab55667). After three washes with Tris-Buffered-Saline-Tween (TBS-T), the membranes were incubated with goat anti-rabbit (111-005-003) or goat anti-mouse (115-005-146) horseradish peroxidase-conjugated IgG (Jackson ImmunoResearch) for 1 hour. All secondary antibodies were diluted 1:5000 in 5% (w/v) skim milk/TBS-T or bovine serum albumin (BSA) according to the manufacturer's recommendations. Membranes were washed three times with TBS-T and immunoreactive proteins were detected using Amersham ECL Western Blotting Detection Reagent (GE Healthcare) or Clarity ECL (Bio-Rad Laboratories) followed by exposure to X-ray film (Fuji Photo Film Co, LTD). Protein level quantification was assessed by densitometry analysis using ImageJ software and was normalized to respective loading control expression level.

3.10 Cell viability assay

Cell viability was assessed using the alamarBlue® Assay with the REDOX indicator resazurin according to the manufacturer's protocol. Briefly, media was removed, cells were washed once with 1X Dulbecco's Phosphate-Buffered Saline (PBS; Corning) and fresh media was added to cells. Resazurin (2.5 mM) was added in a 1:10 dilution. Cells were incubated with resazurin at 37 °C for approximately 45 minutes to 3 hours depending on the cell line. Fluorescence was measured (excitation 530 nm, emission 590 nm) on the Fluoroskan Ascent FL plate reader (Thermo Fischer Scientific).

3.11 Crystal violet cytotoxicity assay

Cytotoxicity was assessed using a crystal violet assay as previously described[163]. At the end of a given experiment, media was removed, cells were washed once with 1X PBS and a

solution of 0.5% crystal violet was added to the cells. Plates were incubated at room temperature on a shaker for 30 minutes, then crystal violet solution was washed three times with water and plates were left to air dry overnight. Once dry, plates were scanned to obtain pictures and were then subjected to crystal violet lift with 500 µl of methanol per well for a 24-well plate or with 250 µl of methanol per well for a 48-well plate. Plates were incubated at room temperature on a shaker for one hour to allow lifting of the crystal violet, then the OD_{570} was read using the Multiskan Ascent plate reader (Thermo Fischer Scientific).

3.12 Pancreatic cancer patient-derived xenograft samples

Patient samples were obtained by endoscopic ultrasound-guided fine-needle aspiration biopsies (EUS-FNA) following protocol 20120112-01H approved by the research ethics board of the Ottawa Hospital Research Institute. All samples were obtained following informed patient consent. Samples implanted subcutaneously in NOD-SCID mice (Charles River Laboratories, Wilmington, MA) were harvested once the tumor reached endpoint and subsequently used for histologic analysis, cored for further experimental analyses or used to establish primary cell lines. Tumor cores (2mm x 2mm) were infected with 1E5 plaque forming units (PFUs) of VSVΔ51-amiR-NTC or VSVΔ51-amiR-4 for 48 hours and 100 µl of the homogenized core samples were titered.

3.13 Tissue processing and immunohistochemistry

Tumors were formalin-fixed, paraffin-embedded and sectioned before being subjected to IHC staining. After deparaffinization and rehydration of tumor block sections, antigen retrieval was performed in boiling sodium citrate buffer (pH 6.0). Tissue specimens were blocked with Dako

Protein Block Serum Free RTU (Dako Cat# X0909) for 10 min at room temperature. Tumor sections were stained against ARID1A (1:300, ab176395) in Dako Antibody Diluent with Background reducing components (Dako Cat# S3022) overnight at 4ºC. After washing twice with PBS, slides were incubated with Secondary OneStep Polymer HRP anti-rabbit (Ready-to-Use) (GTX83399) for 30 minutes at room temperature. After washing twice with PBS, signal was visualized by incubating with ImmPact DAB Peroxidase Substrate (Vector Labs SK 2043) for 2 minutes at room temperature. Samples were counterstained with hematoxylin.

3.14 Rhabdovirus plaque assay

Samples containing rhabdoviruses were serially diluted and titered on Vero cells as previously described[63]. Briefly, a confluent monolayer of Vero cells was infected with serial dilutions of virus-containing samples for 1 hour. Cells were then washed and overlaid with warm 0.5% (w/v) agarose or 3% Carboxymethyl cellulose (CMC) in culture medium and incubated for 24 to 48 hours. MRBΔG viruses were titered using the same protocol on T-Rex™-293 cells in collagen-coated plates. G protein expression was induced by 800 μM DOX. Viral plaques were visualized by staining with 0.05% (w/v) crystal violet in 17% (v/v) methanol. Results are expressed as PFUs per mL or per mg of tissue.

3.15 Synthetic lethality

Cells were seeded into 24-well plates in DMEM 10% FBS. Once confluent, the cells were infected with VSVΔ51-amiR-NTC or VSVΔ51-amiR-4 by removing media, adding virus in serum-free media for 1 hour, removing inoculum and adding supplemented media. Following 18 hour incubation 15 μM GSK126 (Active Biochem) prepared in DMSO or equivalent

volume of DMSO was added to the wells. Supernatant was collected for plaque assays, an alamarBlue® Assay was performed and cells were stained with crystal violet at the end of the experiment. A crystal violet cytotoxicity assay was then performed. See **Appendix 4** for experimental timeline for different cell lines. For SEV transfer experiments, isolated SEVs derived from mock-infected cells or from MRBΔG-amiR-NTC- and MRBΔG-amiR-4-infected cells were transferred to a confluent monolayer of cells in 48-well plates. Treatment plans including SEV amount transferred can be found in **Appendix 8**.

3.16 Measurement of infection and cell death by flow cytometry

HPAF-II, 786-0 and 4T1 cells were infected with VSVΔ51-amiR-4 and treated with or without the GSK126 small molecule inhibitor (15 μM) following the treatment plan outlined in Appendix 5 before staining with polyclonal rabbit anti-VSV primary antibody (1:15000)[62] followed by anti-rabbit Alexa Fluor 647 secondary antibody (1:15000; Jackson ImmunoResearch). Stained cells were analyzed on the BD LSR Fortessa (Becton Dickinson [BD], Franklin Lakes, NJ) and data was analyzed using FlowJo v10 (FlowJo, LLC, Ashland, OR). FSC/SSC was used to identify cells and FSC-A/H was used to determine single cells. Gates for infected cells were set using an uninfected stained sample.

3.17 Extracellular vesicle isolation

EVs were collected using differential centrifugation of conditioned media. Cells were infected at MOI 5 with MRBΔG viruses in serum-free media. After 2 hours, media was changed for DMEM with exosome-depleted serum (Thermo Fisher Scientific) and the cells were incubated for 24 hours at 37 °C. Samples were first subjected to 2,000 x g (15 minutes) and 12,000 x g

(35 minutes) centrifugation steps (Thermo Scientific Sorvall ST 40R Centrifuge and Beckman Coulter Avanti J-E, respectively) to eliminate cells, cellular debris and large EVs. Small EVs were pelleted using ultracentrifugation (Beckman Coulter Optima L-100 XP Ultracentrifuge or Thermo Scientific Sorvall wX+ Ultra Series Centrifuge) at 120,000 x g for three hours and collected in 1X PBS. A schematics of the experimental layout can be found in **Figure 4.15**.

3.18 Nanoparticle tracking analysis

To determine size distribution and concentration of EV preparations, nanoparticle tracking analysis (NTA) was carried out using the ZetaView® (Particle Metrix). The instrument was calibrated with 102 nm beads (1:250 000 dilution). 11 camera positions were used with a frame rate of 30 at room temperature. EVs suspended in 1X PBS were diluted from 100 to 1000 fold. To ensure consistency in concentration readouts, measurements were performed using identical settings using the ZetaView 8.03.08 [0106] software. All particles were taken into account for the concentration count.

3.19 Cryo-electron microscopy

Electron microscopy (EM) grids were prepared with 3µl of purified EV preparation onto 200 mesh grids with 2 µm holes (Quantifoil R2/2, Quantifoil Micro Tools, GmbH, Germany). Grids were glow discharged for 30 seconds prior to applying the sample (Cressington, UK). Grids were plunge-frozen in liquid ethane cooled by liquid nitrogen using a FEI Vitrobot IV (FEI, The Netherlands) at 90% relative humidity, and a chamber temperature of 4 °C. Micrographs were imaged using the FEI Titan Krios EM (Astbury Biostructure Laboratory, University of Leeds) at 300 kV, using a total electron dose of 60 e-/Å^2 and a magnification of

75,000x. Micrographs were acquired using an energy filtered K2 Summit direct electron detector (Gatan, USA), with a final object sampling of 1.07 Å/pixel.

3.20 Immunofluorescence microscopy

SEVs derived from 786-0 cells infected with MRBΔG-amiR-4 were stained with CFSE (Invitrogen) at a final concentration of 15 μM for 10 minutes at 37 °C. Excess dye was removed from SEVs using the Exosome Spin Columns (MW 3000; Invitrogen). SEVs were then transferred onto naïve 786-0 cells grown on coverslips in a 6-well plate and incubated for 2 hours at 37 °C at a final concentration of 2.5E8 particles/mL of media. Cells were then washed 3 times with 1X PBS, fixed using 1% PFA for 5 minutes, washed 3 times with 1X PBS, stained using Hoechst 33342 nucleic acid stain (Invitrogen) for 10 minutes and washed 3 times with 1X PBS. Coverslips were then mounted on slides using Vectashield H-1000 (Vector Laboratories). Samples were imaged on the Axio imager.M1 microscope (Zeiss) with the AxioCam HRm camera (Zeiss).

3.21 RNA protection assay

To evaluate the presence of non-encapsulated RNA in the EV preparations, EVs were subjected to RNase treatment. EV preparations were treated with 1 unit of RNase A for 30 minutes at 37 °C. EV-encapsulated RNA was then extracted using TRIzol™ reagent (Invitrogen) and subjected to RT-qPCR. A sample containing extracted RNA from 786-0 cells was used as control following the same treatment and was resolved on a 1.2% agarose gel alongside an untreated sample to show RNase A activity.

3.22 Transwell assay

4T1 wild-type or Rab27a knockout cells were seeded in the upper compartment of a transwell cell culture insert with 0.4 μm pore diameter (Corning) and were infected with MRBΔG-amiR-4 at MOI 3 for 2 hours. The transwell cell culture inserts were then washed twice with 1X PBS and transferred to a plate containing naïve (uninfected) wild-type cells in the lower compartment. A schematics of the experimental layout can be found in **Figure 4.18a**. The plates were incubated at 37 °C for 48 hours and wild-type cells at the bottom of the transwell chamber were harvested in Trizol before being subjected to RNA extraction and RT-qPCR.

3.23 Animal studies

All animal studies complied with ethical regulations and were approved by the Institutional Animal Care Committee of the University of Ottawa and carried out in accordance with guidelines of the National Institutes of Health and the Canadian Council on Animal Care.

3.23.1 Biodistribution

To assess the biodistribution of VSVΔ51-amiR-4 and ensure no or minimal effect of the virus on normal tissues, C57BL/6 mice (Charles River Laboratories, Wilmington, MA) were injected IV with 1E8 PFU of VSVΔ51-amiR-4 or VSVΔ51-miR-NTC. Mice were sacrificed 48 hours post injection and key organs were harvested. Liver, kidney, lungs, ovary and brain were flash frozen, homogenized using the QIAGEN TissueLyser II and tittered on Vero cells.

3.23.2 Subcutaneous animal tumor model

HPAF-II cells (1E7 cells/tumor) were injected subcutaneously (SC) in nude CD-1 mice (Charles River Laboratories, Wilmington, MA). To compare viral titers of VSVΔ51-amiR-4 and VSVΔ51-amiR-NTC, 5E7 PFUs were injected intratumorally (IT) once tumors reached ~100 mm^3. Equivalent volume of 1X PBS was injected in control mice. After 48 hours, mice were sacrificed and tumors were collected, flash frozen and titered. To compare the efficacy of VSVΔ51-amiR-4 and VSVΔ51 to control tumor growth, 5E7 PFUs were injected IT on days 29–31 and 36–38. To assess the synthetic lethal effect induced by amiR-4 and GSK126, ~100 mm^3 tumors were injected with VSVΔ51-amiR-4 or VSVΔ51 on days 20–22 and 27–29. GSK126 (50 mg/kg) or the equivalent volume of Captisol 20% (vehicle control; Ligand Pharmaceuticals, Inc) was injected intraperitoneally (IP) for 10 consecutive days starting on day 21. Tumor size was measured three times a week using calipers (Fowler, Newton, MA) and tumor volume was calculated using a modified ellipsoidal formula; tumor volume = 1/2 (length × $width^2$)[164].

3.23.3 Orthotopic animal tumor model

TH04 mouse pancreatic cancer cells (1E4) were injected in the tail of the pancreas of immune competent C57BL/6 mice (Charles River Laboratories, Wilmington, MA) to assess the survival advantage of VSVΔ51-amiR-4 compared to VSVΔ51-amiR-NTC. 3E8 PFUs of the viruses or equivalent volume of 1X PBS was injected IP on days 5–7 and 12–14.

3.23.4 Intraperitoneal animal tumor model

B16-F10 cells (2E5 cells/animal) were injected IP in C57BL/6 mice (Charles River Laboratories, Wilmington, MA). To compare the survival rates of mice treated with VSVΔ51-

amiR-4 and VSVΔ51, 3E8 PFUs were injected IP on days 5–7 and 12–14. Equivalent volume of 1X PBS was injected in control mice. To assess the synthetic lethal effect induced by amiR-4 and GSK126, mice were then injected with GSK126 (50 mg/kg) or the equivalent volume of Captisol 20% (vehicle control) IP for 10 consecutive days starting on day 6.

3.24 Statistical analysis and reproducibility

All *in vitro* experiments were repeated at least twice unless otherwise stated. Mouse studies were performed once unless otherwise stated in the figure legend. All measurements were taken from distinct biological replicate samples. Animal cohorts were randomized following tumor implantation before initiation of treatment plan. In the animal experiments, outliers were excluded of sample analysis if the tumor of an animal within a given group differed by 2 standard deviations or more. When sample size was less than 3, no statistical analyses were performed. Statistical analyses were performed using GraphPad Prism 6 and 7 (GraphPad). Quantitative data is reported as mean ± s.e.m or s.d. as indicated in the figure legends. Statistical analysis was performed on raw data by Student's t test to compare two independent conditions, one-way ANOVA to compare three conditions or more, two-way ANOVA with Tukey's or Sidak's correction to compare groups influenced by two variables and the Kaplan-Meier method followed by log rank test for survival analysis. All tests were two-sided. The statistical significance of all *p*-values are: $*p < 0.05$, $**p < 0.01$, $***p < 0.001$ and $****p < 0.0001$. Differences between experimental groups were considered significant at $p < 0.05$. Exact *p*-values are provided in the text whenever suitable.

4. RESULTS

4.1 Selection of an artificial microRNA that enhances oncolytic virus anticancer potency

In order to discover novel amiRNAs with the ability to enhance oncolytic virus replication and cytotoxicity within pancreatic cancer cells without bias, a replicating SV library encoding some 16,000 unique amiRNAs was used (**Figure 4.1**). Although SV is not our oncolytic virus platform of choice, the SV library is a useful tool to identify sequences that enhance the replication of oncolytic viruses with RNA genomes since it can be engineered in a high throughput fashion to generate a high number of individual viruses each encoding an individual amiRNA. The SV library was passaged in a panel of human (MIA PaCa-2) and mouse (Panc02) cancer cell lines, human pancreatic CAFs (PCa-CAF) and normal human skin fibroblast cultures (GM38). After the fourth passage, Next-generation sequencing (NGS) analysis was carried out to compare the passaged viral output to the input, unpassaged library. NGS analysis identified a selection of five amiRNA candidates encoded by SV that led to a substantial fold enrichment following passaging versus the input library across all cell lines tested (**Figure 4.2 and Table 3.1**). These top five candidates are herein arbitrarily named amiR1-5. From the RNA sequencing analysis, we can hypothesize that amiR-4 is the most viable candidate, since it does not enhance the replication of SV in normal cells (GM38), but does confer a replication advantage in pancreatic cancer cells (MIA PaCa-2 and Panc02). Although the SV library can provide us with potential amiRNA candidates that enhance oncolytic SV replication within pancreatic cancer cells, the validity needs to be assessed and confirmed in VSVΔ51 since these two viruses possess a few differences in their life cycles since they have RNA genomes with different polarities. Indeed, SV and VSV are both viruses

Figure 4.1 Schematic flowchart of the Sindbis virus-based artificial microRNA library screen for the selection of pro-viral amiRNAs under pancreatic cancer cell selection. The SV-amiRNA library was serially passaged four times in pancreatic cancer cells to enrich for pro-viral and anti-cancer amiRNA sequences. To identify enriched amiRNA sequences, viral output was sequenced using pre-miR-30-specific primers (see amiR design in Figure 4.3). Identified sequences were then cloned in select oncolytic rhabdoviruses for further characterization and validation.

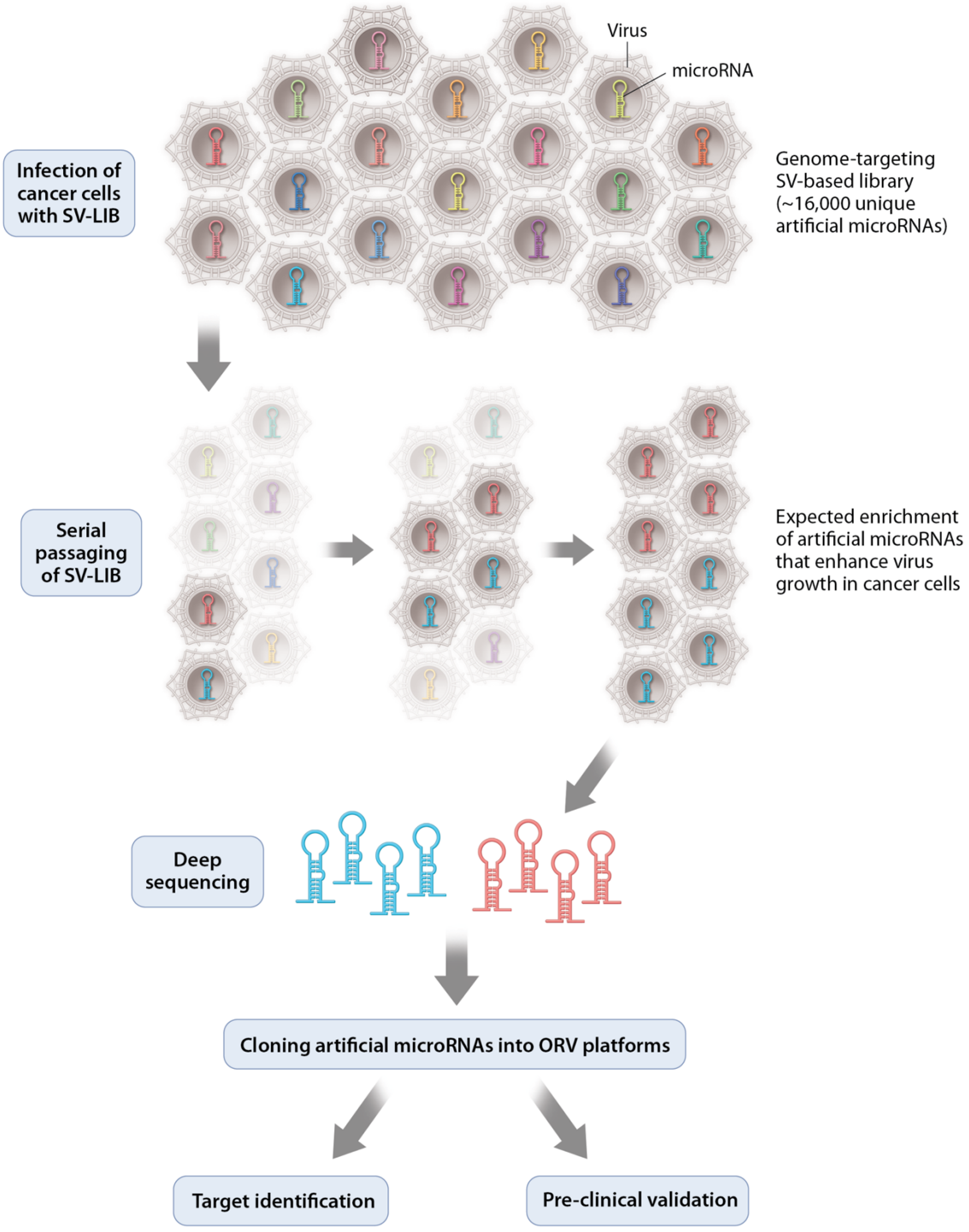
Virus
microRNA
Infection of cancer cells with SV-LIB
Genome-targeting SV-based library (~16,000 unique artificial microRNAs)
Serial passaging of SV-LIB
Expected enrichment of artificial microRNAs that enhance virus growth in cancer cells
Deep sequencing
Cloning artificial microRNAs into ORV platforms
Target identification
Pre-clinical validation

Figure 4.2 Screening of the Sindbis virus-based artificial microRNA library identifies five artificial microRNA sequences of interest. Fold increase in deep sequencing amiRNA hits of the top five most enriched amiRNAs compared to the library in GM38 (human untransformed skin fibroblasts), patient fibroblasts (human CAF-like cells), MIA PaCa-2 (human pancreatic cancer cells) and Panc02 cells (mouse pancreatic cancer cells). n=5 per condition. ND = not detected. Analysis performed by Dr. Carolina Ilkow.

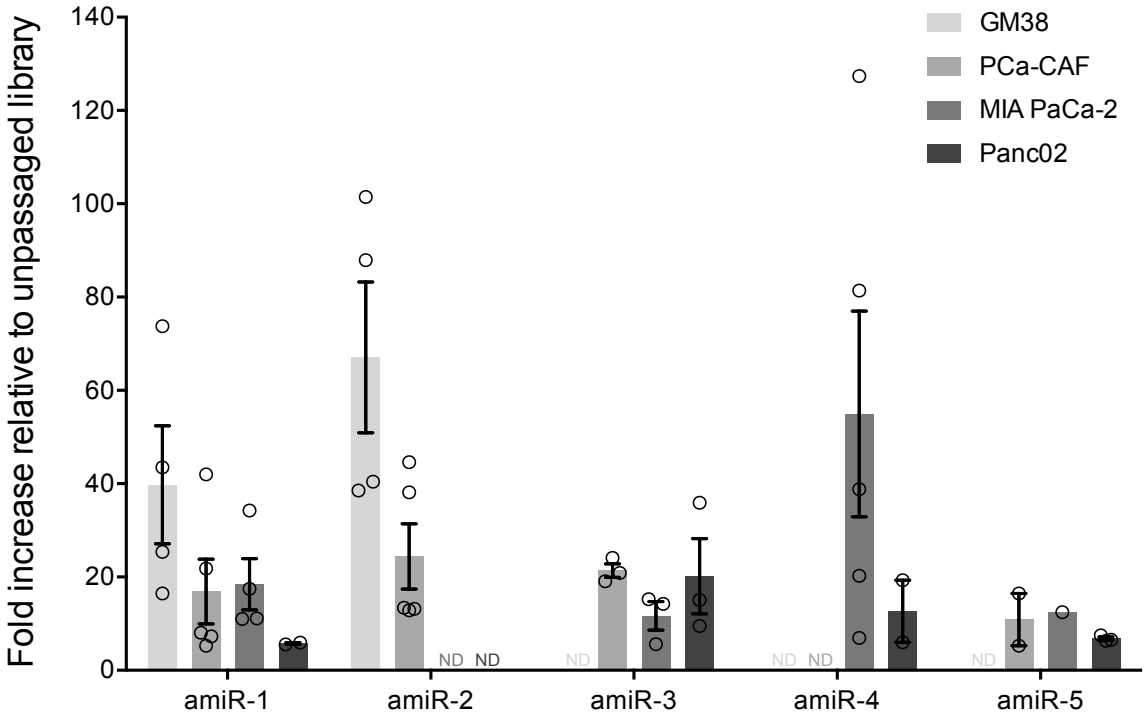
Fold increase relative to unpassaged library
140
120
100
80
60
40
20
0
GM38
PCa-CAF
MIA PaCa-2
Panc02
ND ND
ND
ND ND
ND
amiR-1
amiR-2
amiR-3
amiR-4
amiR-5

with single-stranded RNA (ssRNA) genomes, but the former has a positive sense RNA genome whereas the latter has a negative sense RNA genome.

4.2 Oncolytic rhabdovirus platforms can express artificial microRNAs

To test the ability of these amiRNAs to enhance the replication and oncolysis of the clinically staged oncolytic VSVΔ51[86] and MRB[79] rhabdovirus platforms, the top five selected amiRNAs from the SV library screen were cloned into these platforms (**Figure 4.3**). As predicted and previously shown[165], the insertion of these artificial miRNA sequences did not hinder the rescue or replication ability of these viruses (results not shown). In order to confirm the expression of the amiRNAs from the VSVΔ51 platform, the sense amiRNA strand expression following infection of cancer cells was confirmed by RT-qPCR using primers for the mature amiRNA (**Appendix 1**).

4.3 Selection of amiR-4 as a pro-viral and anti-cancer artificial microRNA

The ability of these amiRNA-expressing viruses to enhance OV-induced cell death and replication was assessed in a panel of cancer cell lines and PDX tumor cores. Assessment of cell viability revealed that among the five selected amiRNAs, amiR-4 induced significantly greater cell death compared to control virus in 786-0, BxPC-3 and HPAF-II tumor cell lines that were otherwise highly resistant to VSVΔ51-mediated killing (**Figure 4.4a**). Furthermore, an increase in virus replication in *ex vivo* PC PDX tumor-derived cores was evident following VSVΔ51-amiR-4 infection compared to a control VSVΔ51 virus expressing a non-targeting control amiRNA (VSVΔ51-amiR-NTC) (**Figure 4.4b)**. Importantly, expression of amiR-4 did not lead to significant enhanced killing by VSVΔ51 in healthy GM38 fibroblasts compared to

Figure 4.3 Schematic of the VSVΔ51 and MRBΔG genomes encoding amiRNA sequences built in the pre-miR-30 backbone. Pre-miR-30 sequences containing the amiRNAs of choice were inserted between the VSVΔ51 G and L genes or the MRBΔG M and L genes.

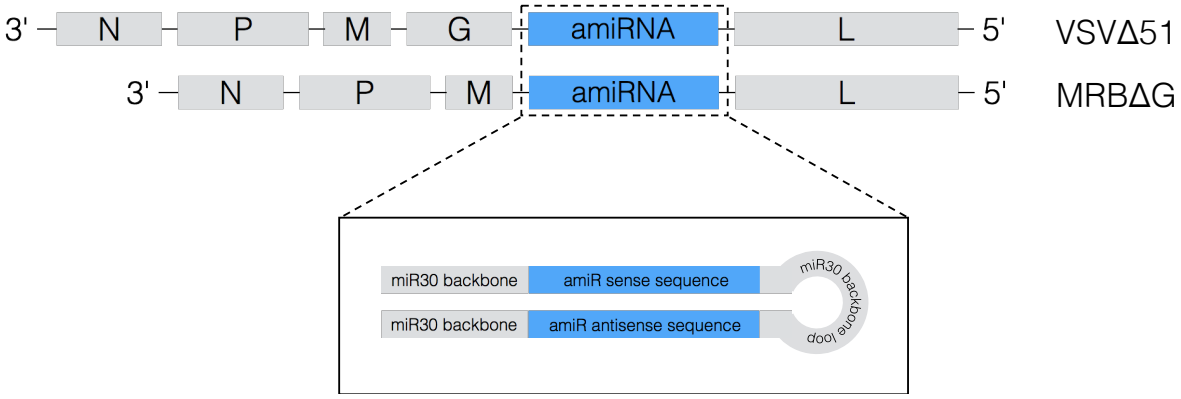
3'
N
P
M
G
amiRNA
L
5'
VSVΔ51
3'
N
P
M
amiRNA
L
5'
MRBΔG
miR30 backbone
amiR sense sequence
miR30 backbone
amiR antisense sequence
loop
miR30 backbone

Figure 4.4 Screening of the Sindbis virus-based artificial microRNA library identifies artificial miRNA-4 as an anti-cancer and pro-oncolytic virus amiRNA sequence. (**a**) Relative percentage of cell viability of 786-0, BxPC-3 and HPAF-II cells infected for 48 hours (786-0 and BxPC-3) or 72 hours (HPAF-II) with indicated amiRNA-expressing viruses at MOI 1, 5 and 3, respectively, compared to uninfected cells. Differences between amiRNA-expressing viruses and control virus were assessed by two-way ANOVA with Dunnett's multiple comparisons test, ** $p < 0.01$, **** $p < 0.0001$. Data represents mean ± s.e.m of five independent biological replicates. (**b**) Relative fold change in titers of amiRNA-expressing VSVΔ51 viruses compared to VSVΔ51-amiR-NTC following *ex vivo* infection of 8 mm^3 patient-derived tumor cores. Ordinary one-way ANOVA with Dunnett's multiple comparisons test, * $p < 0.05$, *** $p < 0.001$. Data represents mean ± s.e.m of three independent biological replicates. Experiments performed by Dr. Carolina Ilkow.

a

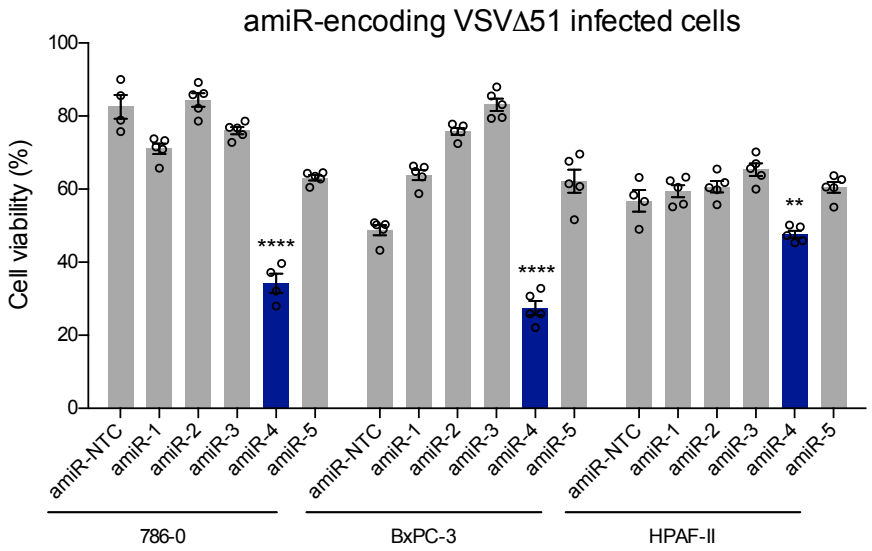
amiR-encoding VSVΔ51 infected cells
Cell viability (%)
100
80
60
40
20
0
****
****
**
amiR-NTC
amiR-1
amiR-2
amiR-3
amiR-4
amiR-5
786-0
BxPC-3
HPAF-II

b

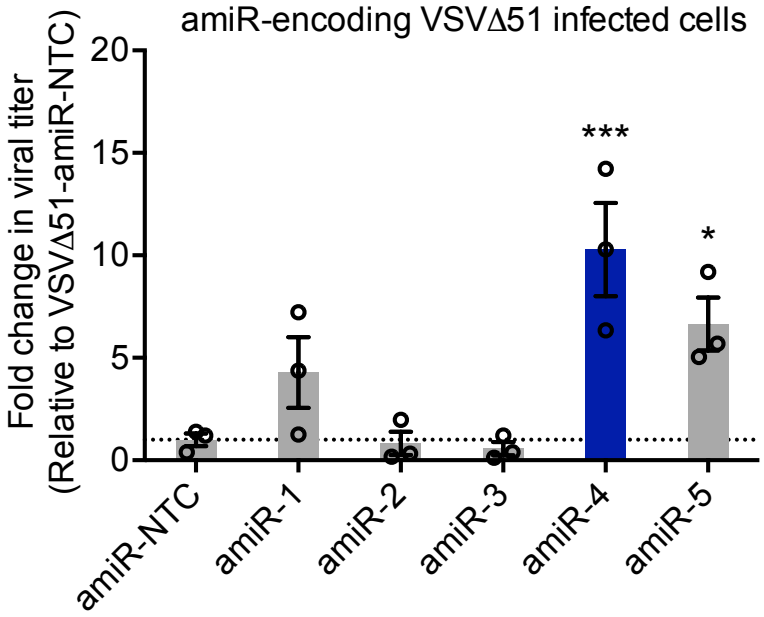
amiR-encoding VSVΔ51 infected cells
Fold change in viral titer
(Relative to VSVΔ51-amiR-NTC)
20
15
10
5
0
***
*
amiR-NTC
amiR-1
amiR-2
amiR-3
amiR-4
amiR-5

virus control 72 hours post-infection (hpi) and does not compromise viral biodistribution in a tumor-free mouse model (**Figure 4.5**). Indeed, we did not observe a significant increase in viral titers in organs of mice treated with VSVΔ51-amiR-4 compared to their VSVΔ51 ctrl-treated counterparts, indicating that amiR-4 does not enhance VSVΔ51 replication and cytotoxicity in normal tissues. Moreover, mice treated with VSVΔ51-amiR-4 did not show any signs of major weight loss or mobility and respiratory issues and were considered healthy according to the National Institutes of Health standards[166] (results and observations not shown).

4.4 amiR-4 enhances the oncolytic capacity of VSVΔ51

amiR-4 was found to significantly enhance virus-induced cytotoxicity *in vitro* in a panel of tumor cell lines (**Figure 4.6a**). In addition to enhancing OV activity in pancreatic cancer cell lines, VSVΔ51-encoded amiR-4 was found to be beneficial in human renal carcinoma (786-0), mouse breast cancer (4T1) and mouse melanoma (B16-F10) cell lines. To determine whether this enhanced oncolytic activity was also observed *in vivo*, immunocompromised mice bearing human pancreatic HPAF-II SC tumors were treated with either VSVΔ51-amiR-NTC or VSVΔ51-amiR-4. Tumors were collected 48 hpi and plaque assays were performed to quantify intratumoral virus replication. Although modest, a significant increase (p-value = 0.014) in viral output was observed in tumors treated with VSVΔ51-amiR-4 compared to VSVΔ51-amiR-NTC control. This enhanced viral production indicates that the expression of amiR-4 within tumors enhances tumor-associated viral replication *in vivo* (**Figure 4.6b**). To determine whether this enhanced replication resulted in tumor debulking and shrinkage, immunocompromised animals bearing HPAF-II SC tumors were treated with vehicle control

Figure 4.5 Functional expression of amiR-4 from a VSVΔ51 oncolytic rhabdovirus platform is safe in normal cells compared to a VSVΔ51 control virus. (**a**) GM38 cells were infected with VSVΔ51-amiR-NTC (control) or VSVΔ51-amiR-1-5 at MOI 1. Cell viability was measured using the alamarBlue® Assay at indicated time points and compared to virus control. Two-way ANOVA with Tukey's multiple comparison test; * $p < 0.05$, ** $p < 0.01$, *** $p < 0.001$. Error bars represent s.e.m. for 5 biological replicates per condition. Experiment performed by Dr. Carolina Ilkow. (**b**) Quantification of VSVΔ51-amiR-NTC or VSVΔ51-amiR-4 infectious particles from different organs obtained from mice IV-treated with the indicated viruses (1E8 pfu/mice) for 48 hours. Data represents mean + s.e.m. of 7 and 8 independent biological replicates for VSVΔ51-amiR-NTC and VSVΔ51-amiR-4, respectively. Two-way ANOVA with Sidak's multiple comparisons test; ns $p > 0.05$, **** $p < 0.0001$. ND = not detected.

a

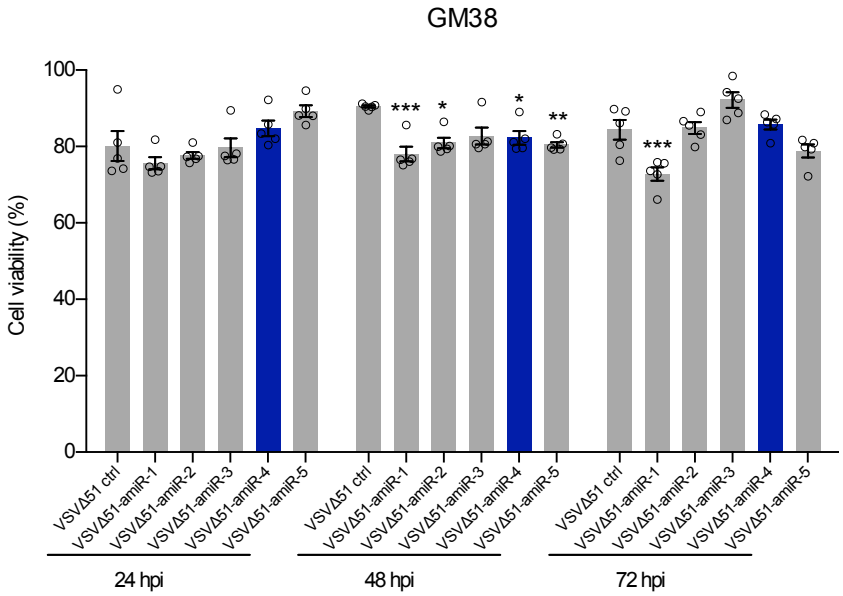
GM38
Cell viability (%)
100
80
60
40
20
0
VSVΔ51 ctrl
VSVΔ51-amiR-1
VSVΔ51-amiR-2
VSVΔ51-amiR-3
VSVΔ51-amiR-4
VSVΔ51-amiR-5
24 hpi
48 hpi
72 hpi

b

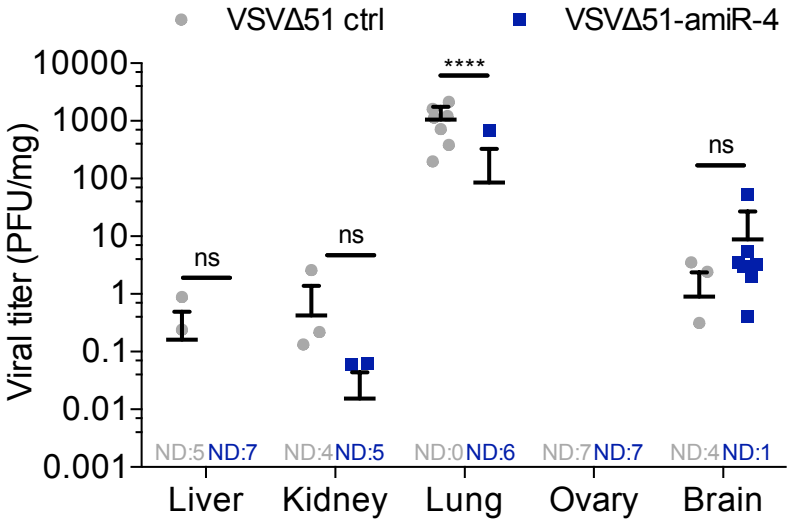
VSVΔ51 ctrl
VSVΔ51-amiR-4
Viral titer (PFU/mg)
10000
1000
100
10
1
0.1
0.01
0.001
ns
ns
****
ns
ND:5 ND:7
ND:4 ND:5
ND:0 ND:6
ND:7 ND:7
ND:4 ND:1
Liver
Kidney
Lung
Ovary
Brain

Figure 4.6 amiR-4 enhances viral replication *in vitro* and *in vivo*. (**a**) Cell viability of indicated cell lines after VSVΔ51-amiR-NTC or VSVΔ51-amiR-4 infection (MOI 0.1; 48 hours) compared to mock-infected cells was measured using the alamarBlue® Assay. Data indicates mean ± s.e.m. of five biological replicates. Two-way ANOVA with Sidak's multiple comparisons test. ns $p > 0.05$, ** $p < 0.01$, *** $p < 0.001$, **** $p < 0.0001$. Experiment performed in collaboration with Dr. Carolina Ilkow. (**b**) A single dose of VSVΔ51 expressing amiR-NTC or amiR-4 was delivered IT into HPAF-II SC tumours. After 48 hours, virus titers were quantified. Unpaired two-tailed t-test, $p = 0.014$. Data represent ± s.e.m (n =10 per group; data of two pooled independent experiments). (**c**) Six doses of PBS, VSVΔ51-amiR-NTC or VSVΔ51-amiR-4 were delivered IT into mice bearing HPAF-II SC tumours. Two-way ANOVA with Tukey's multiple comparison test (VSVΔ51-amiR-4 compared to VSVΔ51-amiR-NTC), * $p < 0.05$. Mean tumour volume ± s.e.m is shown (n=5 per group). (**d**) Kaplan-Meier survival analysis of orthotopic TH04 tumour-bearing mice (n=5 per group) treated with six IP doses of PBS, VSVΔ51-amiR-NTC or VSVΔ51-amiR-4. Log-rank (Mantel-Cox) test, ** $p < 0.01$.

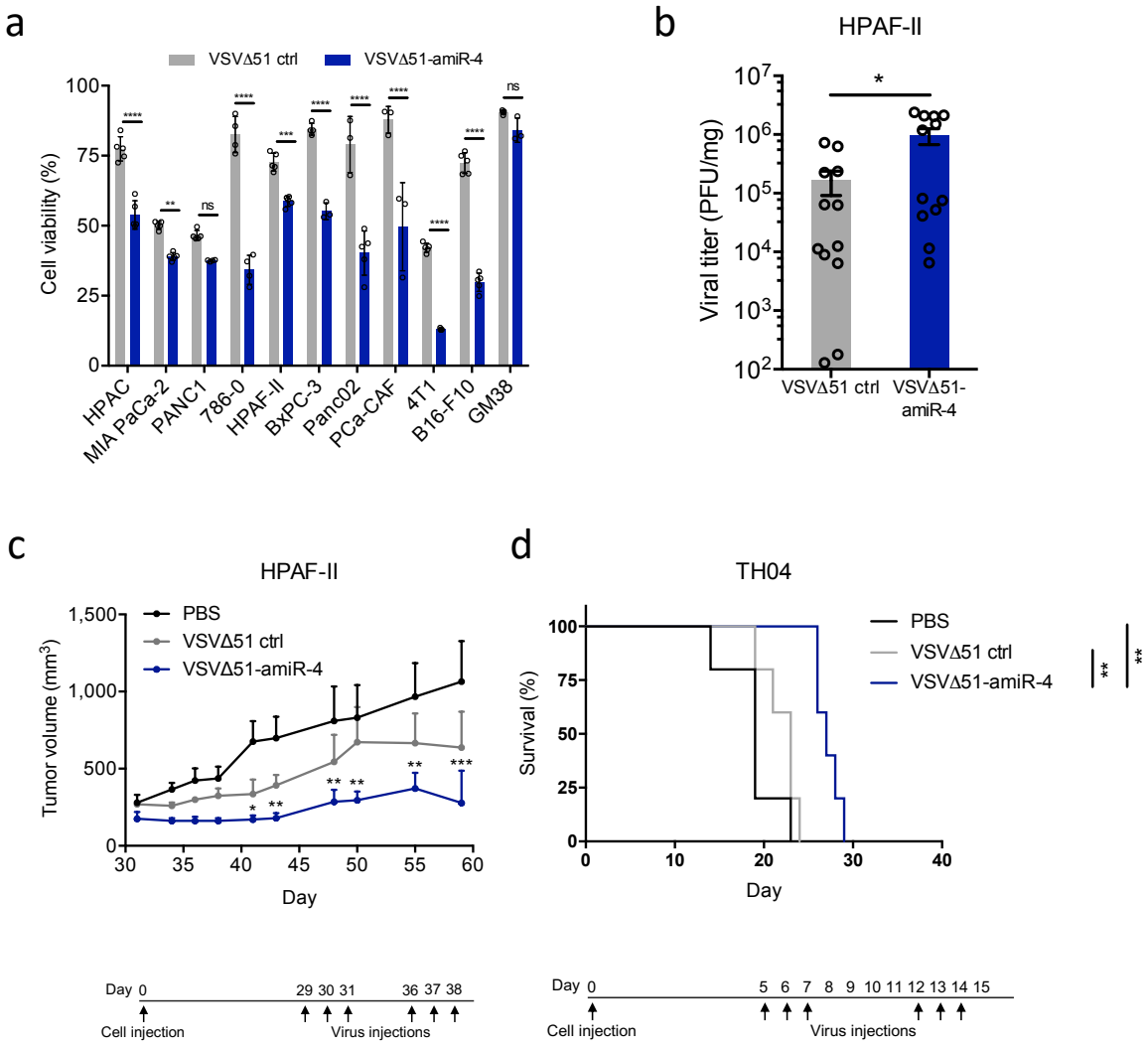
a
VSVΔ51 ctrl
VSVΔ51-amiR-4
Cell viability (%)
HPAC
MIA PaCa-2
PANC1
786-0
HPAF-II
BxPC-3
Panc02
PCa-CAF
4T1
B16-F10
GM38
b
HPAF-II
Viral titer (PFU/mg)
VSVΔ51 ctrl
VSVΔ51-amiR-4
c
HPAF-II
PBS
VSVΔ51 ctrl
VSVΔ51-amiR-4
Tumor volume (mm3)
Day
Day 0
29 30 31
36 37 38
Cell injection
Virus injections
d
TH04
PBS
VSVΔ51 ctrl
VSVΔ51-amiR-4
Survival (%)
Day
Day 0
5 6 7 8 9 10 11 12 13 14 15
Cell injection
Virus injections

(PBS), VSVΔ51 control or VSVΔ51-amiR-4. VSVΔ51-amiR-4 enhanced tumor control compared to treatment control (**Figure 4.6c**) in SC HPAF-II tumors. Survival in immune-competent mice bearing syngeneic orthotopic TH04 pancreatic tumors upon VSVΔ51-amiR-4 treatment was also assessed. While this tumor model is typically extremely aggressive and resistant to immunovirotherapy, a significant increase in survival was evident in animals treated with VSVΔ51-amiR-4 compared to vehicle control (*p*-value = 0.0020) or VSVΔ51 control-treated mice (*p*-value =0.0021) (**Figure 4.6d**). These results thus confirm the replication advantage conferred by the insertion of an amiRNA in VSVΔ51.

4.5 amiR-4 targets cellular factors involved in epigenetic regulation and cytoskeleton stability

In order to find out the cellular targets of amiR-4 involved in OV resistance, bioinformatical prediction tools were put to use. Computational miRNA target prediction pipelines (TargetScanHuman and BLAST) were used to determine potential cellular gene products targeted by amiR-4 based on total energy of duplex or sequence complementarity (**Table 4.1**). Interestingly, all the predicted targets perform epigenetic regulation [AT-Rich Interaction Domain 1A (ARID1A), Minichromosome Maintenance Complex Component 2 (MCM2), histone deacetylase 4 (HDAC-4)] or cytoskeleton stability functions [Plectin (PLEC)]. We then directly tested the ability of VSVΔ51-amiR-4 to selectively reduce the expression of each candidate gene product at both the mRNA and protein levels. We found that the gene products encoded by *ARID1A*, *PLEC* and *HDAC4* but not *MCM2* were specifically decreased following infection with VSVΔ51-amiR-4 as shown by RT-qPCR and immunoblotting analysis (**Figure 4.7**). Our results thus suggest that amiR-4 might potentiate OV-growth and cancer cell

Table 4.1 List of potential amiR-4 targets based on total energy of duplex as predicted by TargetS or on BLAST complementarity

Gene symbol	Gene name	Duplex Free Energy	Number of Complementary Bases	Range	Expect Value	Pos/Neg Strand
ARID1A	AT rich interaction domain 1A (SWI-like)	-77.1698	N/A			
PLEC	Plectin	-74.52005	N/A			
MCM2	Minichromosome maintenance complex component 2	-70.41588	N/A			
HDAC4	Histone deacetylase 4	N/A	16	2-17	5.0	Minus

Predictions done by Dr. Gibbings group at the University of Ottawa

Figure 4.7 Validation of predicted amiR-4 targets. (**a**) Fold change in expression of amiR-4 target genes determined by RT-qPCR in MIA PaCa-2 cells infected for 36 hours with VSVΔ51-amiR-NTC or VSVΔ51-amiR-4 (MOI 1) compared to virus control and normalized to loading control (Rplp0). Unpaired t-test, * $p < 0.05$, **** $p < 0.0001$, error bars show ± s.e.m of five biological replicates. (**b**) Immunoblot analysis showing protein expression levels of amiR-4 predicted targets, GAPDH (loading control), and VSVΔ51 proteins in PANC1 cells subjected or not to VSVΔ51-amiR-NTC or VSVΔ51-amiR-4 infection for 48 hours (MOI 0.1). Experiments performed by Elaine Rose and Dr. Carolina Ilkow.

a

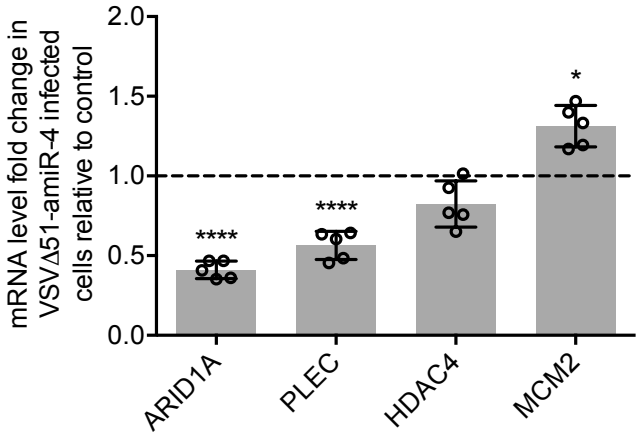
mRNA level fold change in VSVΔ51-amiR-4 infected cells relative to control
2.0
1.5
1.0
0.5
0.0
****
****
*
ARID1A
PLEC
HDAC4
MCM2

b

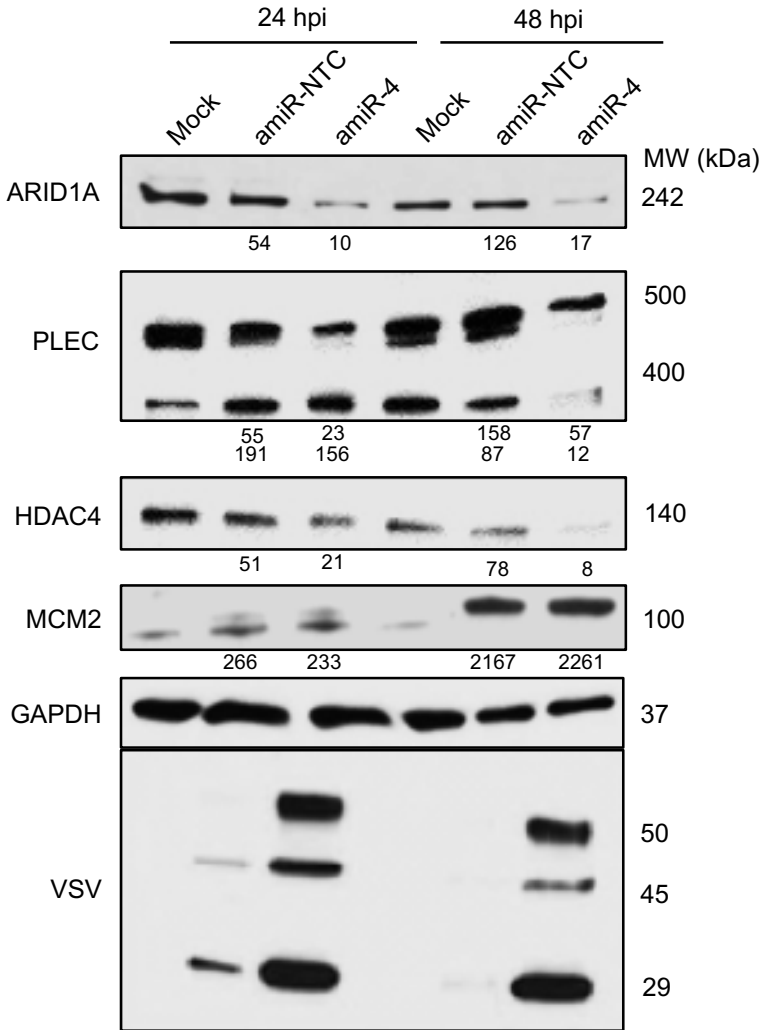
24 hpi
48 hpi
Mock
amiR-NTC
amiR-4
Mock
amiR-NTC
amiR-4
MW (kDa)
ARID1A
242
54
10
126
17
PLEC
500
400
55
191
23
156
158
87
57
12
HDAC4
140
51
21
78
8
MCM2
100
266
233
2167
2261
GAPDH
37
VSV
50
45
29

cytotoxicity via the downregulation of *ARID1A, HDAC4* and *PLEC*. The observation that decreased expression of the *PLEC* gene enhanced virus replication is consistent with earlier studies demonstrating that manipulation of cytoskeletal components enhance VSVΔ51 replication and oncolysis in various tumor models[95,96]. Similarly, multiple reports have previously demonstrated that the inhibition of histone deacetylases boosts the replication of various OV platforms[167–169]. On the other hand, the protein encoded by *ARID1A*, a subunit of the SWI/SNF chromatin remodeling complex which facilitates the access of transcription factors to DNA, was not previously known to hinder OV replication.

4.6 ARID1A plays a role in resistance to oncolytic virus infection

In order to explore the implication of ARID1A in viral resistance, we generated ARID1A CRISPR knockout cell lines. Using *ARID1A* CRISPR knockout 786-0 and PANC1 cancer cells (**Appendix 2**), we demonstrated that *ARID1A*-knockout cells are significantly more sensitive than their parental counterparts to VSVΔ51 infection (p-value < 0.01 at MOI 0.01 and 1; p-value < 0.0001 at MOI 0.1 and 1) (**Figure 4.8a**). Moreover, the benefit of encoding amiR-4 in VSVΔ51 was drastically lost in ARID1A knockout cells, suggesting that ARID1A may be the predominant target of amiR-4 (**Figure 4.8b**). Interestingly, *ARID1A*-knockout cells also display greater susceptibility to other clinically staged OV platforms including VV TK^- VGF^- and oHSV-1 (**Figure 4.8c,d**). We also observed a replicative advantage of VSVΔ51-amiR-4 in *ARID1A*-expressing pancreatic cancer patient-derived samples using our unique biobank of pancreatic cancer patient-derived xenografts (**Figure 4.9**). Most of our PC PDXs express ARID1A, as detected by IHC (**Figure 4.9a**), which is consistent with the literature. Indeed, it is estimated that around 85% of PCs are ARID1A wild-type[21,170,171]. Interestingly, the

Figure 4.8 ARID1A deficient cells are more susceptible to oncolytic virus infection. Representative crystal violet staining pictures and cell viability measured by alamarBlue® Assay of 786-0 WT or ARID1A-KO (ARID1A$^{-/-}$) cells mock-infected or infected at multiple MOIs after 48 hours with VSVΔ51-GFP, VSVΔ51-amiR-4, VV TK^{-} VGF^{-} or oHSV-1 GFP. Crystal violet staining pictures represent cells mock-infected or infected with VSVΔ51-GFP at MOI 1 (**a**), VSVΔ51-amiR-4 at MOI 1 (**b**), VV TK^{-} VGF^{-} at MOI 1 (**c**) or oHSV-1 GFP at MOI 0.1 (**d**) 48 hpi. Two-way ANOVA Tukey's multiple comparison test, ns $p > 0.05$, ** $p < 0.01$, *** $p < 0.001$, **** $p < 0.0001$. Error bars are ± s.e.m of biological triplicate samples.

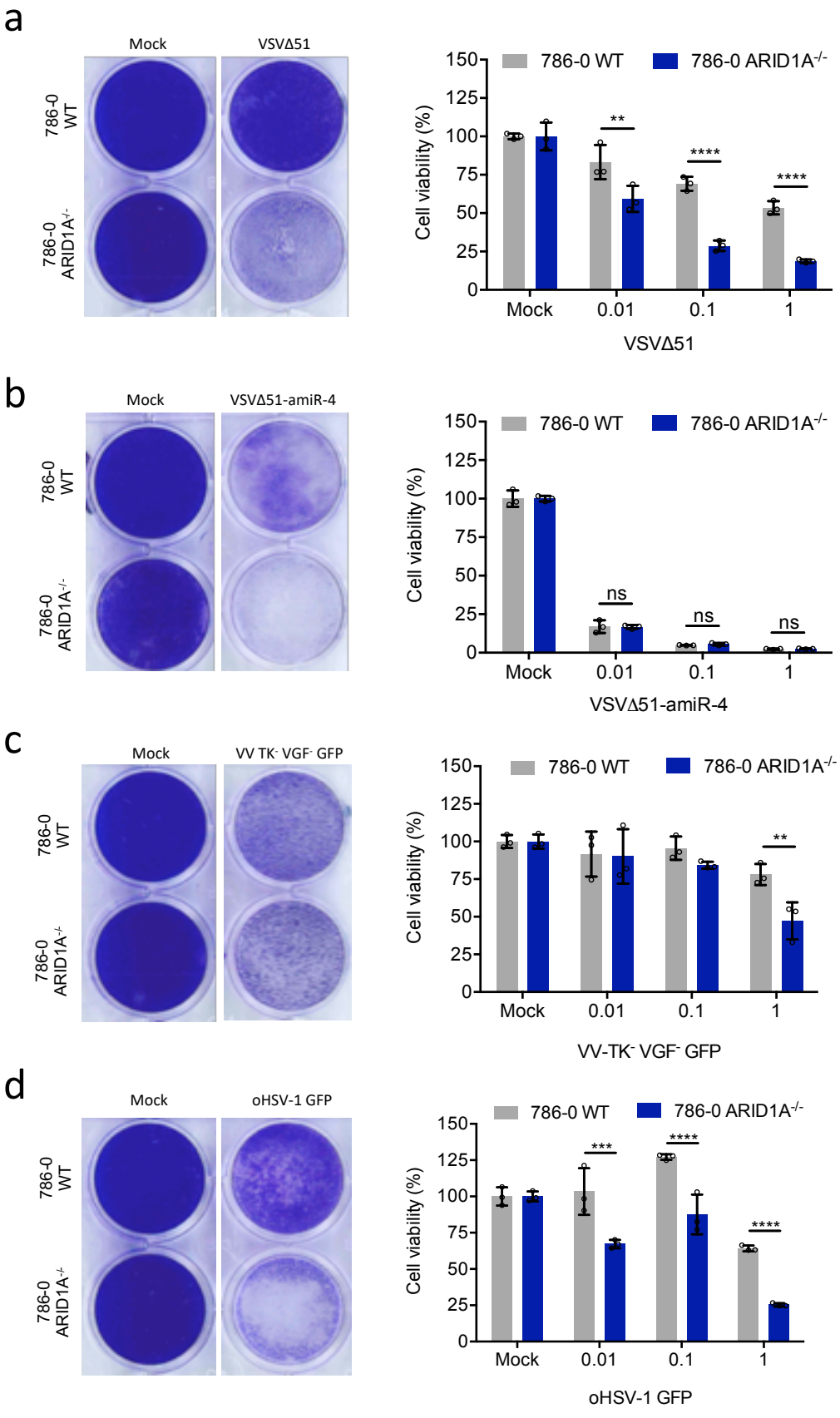
a
Mock
VSVΔ51
786-0 WT
786-0 ARID1A-/-
786-0 WT
786-0 ARID1A-/-
Cell viability (%)
150
125
100
75
50
25
0
**
****
****
Mock
0.01
0.1
1
VSVΔ51
b
Mock
VSVΔ51-amiR-4
786-0 WT
786-0 ARID1A-/-
786-0 WT
786-0 ARID1A-/-
Cell viability (%)
ns
ns
ns
VSVΔ51-amiR-4
c
Mock
VV TK- VGF- GFP
786-0 WT
786-0 ARID1A-/-
786-0 WT
786-0 ARID1A-/-
Cell viability (%)
**
VV-TK- VGF- GFP
d
Mock
oHSV-1 GFP
786-0 WT
786-0 ARID1A-/-
786-0 WT
786-0 ARID1A-/-
Cell viability (%)
***
****
****
oHSV-1 GFP

Figure 4.9 An amiR-4-expressing virus has a replicative advantage in patient samples displaying high levels of ARID1A. (**a**) Immunohistochemistry staining of ARID1A protein expression in representative pancreatic cancer patient-derived xenografts (PDX). Scale bar = 100 μm. (**b**) Viral titers of *ex vivo* infected tumour cores obtained from several pancreatic cancer patient-derived xenografts. Tumour cores were infected with 1E5 PFU of VSVΔ51-amiR-NTC or VSVΔ51-amiR-4 for 48 hours and then samples were processed to quantify infectious viral particles by plaque assay. Two-tailed unpaired t test of individual patient plots, ns $p > 0.05$, * $p < 0.05$, ** $p < 0.01$, *** $p < 0.001$, **** $p < 0.0001$. Experiments performed in collaboration with Christiano Tanese de Souza and Brian Laight.

a

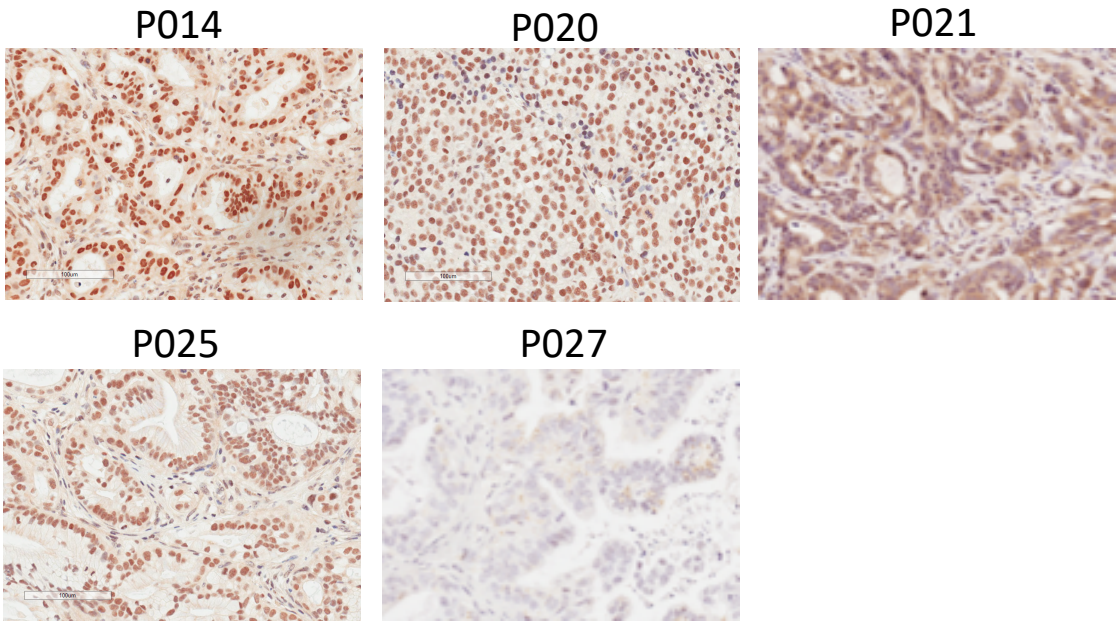
P014
P020
P021
P025
P027

b

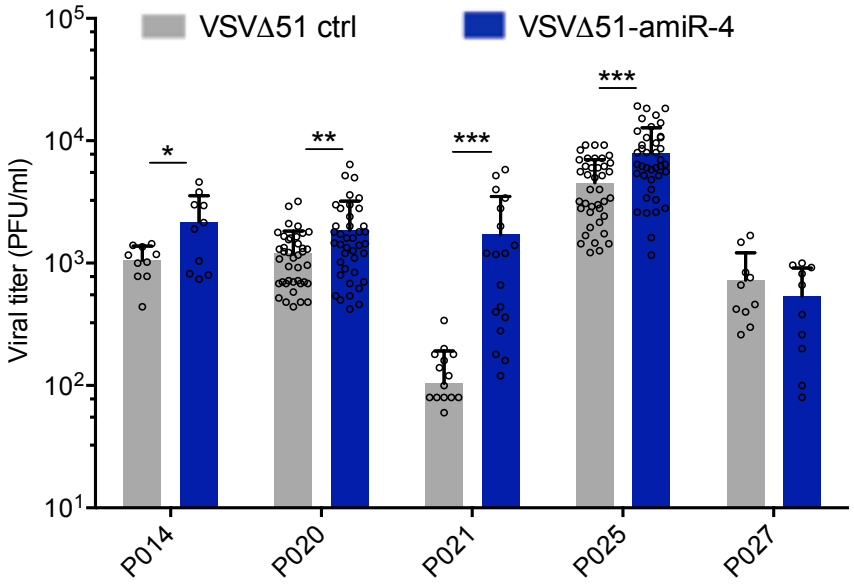
VSVΔ51 ctrl
VSVΔ51-amiR-4
Viral titer (PFU/ml)
10^5
10^4
10^3
10^2
10^1
*
**
***
***
P014
P020
P021
P025
P027

replication advantage is not conferred to VSVΔ51 in a PDX sample with very low ARID1A staining (P027). Altogether, these results suggest that ARID1A possesses antiviral effects and that targeting this gene in cancer cells has the potential to enhance OV replication and subsequent oncolysis. To ascertain the molecular changes in gene expression of *ARID1A*-knockout cells that could lead to virus sensitization, we conducted RNA-sequencing (RNA-seq) analysis. Gene-Ontology (GO) term analysis of these genes in PANC1 WT and ARID1A KO revealed that some primary processes repressed in *ARID1A*-deficient cells are related to type I and II IFN signaling circuits (**Figure 4.10a**). This was confirmed with the transcript expression levels of a few different anti-viral genes (**Figure 4.10b**). A selection of these repressed genes was validated using RT-qPCR (**Appendix 3**). Together, these data indicate that an *ARID1A* wild-type status is associated with resistance to OV therapy and supports the use of an OV encoding amiR-4 to repress residual antiviral responses in cancer cells, thus increasing tumor sensitivity to OV infection for enhanced OV-mediated cell death.

4.7 Combining an amiR-4-expressing oncolytic virus with an EZH2 small molecule inhibitor is beneficial in multiple models

In addition to its novel antiviral role, *ARID1A* represents a particularly interesting amiR-4 target as it has also been demonstrated that ARID1A depletion sensitizes ovarian cancer cells to EZH2 methyltransferase inhibition with the small molecule GSK126 in a synthetic lethal fashion[172]. Here, we hypothesized that an amiR-4-expressing OV could be combined with systemically administered GSK126 to potentiate tumor killing. In fact, combining an amiR-4-expressing virus at very low multiplicities of infection (MOI) with GSK126 drastically and significantly increases cell death *in vitro* in several cancer cell lines in treatment plans spanning

Figure 4.10 ARID1A KO cells display dysregulated antiviral pathways. (**a**) GO-term analysis of biological processes differentially expressed between PANC1 WT and ARID1A-KO cells. Illustrated GO-terms represent all significantly different biological processes (Fisher's exact test) after correction for multiple hypothesis testing (FDR). (**b**) Heatmap showing transcript expression levels (Log2 TPM) of anti-viral genes in uninfected PANC1 wild-type or ARID1A-knockout cells. Experiment performed by Dr. Larissa Pikor and analysis performed by Adrian Pelin.

a

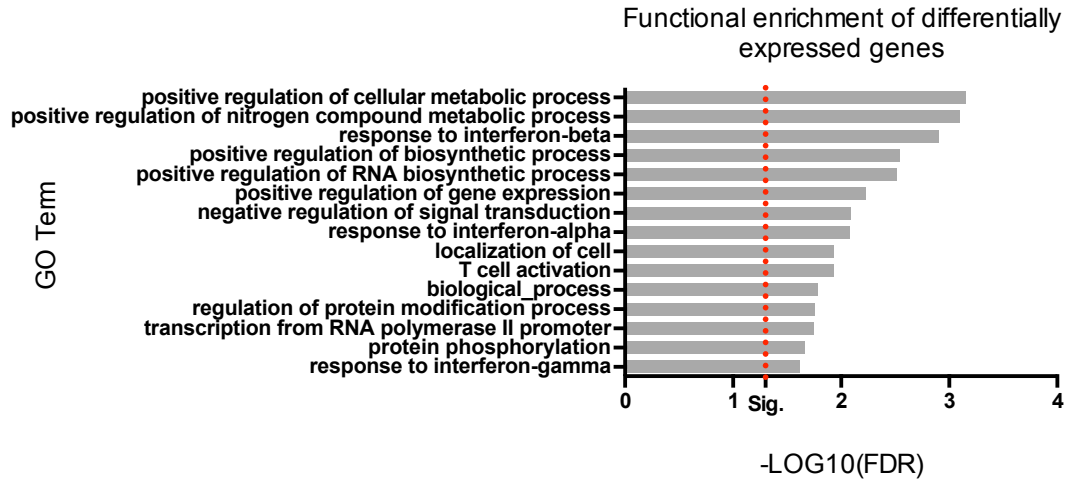
Functional enrichment of differentially expressed genes
GO Term
positive regulation of cellular metabolic process
positive regulation of nitrogen compound metabolic process
response to interferon-beta
positive regulation of biosynthetic process
positive regulation of RNA biosynthetic process
positive regulation of gene expression
negative regulation of signal transduction
response to interferon-alpha
localization of cell
T cell activation
biological_process
regulation of protein modification process
transcription from RNA polymerase II promoter
protein phosphorylation
response to interferon-gamma
0
1
Sig.
2
3
4
-LOG10(FDR)

b

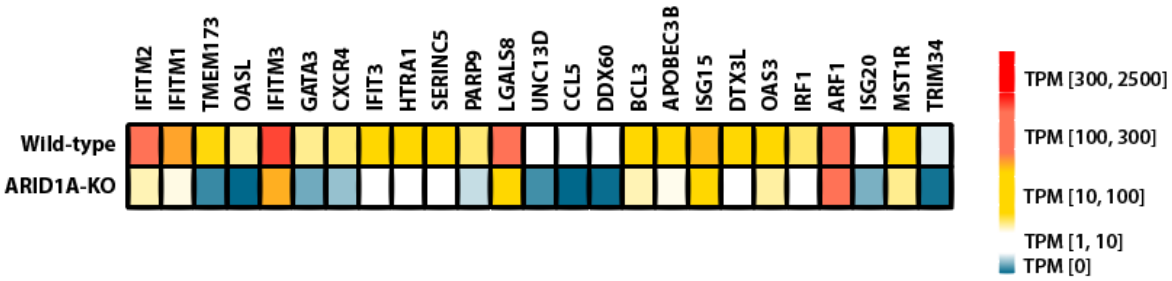
IFITM2
IFITM1
TMEM173
OASL
IFITM3
GATA3
CXCR4
IFIT3
HTRA1
SERINC5
PARP9
LGALS8
UNC13D
CCL5
DDX60
BCL3
APOBEC3B
ISG15
DTX3L
OAS3
IRF1
ARF1
ISG20
MST1R
TRIM34
WIld-type
ARID1A-KO
TPM [300, 2500]
TPM [100, 300]
TPM [10, 100]
TPM [1, 10]
TPM [0]

from 4 to 8 days depending on the cell line (**Figure 4.11 and Appendix 4**). In some cell lines, treatment using only VSVΔ51-amiR4 is more effective than treatment with VSVΔ51 control, but in all cases, GSK126 significantly and drastically increases cell death (**Figure 4.11)**. Moreover, the combination of VSVΔ51-amiR-4 with GSK126 translates into increased tumor cell death and reduced tumor burden in animals bearing human HPAF-II SC tumors compared to VSVΔ51 control virus (**Figure 4.12a**). The combination treatment also improves survival in an immunocompetent mouse model of intraperitoneal carcinomatosis induced by B16-F10 melanoma cells (**Figure 4.12b**).

While we observed enhanced killing with the VSVΔ51-amiR-4 and GSK126 combinatorial treatment compared to either treatment alone (**Figure 4.11**), GSK126 treatment did not increase viral titers (**Figure 4.13a-d**) or the number of infected cancer cells as assessed by flow cytometry (**Figure 4.13e and Appendix 5**). In other words, the combination treatment does not further enhance viral replication. However, since the percentage of tumor cell death observed was much higher than the level of infection, this raised the suspicion that a bystander killing effect could be linked to GSK126 sensitization of uninfected cells via transfer of amiR-4 to neighboring uninfected cells. The prime suspected vector of this hypothesized amiRNA transfer between cells? Extracellular vesicles!

4.8 Oncolytic viruses enhance the production of extracellular vesicles from cancer cells

Interestingly, in agreement with previous studies that show an enhancement of SEV secretion following viral infection[173,174], we have found that SEV secretion by cancer cells is increased upon OV infection (**Figure 4.14 and Table 4.2**). Cells infected with the Maraba MG1 or the

Figure 4.11 VSVΔ51-amiR-4 infection and inhibition of EZH2 via GSK126 promote synthetically lethal conditions in vitro. When exposed to low viral doses of VSVΔ51-amiR-4 and 2–3 doses of GSK126 (15μM) depending on the cell line, cell death is increased in a panel of cancer cell lines (HPAF-II, BxPC-3, 786-0) and a primary patient-derived pancreatic cancer cell line (P025) as assessed by representative crystal violet staining images of four biological replicates (**a**) and corresponding cell viability quantification compared to mock-infected DMSO-treated cells (**b-e**); timeline of treatment procedures can be found in **Appendix 4**. Two-way ANOVA with Sidak's multiple comparisons test, * $p < 0.05$, *** $p < 0.001$, **** $p < 0.0001$. Error bars are mean ± s.e.m of biological triplicates (P025) or quadruplicate (HPAF-II, BxPC-3 and 786-0). Experiments performed in collaboration with Brian Laight.

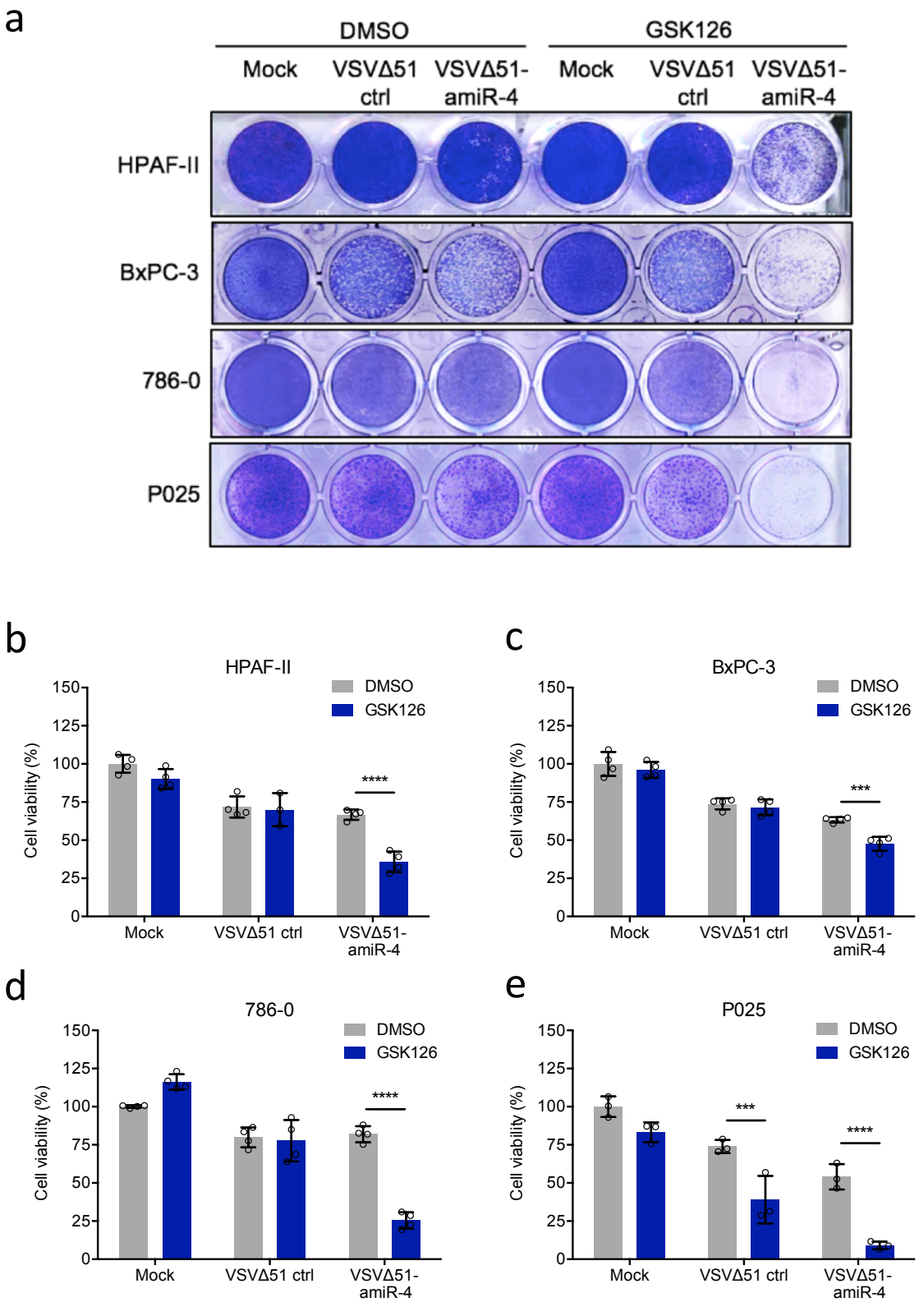
a
DMSO
GSK126
Mock
VSVΔ51 ctrl
VSVΔ51-amiR-4
Mock
VSVΔ51 ctrl
VSVΔ51-amiR-4
HPAF-II
BxPC-3
786-0
P025
b
HPAF-II
c
BxPC-3
d
786-0
e
P025
DMSO
GSK126
Cell viability (%)
150
125
100
75
50
25
0
****
***
Mock
VSVΔ51 ctrl
VSVΔ51-amiR-4

Figure 4.12 Combination therapy with VSVΔ51-amiR-4 and GSK126 is synergistic *in vivo*. (**a**) Growth curve of HPAF-II SC tumours after indicated treatments. Day 60 and 63: Two-way ANOVA with Sidak's multiple comparisons test, ** $p < 0.01$. Mean tumour volume ± s.e.m is shown (n=5 per group). (**b**) Kaplan-Meier survival curves of mice bearing B16-F10 IP tumours and treated as indicated with vehicle controls (PBS and/or Captisol) or with VSVΔ51-amiR-4 or GSK126 (50 mg/kg) or the combination of both monotherapies. Log-rank (Mantel-Cox) test, * $p < 0.05$, ** $p < 0.01$ (n=10 for PBS + GSK126 and VSVΔ51-amiR-4 + GSK126 groups and n=9 for the VSVΔ51-amiR-4 + Captisol group; data represents two pooled individual experiments).

a

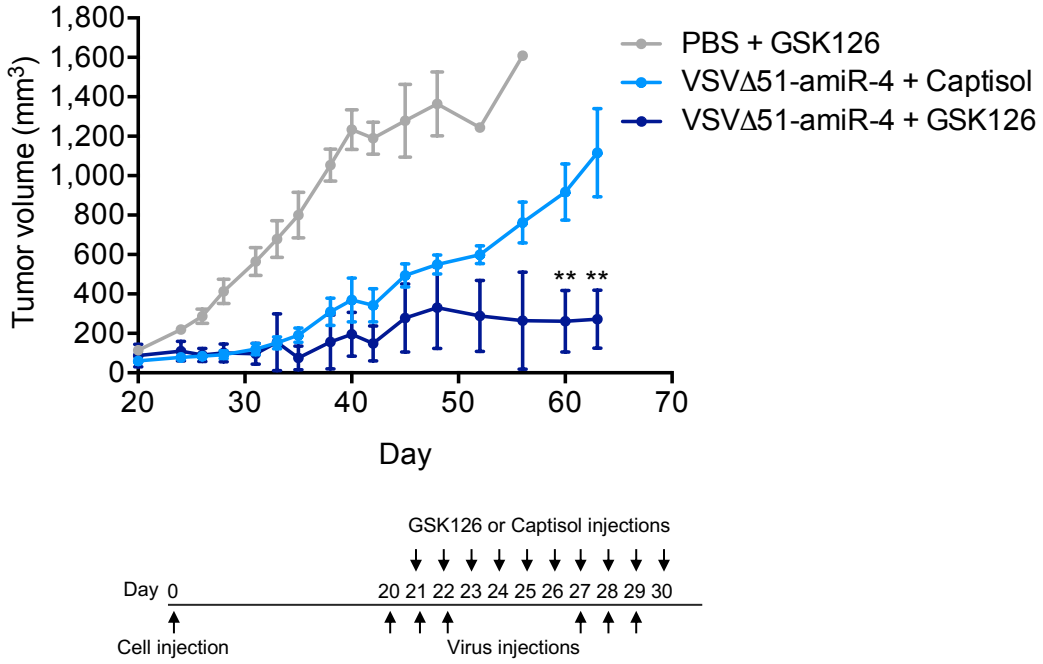
HPAF-II
Tumor volume (mm3)
1,800
1,600
1,400
1,200
1,000
800
600
400
200
0
20
30
40
50
60
70
Day
PBS + GSK126
VSVΔ51-amiR-4 + Captisol
VSVΔ51-amiR-4 + GSK126
** **
GSK126 or Captisol injections
Day 0
20 21 22 23 24 25 26 27 28 29 30
Cell injection
Virus injections

b

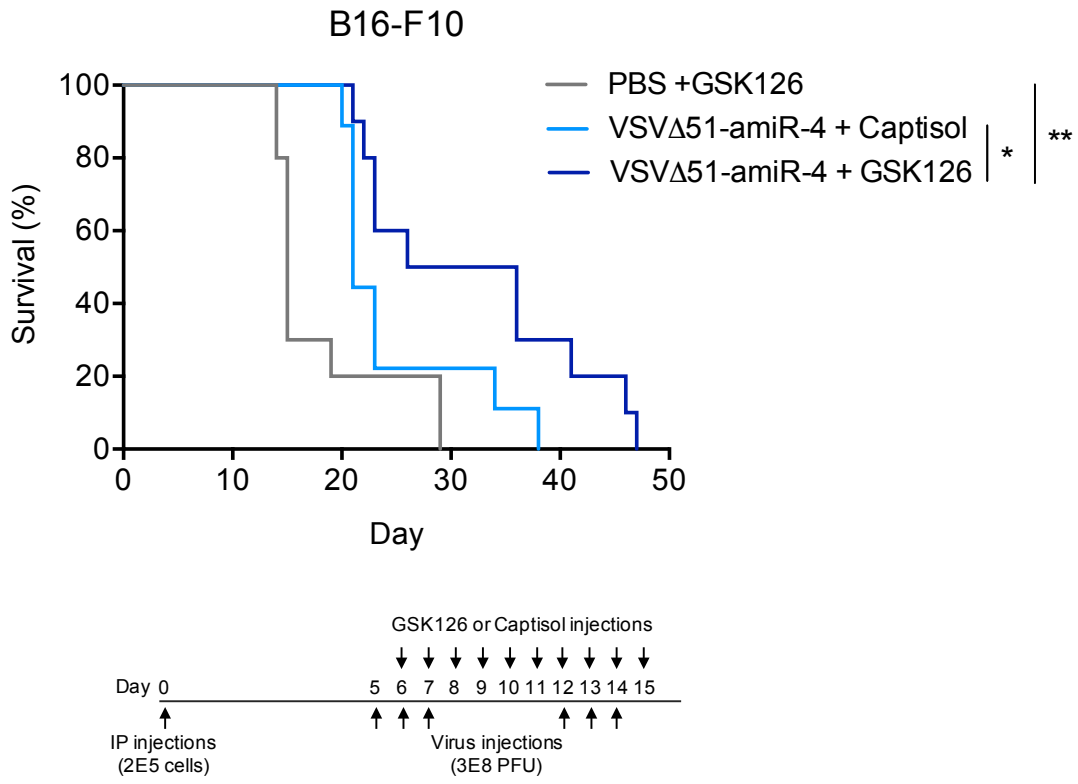
B16-F10
Survival (%)
100
80
60
40
20
0
0
10
20
30
40
50
Day
PBS +GSK126
VSVΔ51-amiR-4 + Captisol
VSVΔ51-amiR-4 + GSK126
*
**
GSK126 or Captisol injections
Day 0
5 6 7 8 9 10 11 12 13 14 15
IP injections
(2E5 cells)
Virus injections
(3E8 PFU)

Figure 4.13 Increased cell death following VSVΔ51-amiR-4 and GSK126 combination treatment is not simply caused by an increase in virus replication. (**a-d**) Viral titers of infected cells at readout following a synthetic lethality treatment plan **Appendix 4**. Two-way ANOVA with Sidak's multiple comparisons test; ns $p > 0.05$, * $p < 0.05$, *** $p < 0.001$, **** $p < 0.0001$. Error bars represent s.e.m. for 5 biological replicates per condition (HPAF-II) or 4 biological replicates per condition (BxPC-3, 786-0 and P025). (**e**) Flow cytometry assessment of infected cells with or without GSK126 treatment (as outlined in **Appendix 5a**). Two-way ANOVA with Sidak's multiple comparisons test; ns $p > 0.05$; *** $p < 0.001$, **** $p < 0.0001$. Error bars represent s.e.m. of biological replicates (HPAF: n=8 per condition; 786-0: n=5 per condition; 4T1: n=4 per condition). Gating strategy used for sample analysis with 4T1 data used as an example can be found in **Appendix 5b**. Experiments performed in collaboration with Brian Laight and Sarwat Tahsin Khan.

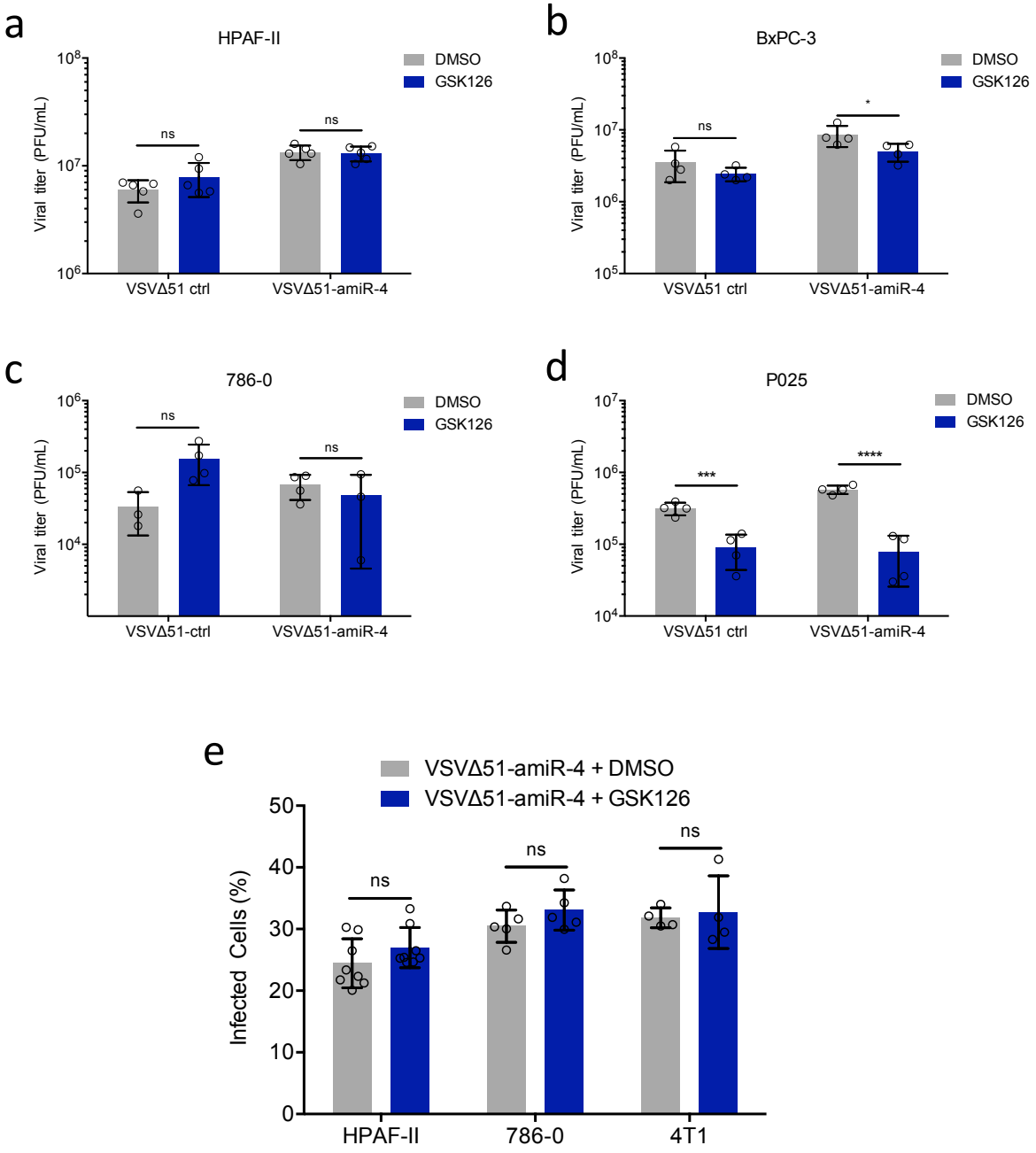
a
HPAF-II
DMSO
GSK126
Viral titer (PFU/mL)
ns
ns
VSVΔ51 ctrl
VSVΔ51-amiR-4
b
BxPC-3
DMSO
GSK126
Viral titer (PFU/mL)
ns
*
VSVΔ51 ctrl
VSVΔ51-amiR-4
c
786-0
DMSO
GSK126
Viral titer (PFU/mL)
ns
ns
VSVΔ51-ctrl
VSVΔ51-amiR-4
d
P025
DMSO
GSK126
Viral titer (PFU/mL)
***
****
VSVΔ51 ctrl
VSVΔ51-amiR-4
e
VSVΔ51-amiR-4 + DMSO
VSVΔ51-amiR-4 + GSK126
Infected Cells (%)
ns
ns
ns
HPAF-II
786-0
4T1

Figure 4.14 Cancer cells infected with oncolytic viruses produce more extracellular vesicles than their uninfected counterparts. (**a**) Immunoblotting analysis of ALIX, CD9 and TSG101 (SEV markers) in total purified SEVs produced by indicated cell lines with or without infection with MRB or MRBΔG at MOI 1. Experiment performed by Drs. Vicki Jennings and Gemma Migneco. (**b**) NTA showing size distribution and quantification of SEVs produced from mock-infected or MRBΔG-infected 786-0 cells at MOI 5 for 24 hours.

a

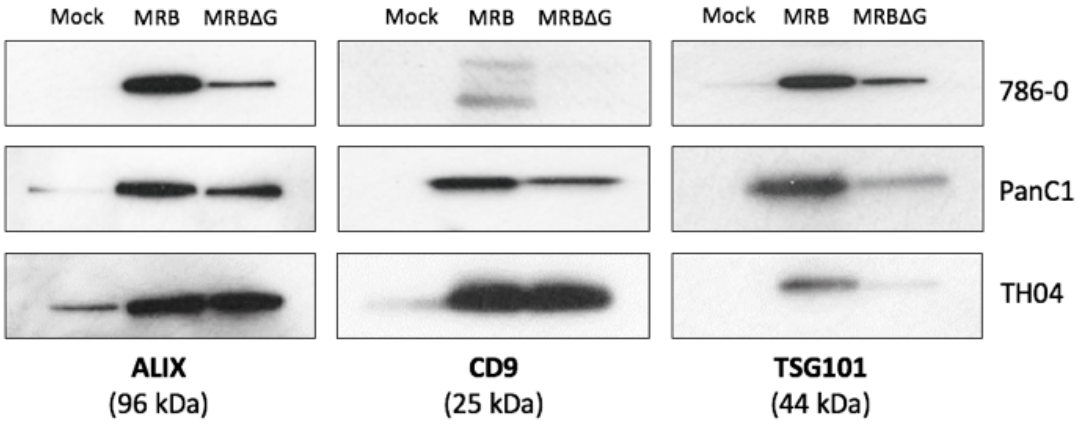
Mock MRB MRBΔG
Mock MRB MRBΔG
Mock MRB MRBΔG
786-0
PanC1
TH04
ALIX
(96 kDa)
CD9
(25 kDa)
TSG101
(44 kDa)

b

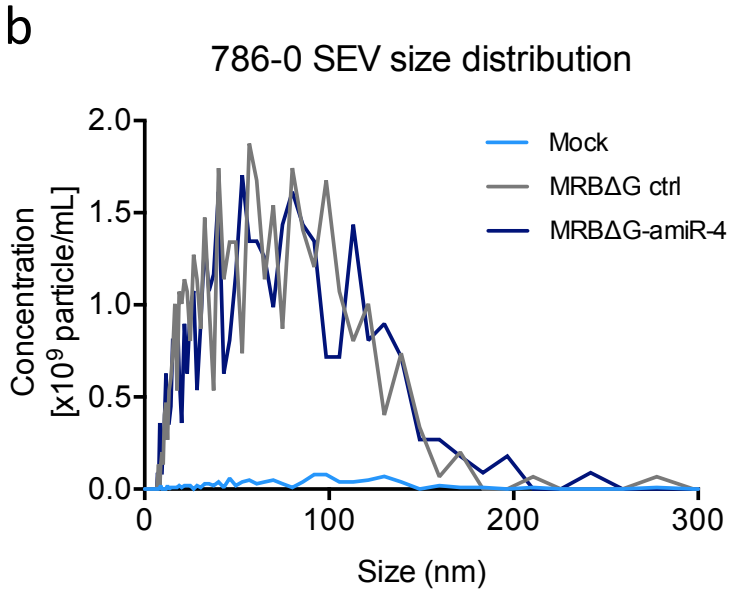
786-0 SEV size distribution
Concentration [x10^9 particle/mL]
2.0
1.5
1.0
0.5
0.0
0
100
200
300
Size (nm)
Mock
MRBΔG ctrl
MRBΔG-amiR-4

Table 4.2 Concentration of small extracellular vesicle samples as determined by nanoparticle tracking analysis

Sample	Concentration (particle/mL)
Mock	1.16E09
MRBΔG-amiR-NTC	4.03E10
MRBΔG-amiR-4	3.80E10

MRBΔG oncolytic rhabdoviruses produce SEVs in higher quantities as assessed qualitatively by immunoblotting analysis of SEV pellets resuspended in equal volumes of buffer with an equal volume ran on gels (**Figure 4.14a**). Immunoblotting analysis shows a greater signal of several SEV markers in cells infected with the rhabdoviruses compared to uninfected cells (mock). Moreover, we observe that although some samples of SEVs derived from the non-replicating virus-infected cells display less SEV-related markers than MRB-infected cells, MRBΔG-infected cells still display enhanced secretion of SEVs compared to uninfected cells. Using a quantitative method, we are able to observe an almost equal enhancement of SEV secretion from MRB MG1- and MRBΔG-infected cells (**Figure 4.14b**). Since OV-infected cells abundantly secrete SEVs, we hypothesized that the previously observed bystander killing of neighbouring uninfected cancer cells could be mediated by amiR-4-containing SEVs derived from VSVΔ51-amiR-4 infected cells.

4.9 Small extracellular vesicles derived from virally infected cells contain artificial microRNAs and are delivered to naïve cells

To validate the role of SEVs in enhancing the therapeutic efficiency of the combination treatment regimen, SEVs were isolated from cells infected with a single-cycle MRB virus. Oncolytic rhabdoviruses can be engineered to be used as single-cycle viruses. These viruses, lacking the G protein gene, can enter cells, replicate within these, but fail to produce a new round of virions with infectible properties. Both being nano-entities, SEVs and viruses are often difficult to separate using common isolation techniques[143]. Since both SEVs and rhabdovirus virions possess similar buoyant and sedimentation velocities, using the MRBΔG facilitates the isolation of SEV preparations devoid of infectious virions (**Figure 4.15**). This

Figure 4.15 Production and isolation of small extracellular vesicles. Schematic representation of the SEV harvesting procedure from infected cancer cells. The supernatant of cells infected with a replication-deficient virus is harvested and further processed via differential ultracentrifugation to obtain SEV preparations devoid of viral particles.

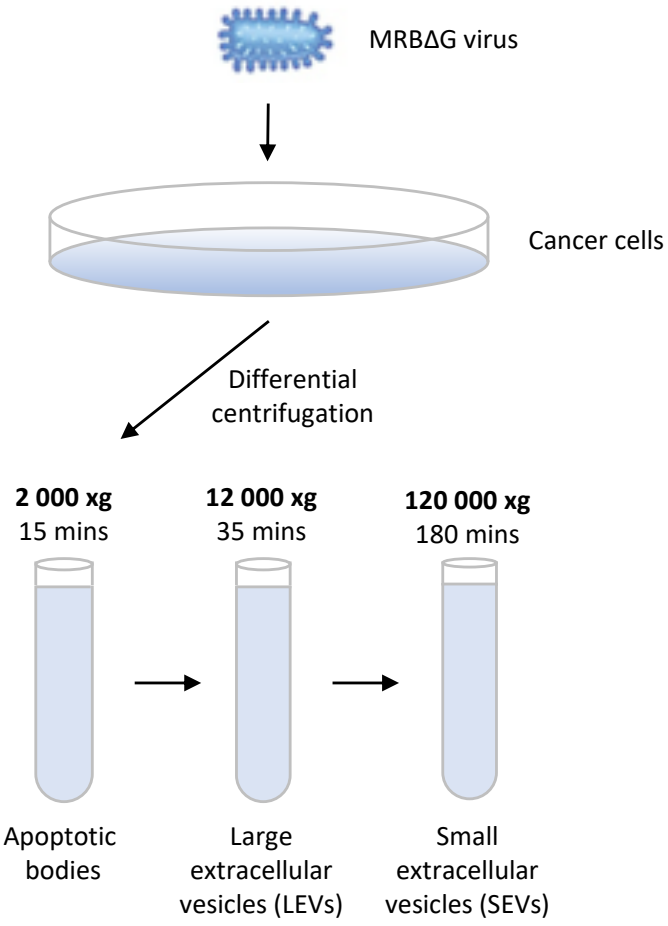
MRBΔG virus
Cancer cells
Differential centrifugation
2 000 xg
15 mins
12 000 xg
35 mins
120 000 xg
180 mins
Apoptotic bodies
Large extracellular vesicles (LEVs)
Small extracellular vesicles (SEVs)

was confirmed by the absence of bullet-shaped MRB virions in several frames of EM imaging (**Appendix 6**).

Using this technique of SEV production with the single-cycle virus, SEVs derived from MRBΔG-amiR-4-infected cells were shown to contain amiR-4 as assessed by qPCR (**Figure 4.16a**). However, in order to validate that the detected amiRNAs are contained within the SEVs, an RNA protection assay was conducted, showing that most RNA detected by qPCR is contained within SEVs (**Appendix 7**). Moreover, it was determined that these SEVs are taken up by uninfected cells when these are educated with fluorescently labeled SEVs (**Figure 4.16b**).

4.10 Small extracellular vesicles derived from virally infected cells mediate a bystander cancer cell killing

In order to validate the contribution of amiR-4 containing SEVs to the hypothesized bystander effect, SEVs were produced from infected or uninfected cells and were transferred to naïve, uninfected cells. This 'education' process was repeated several times and was also combined to the addition of the GSK126 small molecule inhibitor according to the treatment plan found in **Appendix 8**. When naïve uninfected cells were educated with isolated amiR-4-containing SEVs, cell death was observed and cytotoxicity was enhanced in a synthetic lethal fashion with the combination of GSK126 (**Figure 4.17**). Similarly to the infection of cells with VSVΔ51-amiR-4, the sole addition of amiR-4-containing SEVs to naïve cells is sufficient to induce cell death, but the combination of the amiR-4-containing SEVs and GSK126 is synergistic and results in superior cell killing as assessed by crystal violet staining of cells and

Figure 4.16 Small extracellular vesicles derived from MRBΔG-amiR-4-infected cells contain amiR-4 sequences and are delivered to receiving cells. (**a**) RT-qPCR analysis of amiR-4 levels compared to hsa-Let-7f-5p (loading control) in mock cell-associated SEVs and infected cell-associated SEVs derived from 786-0 cells infected with MRBΔG-amiR-4 at MOI 1 (n=3 biological replicates per condition). ND = not detected. (**b**) Representative immunofluorescence images from two biological replicates showing uptake of SEVs derived from MRBΔG-amiR-4-infected 786-0 cells by naïve 786-0 cells. Isolated SEVs were labeled with CFSE and transferred to naïve 786-0 cells. Two hours later, cells were fixed and prepared for fluorescence microscopy. Nuclei were stained with Hoechst stain. Scale bars = 10 μm.

a

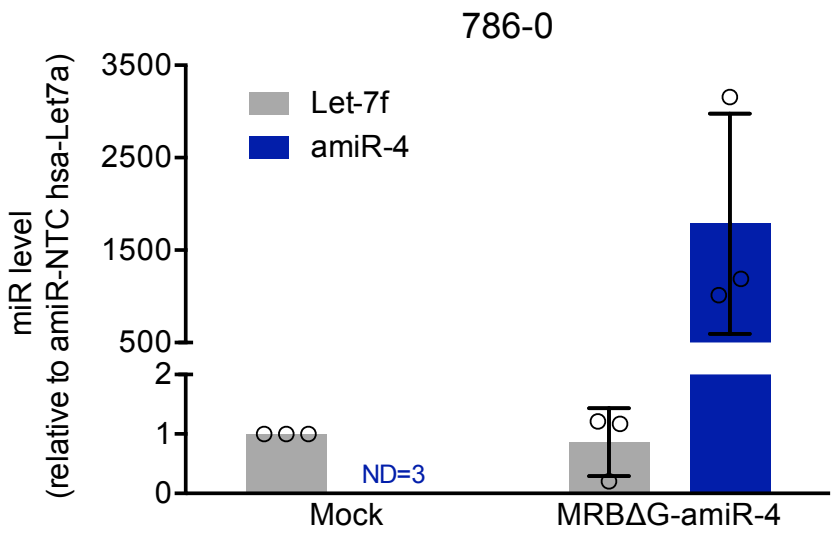
786-0
miR level
(relative to amiR-NTC hsa-Let7a)
3500
2500
1500
500
2
1
0
Let-7f
amiR-4
ND=3
Mock
MRBΔG-amiR-4

b

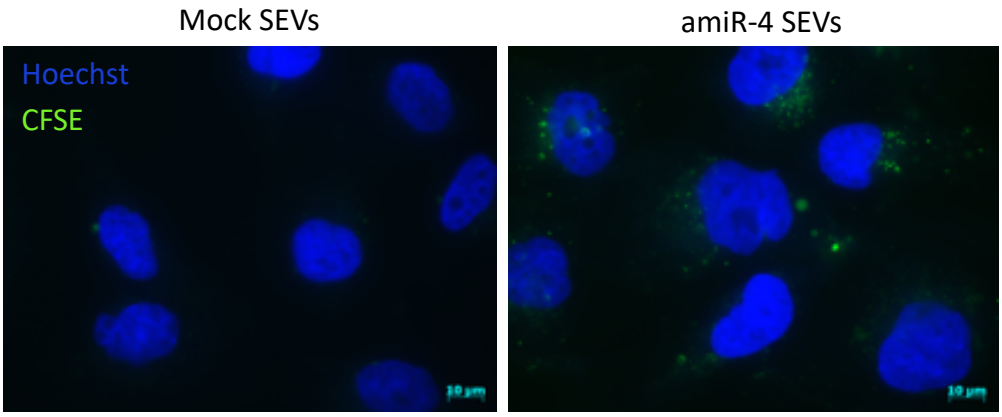
Mock SEVs
amiR-4 SEVs
Hoechst
CFSE

Figure 4.17 amiR-4-containing small extracellular vesicles induce cytotoxicity in educated naïve cells. HPAF-II, BxPC-3, 786-0 and P025 cells were educated with SEVs harvested from mock-infected, MRBΔG-amiR-NTC or MRBΔG-amiR-4-infected cells (MOI 5) and treated with vehicle control (DMSO) or GSK126 (15 μM). Representative crystal violet cell cytotoxicity assay images of three biological replicates (**a**) and their corresponding cell viability quantification compared to mock SEV and DMSO treated cells (**b**) are shown; timeline of treatment procedures can be found in **Appendix 8**. Two-way ANOVA with Sidak's multiple comparisons test, ** $p < 0.01$, *** $p < 0.001$, **** $p < 0.0001$. Error bars are mean ± s.e.m of biological triplicates. Experiments performed in collaboration with Brian Laight.

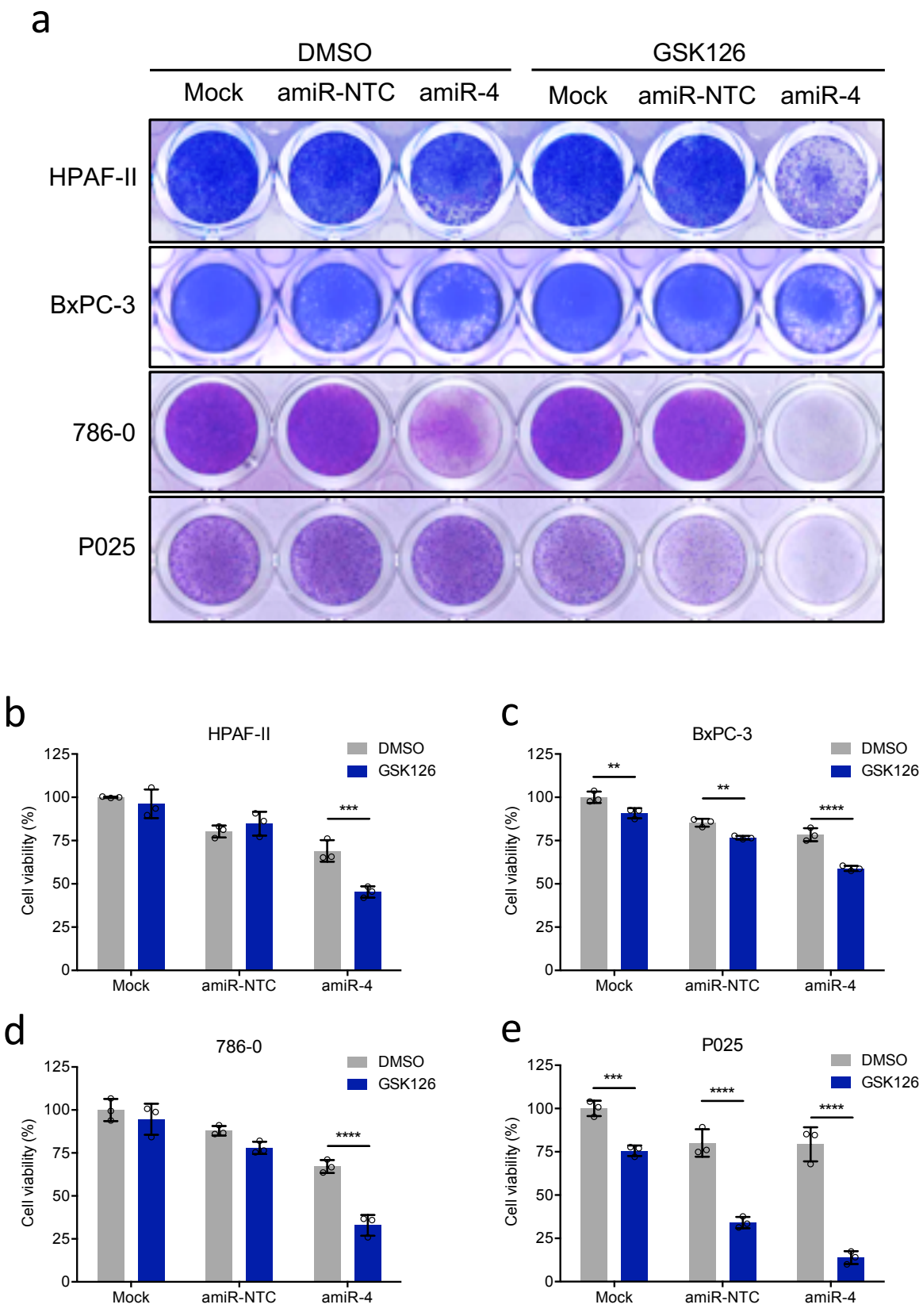
a
DMSO
GSK126
Mock
amiR-NTC
amiR-4
Mock
amiR-NTC
amiR-4
HPAF-II
BxPC-3
786-0
P025
b
HPAF-II
DMSO
GSK126
Cell viability (%)
125
100
75
50
25
0
***
Mock
amiR-NTC
amiR-4
c
BxPC-3
DMSO
GSK126
Cell viability (%)
**
**
****
Mock
amiR-NTC
amiR-4
d
786-0
DMSO
GSK126
Cell viability (%)
****
Mock
amiR-NTC
amiR-4
e
P025
DMSO
GSK126
Cell viability (%)
***
****
****
Mock
amiR-NTC
amiR-4

cell viability assessment (**Figure 4.17**). This affirms the involvement of SEVs in creating a bystander effect that increases therapeutic gain within treated cell monolayers or tumors.

4.11 The bystander effect is abrogated in Rab27a deficient cells

Rab27 GTPases mediate SEV release[175,176]. Thus, in order to validate the transfer of virally encoded amiR-4 to uninfected cells through SEVs, we generated a Rab27a knockout 4T1 cell line and demonstrated that these cells exhibit abrogated SEV secretion (**Appendix 9**), like previously shown with shRNAs directed against Rab27a[176,177], without significantly affecting viral replication (p-value > 0.5 at all MOIs) (**Appendix 10a**). Mouse 4T1 cancer cells reprogrammed with SEVs passively transferred in transwell co-culture system from Rab27a-depleted 4T1 cells infected with MRBΔG-amiR-4 (**Figure 4.18a**) contained significantly less amiR-4 than cells exposed to the infected wild-type counterpart cells (p-value = 0.0066) due to abrogated SEV production in the Rab27a-depleted 4T1 cells (**Figure 4.18b**). Furthermore, while as expected, the combinatorial treatment of VSVΔ51-amiR-4 and GSK126 resulted in a significant decrease in cancer cell viability (p-value = 0.0003), Rab27a-depletion in 4T1 cells abolished these effects (p-value = 0.7193) (**Figure 4.19**). Again, viral replication was unaffected by or GSK126 treatment, but also remained unchanged in a Rab27a deficiency setting (**Appendix 10b,c**). The aforementioned data provides evidence that the transfer of virally expressed amiRNA-4 from infected to uninfected cells via SEVs contributes in part to the bystander sensitization of uninfected cells to GSK126.

Figure 4.18 Rab27a deficiency limits the spread of amiR-4 via extracellular vesicles to neighboring uninfected cells. (**a**) Schematic representation of transwell coculture assays designed to assess the transfer of amiR-4 via infected cell-derived SEVs to uninfected cells. 4T1 WT or Rab27a-defient (Rab27a$^{-/-}$) cells were seeded in the upper compartment and infected with MRBΔG-amiR-NTC control or with MRBΔG-amiR-4 (MOI 3). After 24 hours, inserts were transferred to a new plate containing uninfected 4T1 WT receiving cells in the lower compartment. (**b**) RT-qPCR analysis of amiR-4 levels in receiving cells (lower compartment) after 48 hours of education by cell-secreted factors derived from MRBΔG-amiR-4-infected cells (upper compartment) with three biological replicates per condition. Two-tailed unpaired t-test, ** $p < 0.01$. Experiment performed in collaboration with Dr. Carolina Ilkow.

a

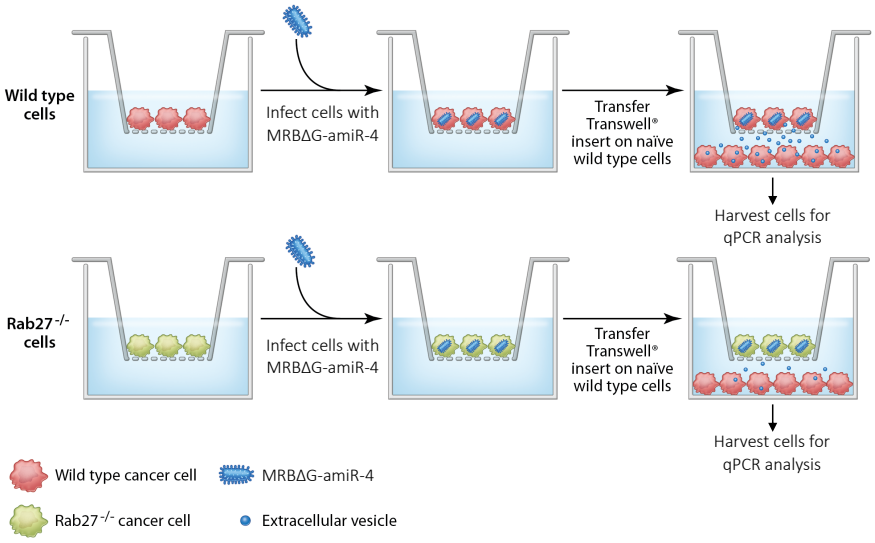
Wild type cells
Infect cells with MRBΔG-amiR-4
Transfer Transwell® insert on naïve wild type cells
Harvest cells for qPCR analysis
Rab27-/- cells
Infect cells with MRBΔG-amiR-4
Transfer Transwell® insert on naïve wild type cells
Harvest cells for qPCR analysis
Wild type cancer cell
MRBΔG-amiR-4
Rab27-/- cancer cell
Extracellular vesicle

b

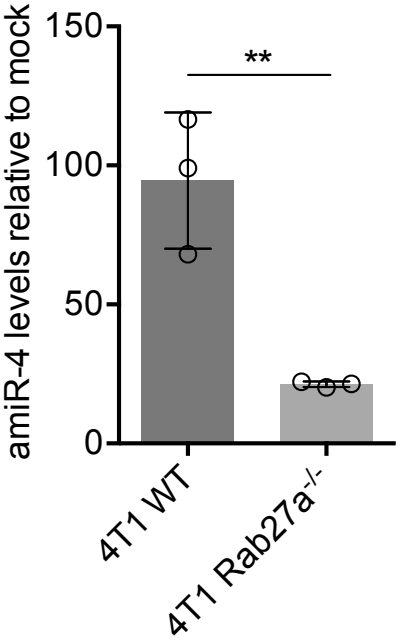
amiR-4 levels relative to mock
150
100
50
0
**
4T1 WT
4T1 Rab27a-/-

Figure 4.19 Reduced SEV biogenesis abrogates the observed amiR-4 bystander effect. (**a**) RT-qPCR analysis of amiR-4 levels in receiving cells (lower compartment; see **Figure 4.18a** for experimental schematic) after 48 hours of education by cell-secreted factors derived from MRBΔG-amiR-4-infected cells (upper compartment) with three biological replicates per condition. Two-tailed unpaired t-test, ** $p < 0.01$. (**b-d**) 4T1 WT (n=4 per condition) or Rab27a$^{-/-}$ cells (n=7 per condition) were mock-treated or infected with VSVΔ51 control or VSVΔ51-amiR-4 (MOI 0.025) and treated with either vehicle control (DMSO) or GSK126 (15 μM). Representative crystal violet cell cytotoxicity assay images of four biological replicates (**b**) and their corresponding quantifications (**c,d**) are shown. Statistical analysis is performed by two-way ANOVA with Tukey's multiple comparison test, ns $p > 0.05$, *** $p < 0.001$. Experiments performed in collaboration with Brian Laight.

a

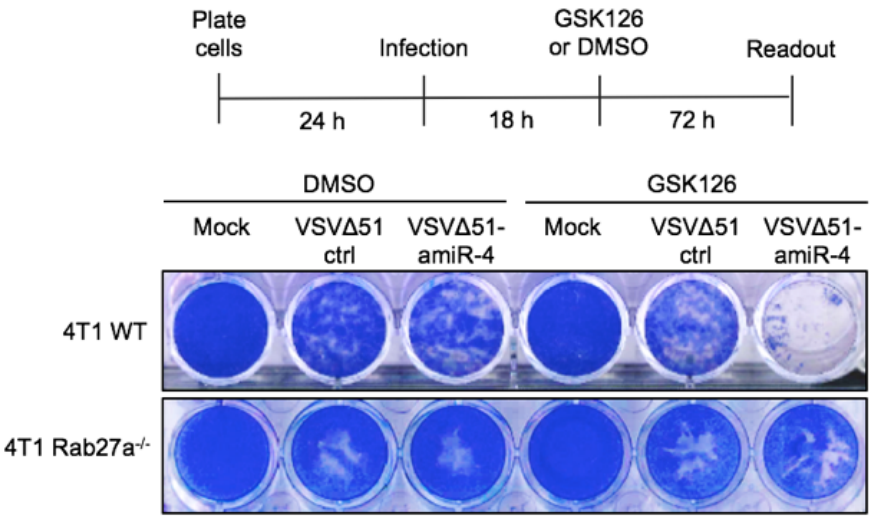
Plate cells
Infection
GSK126 or DMSO
Readout
24 h
18 h
72 h
DMSO
GSK126
Mock
VSVΔ51 ctrl
VSVΔ51-amiR-4
Mock
VSVΔ51 ctrl
VSVΔ51-amiR-4
4T1 WT
4T1 Rab27a-/-

b

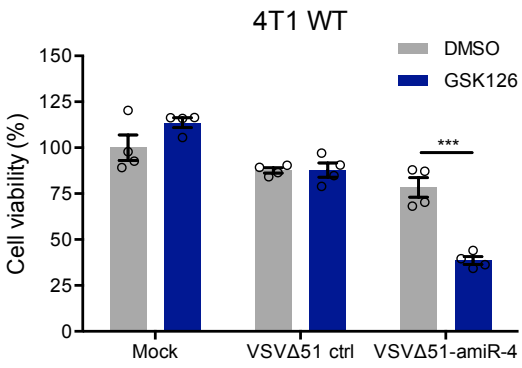
4T1 WT
DMSO
GSK126
Cell viability (%)
150
125
100
75
50
25
0
***
Mock
VSVΔ51 ctrl
VSVΔ51-amiR-4

c

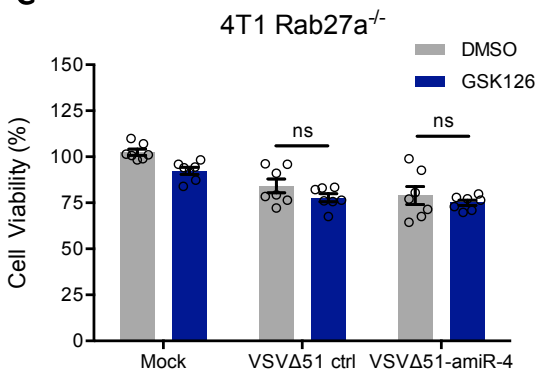
4T1 Rab27a-/-
DMSO
GSK126
Cell Viability (%)
150
125
100
75
50
25
0
ns
ns
Mock
VSVΔ51 ctrl
VSVΔ51-amiR-4

5. DISCUSSION

5.1. Bioselection screening to identify key players of residual antiviral immunity

5.1.1 Delivery of virally encoded microRNAs to the cytoplasm

Thus far, the rise of miRNA therapy has been limited by an *in vivo* delivery problem. Indeed, systemic injections of liposomes or EVs for miRNA delivery often results in accumulation in the liver which poses a challenge for delivery to other organs or tumors, thus limiting greatly the efficacy of these therapies. In addition to posing the same disadvantages, the use of adenoviruses or other gene therapy viral vectors also poses genotoxicity concerns[178,179]. One alluring strategy for delivering miRNAs to cancer cells is the use of OVs possessing a cytoplasmic replication cycle, which are regarded as safe vectors, since their replication does not occur in the nucleus. However, canonical miRNA processing requires a nuclear step. Thus, it was previously thought that OV-encoded miRNA transcripts produced in the cytoplasm could not be properly processed into mature miRNA sequences to exert their therapeutic functions. Yet, the speculation was dismissed after the discovery of a noncanonical mechanism allowing virus-derived cytoplasmic primary miRNA (c-pri-miRNA) processing[180]. Upon viral infection, Drosha has been shown to localize to the cytoplasm to initiate virally encoded miRNA processing without affecting the processing of endogenous miRNAs. This culminates in the production of mature miRNAs with therapeutic knockdown efficacy[165,180–183]. These proof-of-concept experiments have paved the way to the use of oncolytic rhabdovirus-encoded miRNAs for cancer therapeutics by our team and collaborators. Here, we show that VSVΔ51 and MRB MG1 can encode and express amiRNAs with therapeutic potential. We notably identified a functional amiRNA sequence that enhanced OV-mediated cell death within PC cells upon targeting of several cellular proteins.

5.1.2 Sindbis virus artificial microRNA library

In order to select amiRNA sequences able to confer a replicative advantage to oncolytic RNA viruses, a library of ~16,000 unique SV-encoded amiRNAs was passaged in pancreatic cancer cells, pancreatic CAFs and normal skin fibroblasts. This approach selectively enriches sequences conferring a replication advantage to the virus, since the amiRNA sequence has to be transcribed from the viral genome to exert its selective pressure. However, enriched amiRNAs could potentially confer entry or uncoating advantages to the virus in the event that they are disseminated to neighboring cells via EVs and could then have effects on steps happening upstream of viral replication in the virus life cycle. Moreover, this type of screen will select for amiRNAs that target transcripts with a shorter half-life, since the enrichment is limited by the duration of the viral life cycle.

5.1.3 Selection of an artificial microRNA to enhance oncolytic VSV-mediated cell death in pancreatic cancers

The SV-library amiRNA screen was conducted to identify sequences aiding OV-mediated cell death within cancer cells. The results of the screen show an enrichment of the amiR-1- and amiR-2-encoding viruses in normal GM38 fibroblasts, making these amiRNAs unsuitable for safe therapeutic purposes (**Figures 4.2 and 4.5a**). On the other hand, like amiR-4, amiR-3 and amiR-5 were enriched in cancer cells, but not in normal cells, making them interesting candidates to improve OV therapy in PC (**Figure 4.2**). However, our results show that these two amiRNAs do not confer a significant therapeutic advantage to VSVΔ51 in the PC cell lines tested (**Figure 4.4**). This could be explained by the fact that SV and VSVΔ51 do not have identical replication cycles, and while these amiRNAs can confer a replicative advantage to

SV, the same will not necessarily be true for VSVΔ51. Finally, amiR-4 was selected as the prime candidate on the basis that it does not impair the safety profile of VSVΔ51 in normal cells, but significantly improves VSVΔ51-mediated cell death within PC cells (**Figures 4.2, 4.4 and 4.5**).

5.1.4 Identification of artificial microRNAs with cancer-associated fibroblast-targeting potential

Interestingly, VSVΔ51 has previously been shown to replicate within CAFs[63] and thus presents an interesting strategy to target CAFs within PCs, an intervention much needed in PC research. Here, our screen identified amiR-3 and amiR-5 as sequences potentially conferring a replicative advantage in CAFs when expressed from the oncolytic SV, while causing very low cytotoxicity to normal cells (**Figures 4.2 and 4.5a**). It would thus be interesting to further investigate the effects of these amiRNAs in VSVΔ51-potentiated CAF killing.

5.2 Analysis of amiR-4 targets

5.2.1 Exploring different amiR-4 targets

Our target prediction analysis identified several cellular targets involved in epigenetic regulation and cytoskeleton stability. Among those, the protein products of *HDAC4, PLEC* and *ARID1A* were confirmed to be downregulated in VSVΔ51-amiR-4-infected cells. Histone deacetylase (HDAC) enzymes perform important epigenetic regulation functions in normal cells by participating in post-translational modification of the DNA. Their deregulation has been shown to lead to carcinogenesis and HDAC inhibition is an increasingly explored means of treating cancers[184]. Moreover, HDAC inhibition has been shown to synergize with OV

therapy[169,185,186]. Here, we show that the expression of HDAC4 is drastically downregulated in PANC1 cells infected with VSVΔ51-amiR-4 for 48 hours (**Figure 4.7b**), but does not show significant downregulation in MIA PaCa-2 cells 36 hpi (**Figure 4.7a**). This discrepancy in results could be explained by the different sensitivity of cell lines to VSVΔ51 or even the differing time points of data analysis. Therefore, in order to validate the physiological and therapeutic effects of HDAC4 targeting using amiR-4, more experiments are needed. Moreover, PLEC is an important structural protein that holds together different parts of the cytoskeleton, like microtubules and actin microfilaments[187]. In cancer cells, PLEC deregulation can be involved in metastasis. Indeed, two distinct studies each revealed an important role of PLEC in invasion and metastasis in prostate and pancreatic cancers[188,189]. We also know that cytoskeleton manipulation by viruses can ease their spread[190] and that PLEC can play a role in viral infections[191]. Also, previous reports have shown therapeutic potential for targeting components of the cytoskeleton in a synergistic fashion with OV therapy[96]. Here, we show that PLEC is significantly downregulated upon infection of MIA PaCa-2 cells by the VSVΔ51-amiR-4 OV 36 hpi and that the protein levels are drastically decreased in PANC1 cells 48 hpi (**Figure 4.7**). Our results suggest that PLEC merits more attention as a target for enhancing oncolytic virotherapy in PCs.

Moreover, in order to further confirm these targets and to perhaps identify other targets that may have been missed by the prediction tools used, a functional assay to determine amiR-4 targets could be put to use. In order to functionally identify amiR-4 targets, we could make use of an assay for miRNA target identification, like the 3'LIFE assay, a high throughput dual reporter luciferase assay[192]. This method makes use of a library of plasmids encoding human

3'UTR sequences and two different luciferases. By cotransfecting individual plasmids of this library with a plasmid encoding the miRNA of interest in a high throughput fashion, luciferase expression repression can be quantified to identify 3'UTRs of genes targeted by the miRNA. This technique has been shown to be more accurate and can identify a higher number of novel miRNA target genes compared to bioinformatic predictions[192].

Here, since the targeting of HDACs and cytoskeleton proteins have previously been implicated in OV therapeutic gain, our focus shifted prominently to ARID1A.

5.2.2 Spotlight on ARID1A

5.2.2.1 ARID1A targeting in cancers

Since ARID1A's role in antiviral immunity had not previously been explored and exploited for virotherapy, we decided to focus on this target. In humans, ARID1A is part of the SWI/SNF chromatin remodeling complex, a protein complex that breaks down DNA-histone interactions in an ATP-dependent manner. This exposes the DNA to the machinery necessary for the transcription of inducible genes[193]. It is notably involved in normal embryonic development and in the differentiation of different cell types in adults[194]. SWI/SNF subunits are mutated in ~20% of cancers, making them the epigenetic regulators with the highest mutational frequencies across all cancers[170,195]. Moreover, ARID1A is the most commonly mutated SWI/SNF subunit in cancer, its mutation generally causing an inactivated phenotype[194].

5.2.2.2 Role of ARID1A in antiviral immunity

Our RNA-seq analysis revealed a dampening of IFN response elements in *ARID1A*-knockout cells (**Figure 4.10**) consistent with a previously suggested role of ARID1A in the regulation

of the interferon response[196]. Indeed, depleting cancer cells of ARID1A using CRISPR-Cas9 technology or by infecting *ARID1A* wild-type cells with VSVΔ51-amiR-4 renders these cells significantly more sensitive to infection (**Figure 4.8**). Interestingly, our RNA-seq analysis identified IFITM2 as the protein most significantly downregulated in *ARID1A*-knockout cells compared to wild-type cells (**Figure 4.10b**). Previous reports demonstrated a role of IFITM2 in restricting VSV infection in HEK293T cells with increased viral titers upon treatment of cells with a siRNA against IFITM2[197] which also corroborates with our results.

5.2.2.3 Therapeutic targeting strategies of ARID1A deficient cancers

Albeit an undruggable target, naturally occurring ARID1A deficiency has been shown to synergize with therapeutics, notably anti-PD-L1 therapy[198] and systemic administration of small molecule inhibitors targeting synthetic lethal interactions[172,199]. ARID1A has been hypothesized to be a tumor suppressor as it is often functionally lost in cancers[200]. Therefore, ARID1A depletion as a therapeutic intervention is not generally desirable. However, ARID1A loss has been exploited in preclinical treatments as part of synthetic lethal strategies. Indeed, EZH2 methyltransferase inhibition and HDAC6 inhibition have been shown to synergize with ARID1A deficiency to reduce tumor burden[172,199]. In these studies, the ARID1A loss of ovarian cancer tumors is exploited to cause cancer cell death in combination with drugs targeting EZH2 and HDAC6, namely GSK126 and ACY1215 respectively. Here, we hypothesized that ARID1A targeting through the infection of cancer cells with VSVΔ51-amiR-4 combined with EZH2 inhibition using GSK126 would enhance cell death in PC cell lines and tumors. Indeed, targeting ARID1A through amiR-4 is a potent strategy for PCs, since most of these cancers (~85-96%) retain an *ARID1A* wild-type status[21,170], which was validated

in our PC biobank using IHC staining with 4/5 tumors expressing ARID1A (**Figure 4.9a**). We show that the combination therapy with the OV and the small molecule inhibitor enhances cell death *in vitro* (**Figure 4.11**), *ex vivo* (**Figure 4.9b**) as well as in aggressive mouse models of PC (**Figure 4.12**).

5.3 The virally induced extracellular vesicle-mediated bystander effect

5.3.1 Unveiling the oncolytic virus-induced bystander effect

Here, we use the GSK126 small molecule inhibitor to target PCs in a synthetic lethal fashion in combination with our amiR-4-encoding virus as a means to target ARID1A. GSK small molecule inhibitors have been shown to have VSe potential (personal communication with Anabel Bergeron; Diallo laboratory), so we thought that combining the use of GSK126 with VSVΔ51 could potentially further enhance viral replication. However, the combination of these therapeutics did not enhance cytotoxicity in PC cells, except in the P025 PDX-derived cell line (**Figure 4.11**). Moreover, in terms of viral replication, the amount of virus produced from the VSVΔ51 and GSK126 combination treatment was not enhanced in any of the cell lines tested (**Figure 4.13a-d**). This indicates that in these cells, GSK126 does not act as a VSe. However, a drastic increase in cell death can be observed when cells are treated with a combination of VSVΔ51-amiR-4 and GSK126 (**Figure 4.11**). This also translates into impressive therapeutic gain in models of highly aggressive PC and intraperitoneal carcinomatosis (**Figure 4.12**). At first glance, this increase in cell death can be attributed to the synthetic lethality occurring by the targeting of both ARID1A and EZH2 simultaneously in the combination treatment groups which was indeed hypothesized to enhance cytotoxicity. However, by taking a closer look, we observed that at very low infection rates (~30% of

infected cells; **Figure 4.13e**), the cell monolayer was destroyed in most cases (**Figure 4.11a**) and 50-90% of cells lacked metabolic activity (**Figure 4.11b-e**). We have also shown that this observed phenomenon is not due to an enhancement in viral replication, as demonstrated by titer levels and infectivity rates using flow cytometry (**Figure 4.13**). We then suspected the occurrence of a bystander effect where amiRNAs derived from VSVΔ51-amiR-4-infected cells could be transferred from infected to uninfected cells, which we hypothesized was happening through cell-cell communication mediated by EVs.

5.3.2 Repurposing tumors into therapeutic extracellular vesicle factories

To demonstrate that EVs are indeed involved in this hypothesized bystander effect, we conducted *in vitro* EV education experiments. This confirmed that 1) EVs containing amiR-4 are sufficient to induce cytotoxicity in uninfected cells and that 2) combining amiR-4-containing EVs and GSK126 is synthetic lethal (**Figure 4.17**). This second observation indicates that EVs derived from VSVΔ51-amiR-4 contain cytotoxic amiRNAs (**Figure 4.16a**) and that these EVs localize to neighboring uninfected cells (**Figure 4.16b**) to sensitize these cells to EZH2 inhibition via the targeting of ARID1A. This sensitization thus enables the synthetic lethality to occur in vulnerable cells. The implication of SEV's involvement in this type of intercellular communication network was further confirmed in a breast cancer Rab27a KO cell line of mouse origin that was readily available in our lab. Using this cell line with an abrogated SEV secretion mechanism, we were able to show that this bystander effect is consequentially also abrogated (**Figures 4.18 and 4.19**). In order to further validate the involvement of EVs in this phenomenon, *in vivo* studies in a PC model will be needed and are currently underway.

We show here a proof of concept that *in situ* production of therapeutic EVs within the tumor bed is a strategy possible for cancer therapy. Indeed, OVs can be used as vectors for amiRNA expression within tumor cells, which can then be exported from infected cells via EVs to reach neighboring naïve cells to spread the therapeutic cytotoxic cargo and sensitize said cells to small molecule inhibitors. This bypasses the production, delivery and specificity issues associated to current EV production and delivery strategies. However, it is important to note that these EVs could also find their way to normal tissues and harm them. We did not observe severe off target effect and cytotoxicity issues in this study. We are, however, still addressing this concern by engineering in OVs proteins that will allow specific EV tropism to tumor cells or other cells of the TME we wish to target using amiRNA cytotoxic cargoes.

5.3.3 Extracellular vesicles vs. virions vs. defective interfering particles

Even though we have shown that our EV preparations are devoid of bullet-shaped virions (**Appendix 6**) and we have used cell lines with reduced EV biogenesis to validate the bystander effect (**Figures 4.18 and 4.19**), other experiments are needed to have a higher degree of certainty that the observed effect is undoubtedly due to EVs. Other strategies that could come into play that cannot be ignored include, but may not be limited to, the spread of the viral genomes by EVs or the involvement of viral defective interfering particles (DIPs). EVs have been shown to have the capacity to contain and transfer partial or complete viral genomes between cells[201]. It will thus be of high importance to experimentally test whether we are able to detect the VSVΔ51 genome within EVs to ensure the involvement of EV-associated amiRNA delivery in our hypothesized sensitization strategy. Moreover, DIPs are particles known to be formed concomitantly with virions during infections. They cannot replicate on

their own, but will compete for viral proteins in infectious virion-infected cells and can thus interfere with the production of infectious particles[202]. Although DIPs have been described, their specific functions in viral infection and spread remain elusive. Therefore, we cannot completely dismiss their involvement, if any, in the therapeutic effects shown here and this thus merits further investigation.

5.4 Combination with immune checkpoint inhibitors

Immunotherapy has taken the world of cancer therapy by storm. Checkpoint blockade, which consists of blocking inhibitory checkpoints of immune cells can restore the ability of the immune system to clear cancer cells[203,204]. Moreover, it is now well established that due to the high heterogeneity and fast adaptability of tumors, combination therapies are more successful than the use of a single therapeutic agent to treat cancer. Therefore, novel therapeutics are now, most often than not, tested in combination with immune checkpoint inhibitors (ICIs), due to their impressive track record in clinical successes[205]. OVs have been shown to synergize with ICIs[205–207]. Indeed, OVs are able to modify the immune TME landscape to make tumors 'hotter'. The release of PAMPs and DAMPs in the TME following OV infection enhances TIL homing to tumors, which are required for generating potent antitumor immune responses using ICIs[68,206]. Interestingly, ARID1A and EZH2 deficiency also work in synergy with ICIs. Shen and colleagues have found that ARID1A deficient ovarian cancers harbor more TILs and have higher PD-L1 expression than ARID1A WT tumors which renders them cooperative with anti-PD-L1 therapy[198]. Moreover, inhibition of EZH2 in melanoma has been shown to synergize with anti-CTLA-4 immunotherapy[208]. Therefore, we hypothesize that ARID1A targeting using an OV coupled with the inhibition of EZH2 using GSK126 will render tumors susceptible to

ICIs, thus further enhancing therapeutic efficacy in models of PC. These studies are currently underway.

5.5 Exploring effects of the combination therapy on the pancreatic cancer tumor microenvironment

As previously stated, the PC TME is a harsh environment that is poorly immunogenic. However, OV infection can circumvent this and increase responsiveness of tumors to ICIs. In order to uncover the mechanism(s) underlying enhanced therapeutic effects *in vivo*, an immune profile of treated tumors needs to be obtained. This information will also allow to predict responsiveness of OV- and small molecule-treated tumors to anti-PD-1/anti-PD-L1 therapy. Preliminary flow cytometry analysis indicates an increase in $CD8^+$ T cell infiltration and activation in tumors treated with the combination treatment compared to control-treated tumors (data not shown; experiments performed in collaboration with Sarwat Tahsin Khan). Other experiments are currently underway to determine the extent of infiltration and activation of other TILs as well as expression of PD-1/PD-L1 in treated tumors which will be useful in predicting whether treated tumors will respond to checkpoint blockade. In addition, conducting similar experiments in PC PDX tumor cores with exogenous addition of human PBMCs will also provide a good degree of certainty as to whether this strategy would translate into sufficient therapeutic gain in the clinic.

5.6 Broadening the scope of this novel treatment plan

Although we tested the efficacy of the VSVΔ51-amiR-4 and GSK126 combination treatment more thoroughly in PC cell lines and models, this therapeutic strategy would hypothetically

work similarly in other ARID1A WT cancers. Notably, hepatocellular, colorectal, melanoma, lung and breast cancers are other cancers displaying low ARID1A mutation rates, with less than 15% of these cancers presenting with ARID1A mutations[170]. Thus, the majority of these tumors retain an ARID1A WT status and would be ideal candidates for this type of therapy. Other tumor models are currently being tested.

6. CONCLUSION

To conclude, OVs can be engineered and used as replication-competent amiR vectors to enhance viral replication in cell lines and tumors otherwise resistant to OV therapy. Additionally, these OV-encoded amiRs can be used along with systemically administered small molecule inhibitors to create a synthetic lethal effect within tumors that significantly enhance cell death. Moreover, the combination treatment of the amiR-expressing OV and the small molecule inhibitor allowed the discovery of an EV-mediated bystander effect occurring after the secretion of amiRs contained within vesicles derived from infected cells which have the ability to sensitize naïve neighboring cells to OV therapy or to small molecule inhibition. This strategy consists of a novel method to target cells normally resistant to OV therapy (**Figure 6.1**) and ultimately provides new hope to fight the notorious disease that is PC.

Figure 6.1 Proposed model of the effects induced by the VSVΔ51-amiR-4 and GSK126 combinatorial therapy. In our models, cell death can occur as a direct effect of oncolysis **or** via SEV delivery of amiR-4 to uninfected neighboring cells which causes a synthetic lethal effect in cells when combined with the GSK126 small molecule inhibitor.

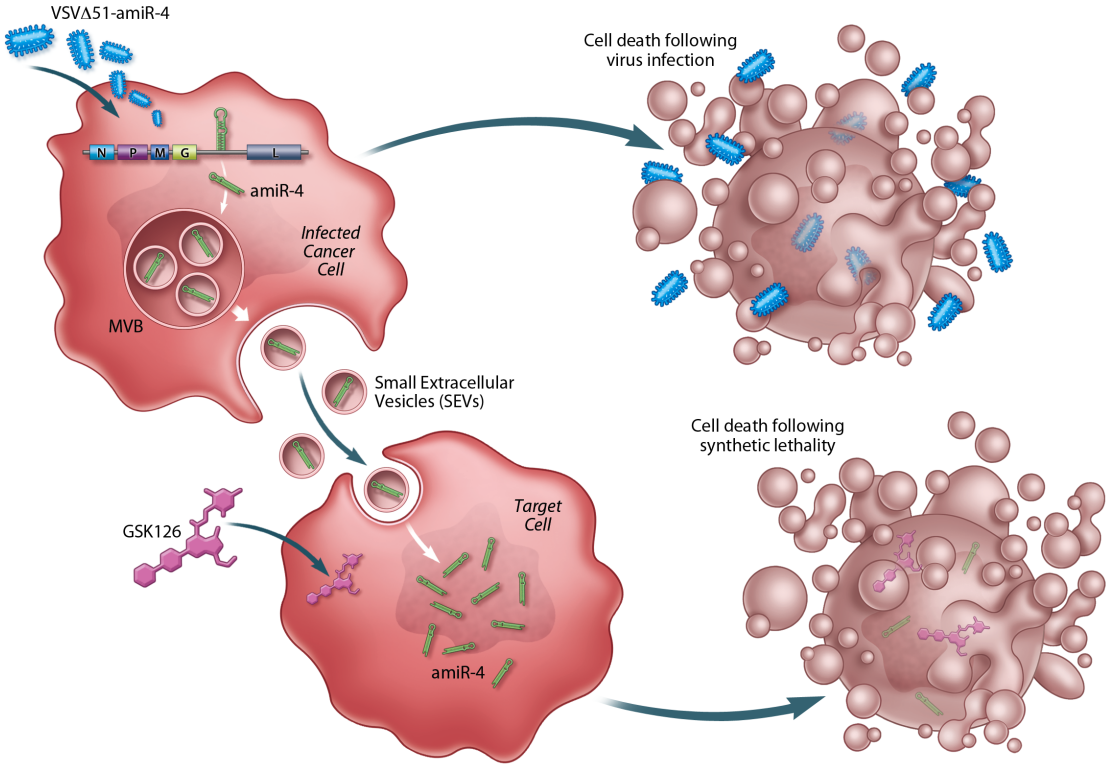
VSVΔ51-amiR-4
N
P
M
G
L
amiR-4
Infected Cancer Cell
MVB
Small Extracellular Vesicles (SEVs)
GSK126
Target Cell
amiR-4
Cell death following virus infection
Cell death following synthetic lethality

APPENDICES

Appendix 1. Validation of amiR expression from VSVΔ51. Quantitative RT-PCR expression analysis of amiR1-5 transcripts from VSVΔ51. The copies per reaction were calculated based on a relative standard curve of the sample. Error bars represent ± s.e.m of three biological replicates. ND = not detected. Experiment performed by Hayley McKay.

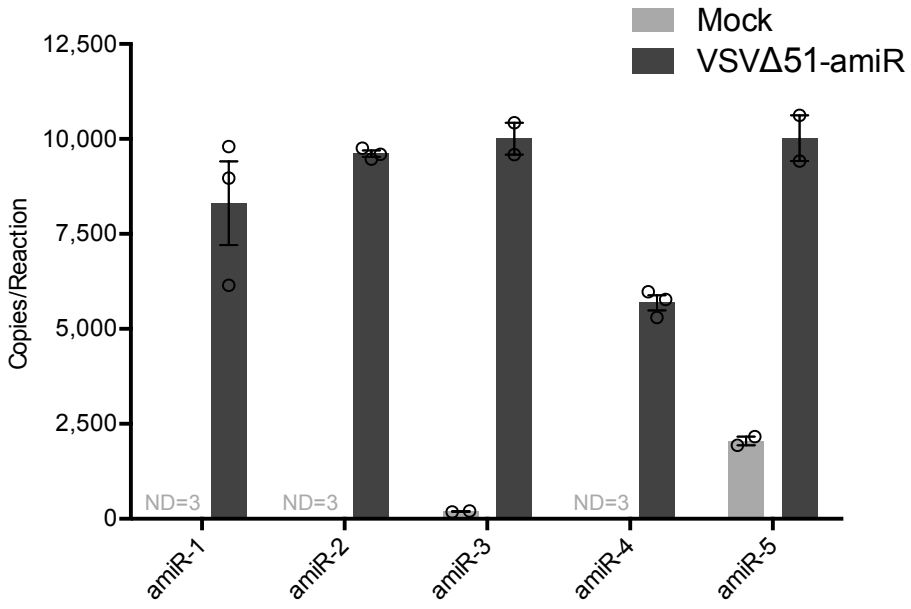
Mock
VSVΔ51-amiR
12,500
10,000
7,500
5,000
2,500
0
Copies/Reaction
ND=3
ND=3
ND=3
amiR-1
amiR-2
amiR-3
amiR-4
amiR-5

Appendix 2. ARID1A CRISPR-Cas9 knockout validation. (**a**) ARID1A expression levels of PANC1 and 786-0 WT, ARID1A KO bulk populations and clonal populations compared to GAPDH loading control expression determined by Western blotting. (**b**) T7 assay on genomic DNA of PANC1 and 786-0 WT, ARID1A KO bulk populations and clonal populations. Primers sets specific for gRNA targeting regions of the ARID1A gene were used to amplify this specific portion of the gene before performing the T7 assay. PCR products were resolved by agarose gel electrophoresis and expected amplicon size is indicated. Assays performed by Hayley McKay and Dr. Larissa Pikor.

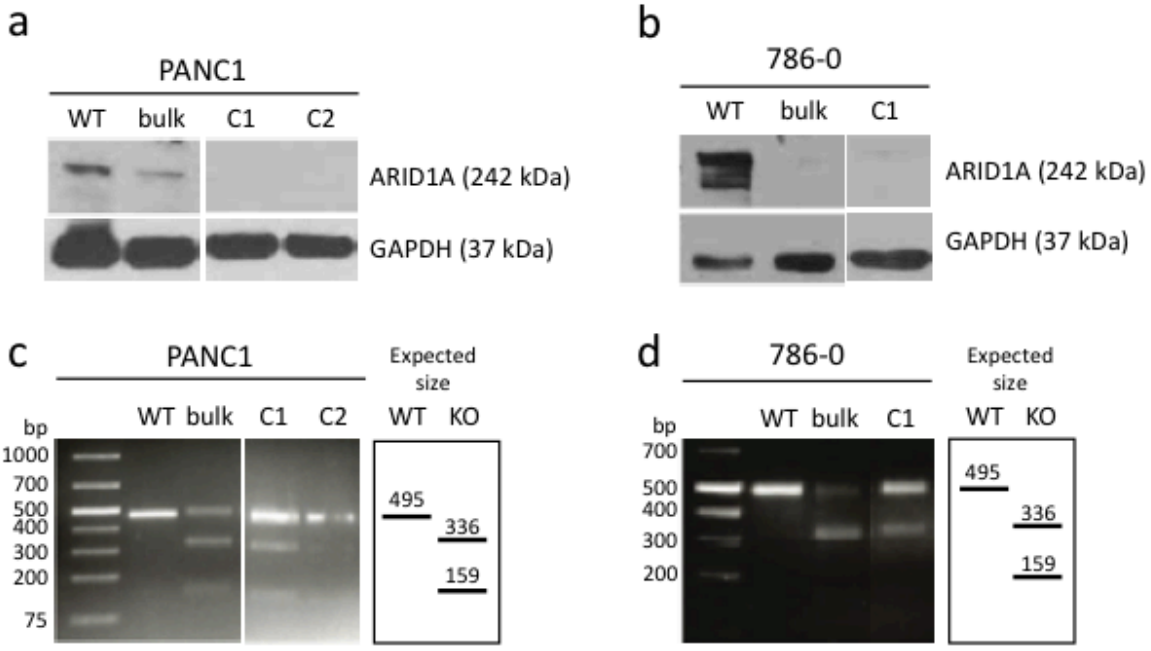
a
PANC1
WT
bulk
C1
C2
ARID1A (242 kDa)
GAPDH (37 kDa)
b
786-0
WT
bulk
C1
ARID1A (242 kDa)
GAPDH (37 kDa)
c
PANC1
Expected size
WT
KO
bp
1000
700
500
400
300
200
75
495
336
159
d
786-0
Expected size
WT
KO
bp
700
500
400
300
200
495
336
159

Appendix 3. RT-qPCR validation analysis of differentially expressed genes involved in immune function found to be downregulated in ARID1A$^{-/-}$ PANC1 cells compared to WT by NGS. (**a**) A selection of viral immunity-related genes was chosen from the NGS results. Selection performed by Adrian Pelin. (**b**) Validation of expression was conducted in ARID1A$^{-/-}$ PANC1 clone 1 (C1) and clone 2 (C2) cells; two distinct clonal populations. Gene expression fold change relative to WT cell expression of transcripts was calculated and plotted. Error bars represent s.e.m. for 2 biological replicates per condition. Experiment performed by Hayley McKay.

a

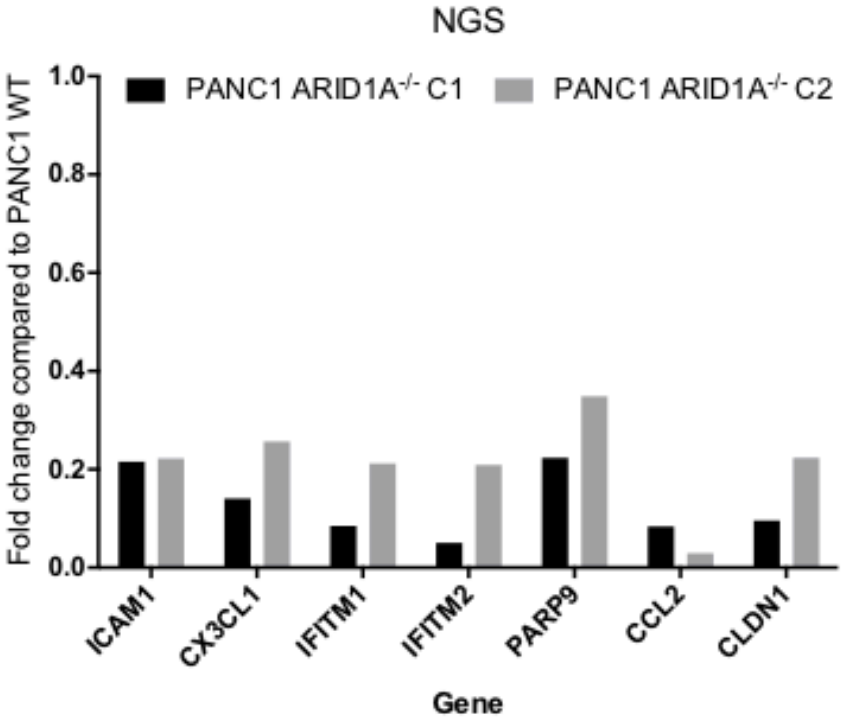
NGS
PANC1 ARID1A-/- C1
PANC1 ARID1A-/- C2
Fold change compared to PANC1 WT
1.0
0.8
0.6
0.4
0.2
0.0
ICAM1
CX3CL1
IFITM1
IFITM2
PARP9
CCL2
CLDN1
Gene

b

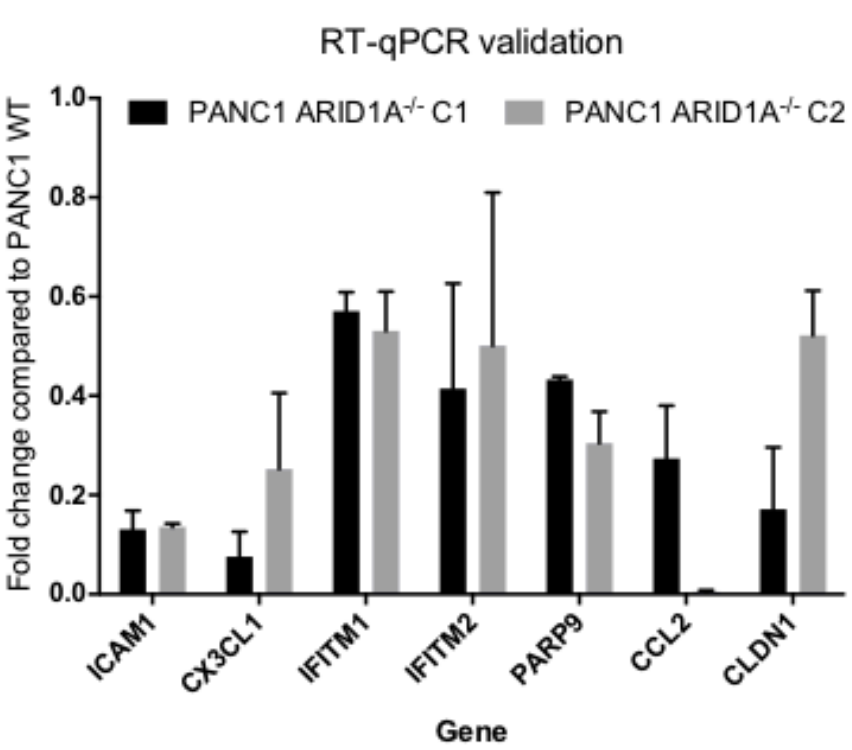
RT-qPCR validation
PANC1 ARID1A-/- C1
PANC1 ARID1A-/- C2
Fold change compared to PANC1 WT
1.0
0.8
0.6
0.4
0.2
0.0
ICAM1
CX3CL1
IFITM1
IFITM2
PARP9
CCL2
CLDN1
Gene

Appendix 4. Experimental outlines of VSVΔ51-amiR-4 and GSK126 treated cell lines in Figure 4.11.

HPAF-II

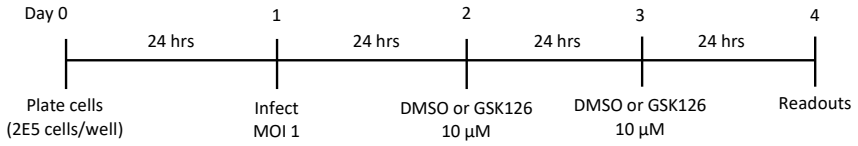

BxPC-3

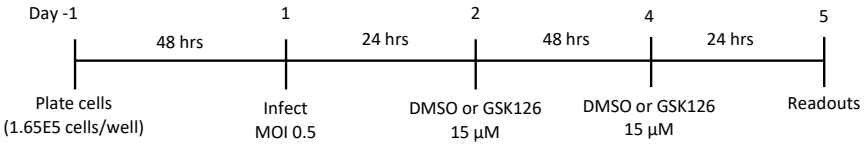

786-0

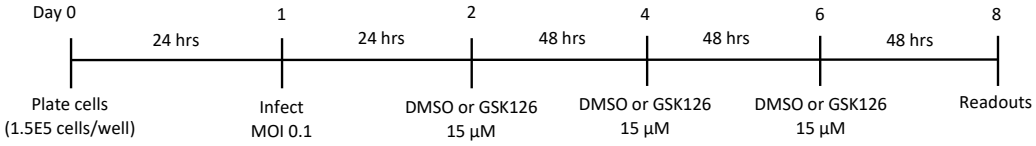

P025

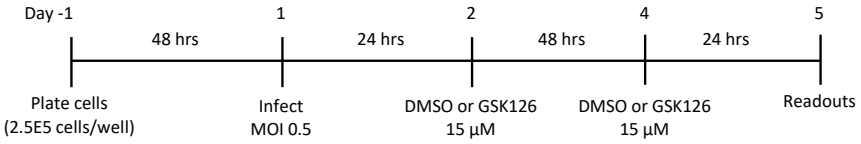

Appendix 5. Additional information on flow cytometry assessment of infected cells with or without GSK126 treatment. (**a**) Experimental outline of cell treatment carried in **Figure 4.13e** and (**b**) gating strategy used for sample analysis with 4T1 data used as an example.

a

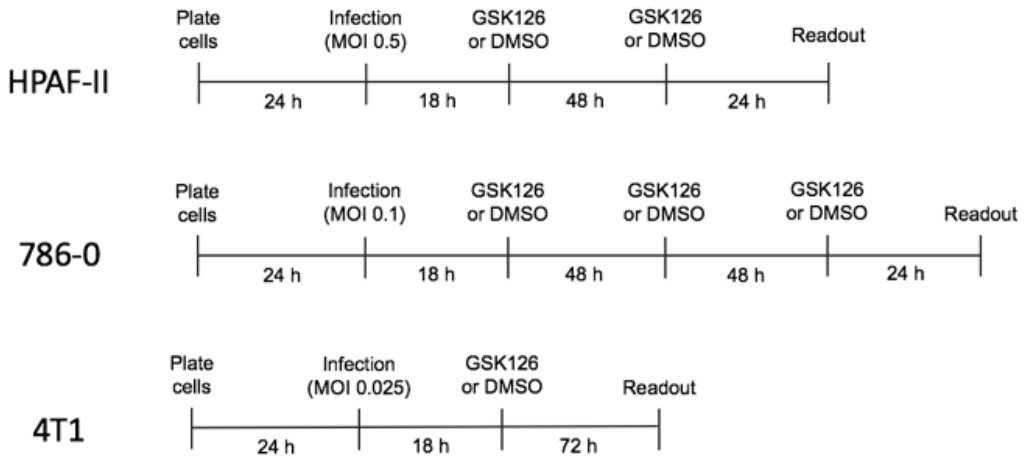
HPAF-II
Plate cells
Infection (MOI 0.5)
GSK126 or DMSO
GSK126 or DMSO
Readout
24 h
18 h
48 h
24 h
786-0
Plate cells
Infection (MOI 0.1)
GSK126 or DMSO
GSK126 or DMSO
GSK126 or DMSO
Readout
24 h
18 h
48 h
48 h
24 h
4T1
Plate cells
Infection (MOI 0.025)
GSK126 or DMSO
Readout
24 h
18 h
72 h

b

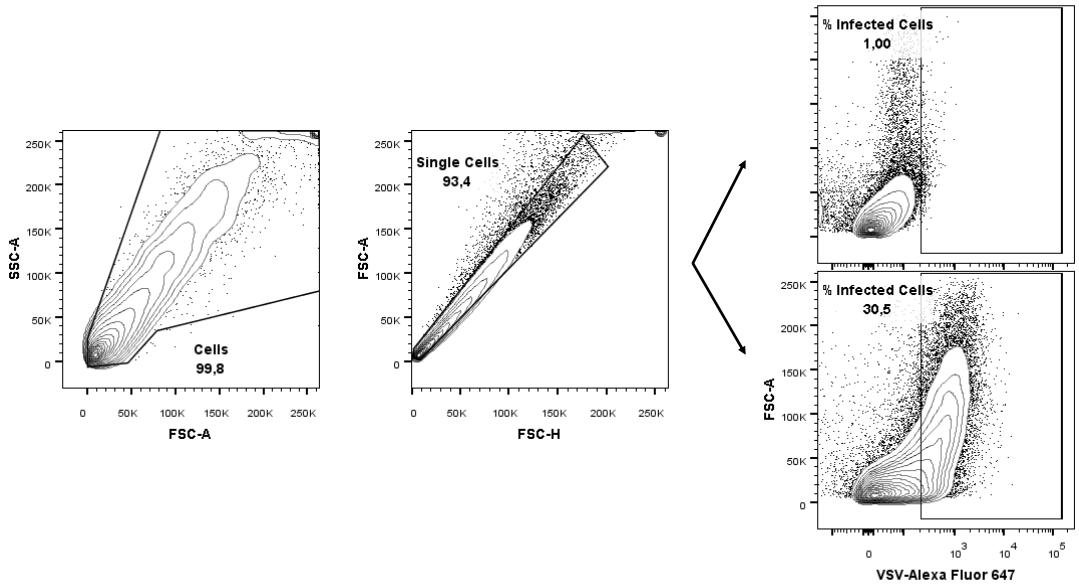
SSC-A
FSC-A
Cells
99,8
FSC-A
FSC-H
Single Cells
93,4
% Infected Cells
1,00
% Infected Cells
30,5
FSC-A
VSV-Alexa Fluor 647

Appendix 6. Characterization of small extracellular vesicles. (**a**) Representative electron microscopy photomicrographs of Mel888 human melanoma-derived SEVs infected with MRBΔG at MOI 1. Pictures show the absence bullet-shaped rhabdovirus virions from SEV preparation. Scale bar = 100 nm. (**b**) ALIX (SEV marker) and calreticulin (specific cell-associated marker) immunoblotting analysis of purified SEVs and whole Mel888 cell lysates. Experiments performed by Dr. Vicki Jennings.

a

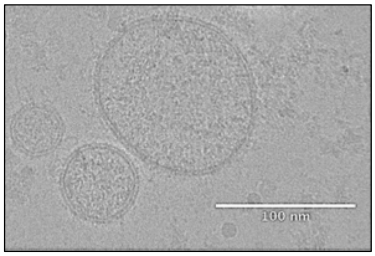

b

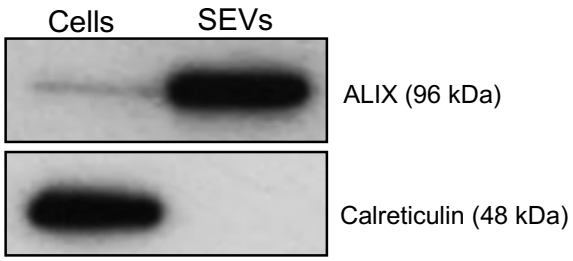

Appendix 7. Assessment of relative levels of extracellular vesicle-encapsulated miRNA compared to free miRNAs or externally attached miRNAs on extracellular vesicles. (**a**) SEVs collected from 786-0 and HPAF-II cells infected or not with MRBΔG-amiR-4 at MOI=1 48 hpi. To remove free, non-encapsulated RNA, an RNase protection assay was performed (RNase A, 1 unit/sample, 30 min). RT-qPCR analysis of amiR-4 levels was conducted on purified SEV RNA. n=1 per condition. (**b**) To show RNase A activity, 1 µg 786-0 cellular RNA was treated with or without 1 unit of RNase A for 30 min. Samples were then resolved using agarose gel electrophoresis.

a

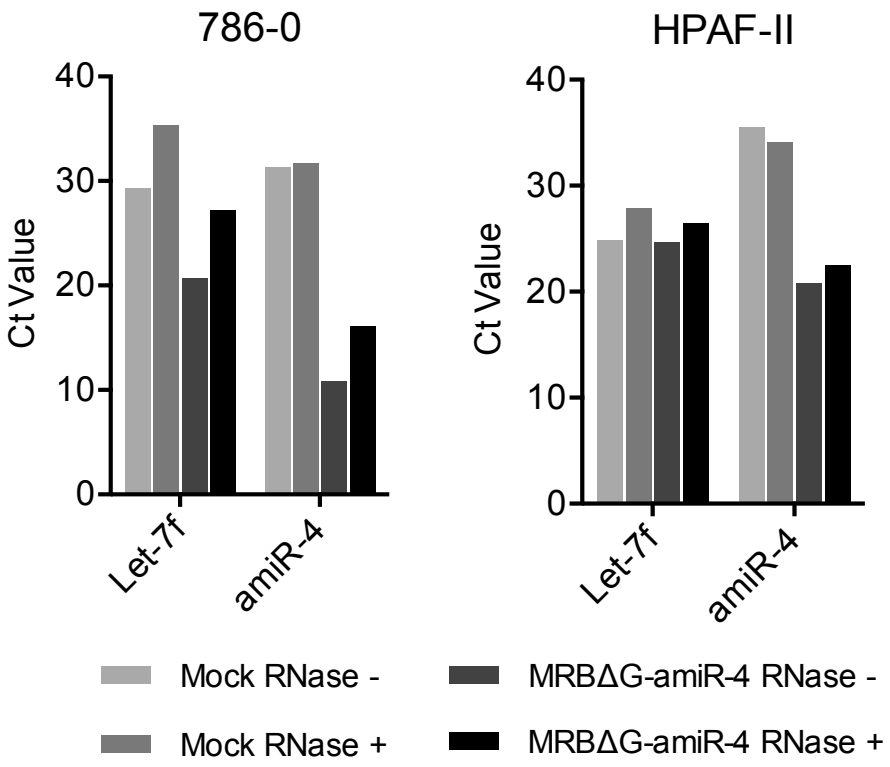

b

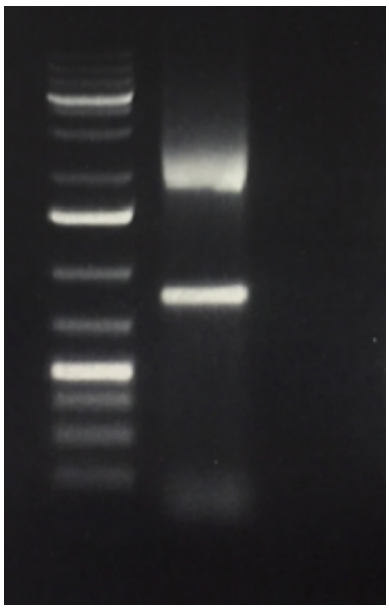

1. 1 kb Plus DNA ladder
2. Untreated RNA
3. RNase A treated RNA

Appendix 8. Experimental outlines of extracellular vesicle education and GSK126 treatment of naïve cells. Experimental outlines of SEV-educated and GSK126-treated cell lines in **Figure 4.17** are shown.

HPAF-II

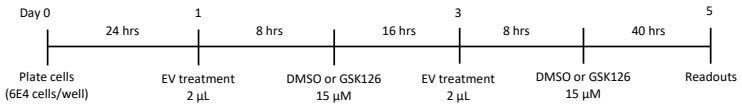

HPAF-II

Condition	SEVs transferred/well
Mock	2.3E6
MRBΔG-amiR-NTC	8.1E7
MRBΔG-amiR-4	7.6E7

BxPC-3

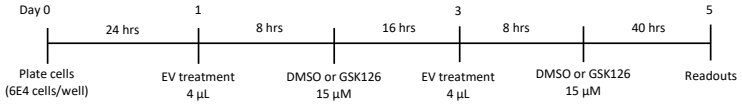

BxPC-3

Condition	SEVs transferred/well
Mock	4.6E6
MRBΔG-amiR-NTC	1.8E8
MRBΔG-amiR-4	1.5E8

786-0

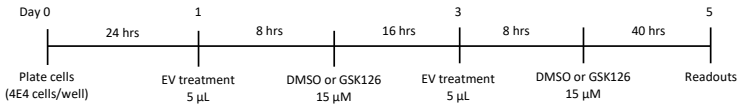

786-0

Condition	SEVs transferred/well
Mock	5.8E6
MRBΔG-amiR-NTC	2.0E8
MRBΔG-amiR-4	1.9E8

P025

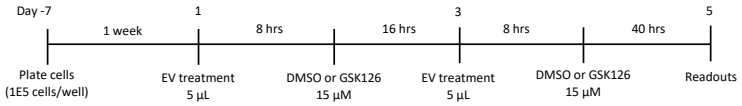

P025

Condition	SEVs transferred/well
Mock	5.8E6
MRBΔG-amiR-NTC	2.0E8
MRBΔG-amiR-4	1.9E8

Appendix 9. Characterization of 4T1 Rab27$^{-/-}$ cells and their derived extracellular vesicles. (**a**) Immunoblotting analysis of 4T1 WT and Rab27a CRISPR-Cas9 KO clonal cell lines. β-tubulin is included as a loading control. (**b**) NTA quantification and size distribution profiles of 4T1 WT and Rab27a$^{-/-}$ cell-derived SEVs. ND = not detected.

a

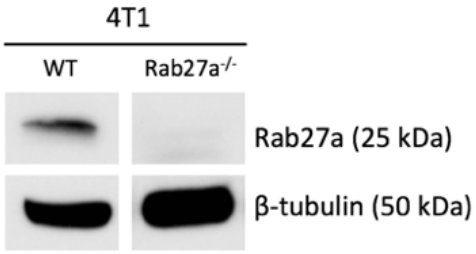
4T1
WT
Rab27a-/-
Rab27a (25 kDa)
β-tubulin (50 kDa)

b

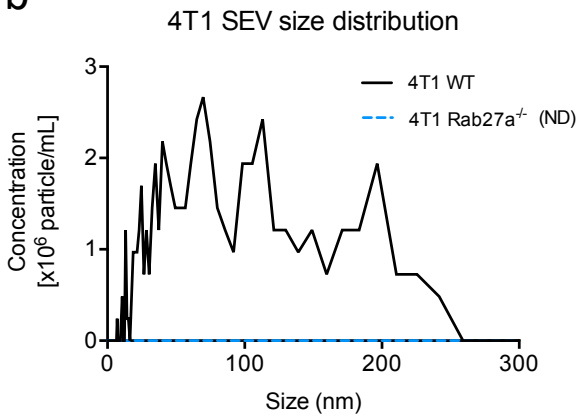
4T1 SEV size distribution
4T1 WT
4T1 Rab27a-/- (ND)
Concentration [x10^6 particle/mL]
0
1
2
3
0
100
200
300
Size (nm)

Appendix 10. Viral titers remain unchanged in 4T1 Rab27a$^{-/-}$ cells compared to 4T1 WT cells. (**a**) 4T1 WT or Rab27a$^{-/-}$ cells produce similar amounts of virus following VSVΔ51 infection at indicated MOIs 48 hpi as quantified by plaque assay. Two-way ANOVA with Sidak's multiple comparison test, ns $p > 0.05$. Error bars represent s.e.m. of three biological replicates. (**b,c**) 4T1 WT or Rab27a$^{-/-}$ cells infected with VSVΔ51 or VSVΔ51-amiR-4 (MOI 0.025) and treated with vehicle control (DMSO) and GSK126 (15 μm) for 72 hours. Production of infectious particles for each condition was quantified by plaque assay. Two-way ANOVA with Sidak's multiple comparison test, ** $p < 0.01$. Data represent ± s.e.m. of four biological replicates for wild-type cells and two for Rab27a$^{-/-}$ cells. Experiments performed in collaboration with Brian Laight.

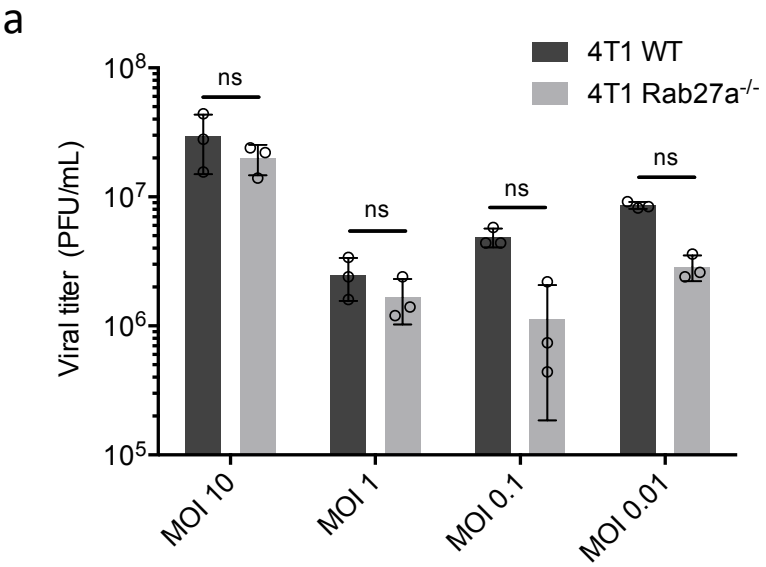
a
4T1 WT
4T1 Rab27a-/-
Viral titer (PFU/mL)
ns
MOI 10
MOI 1
MOI 0.1
MOI 0.01

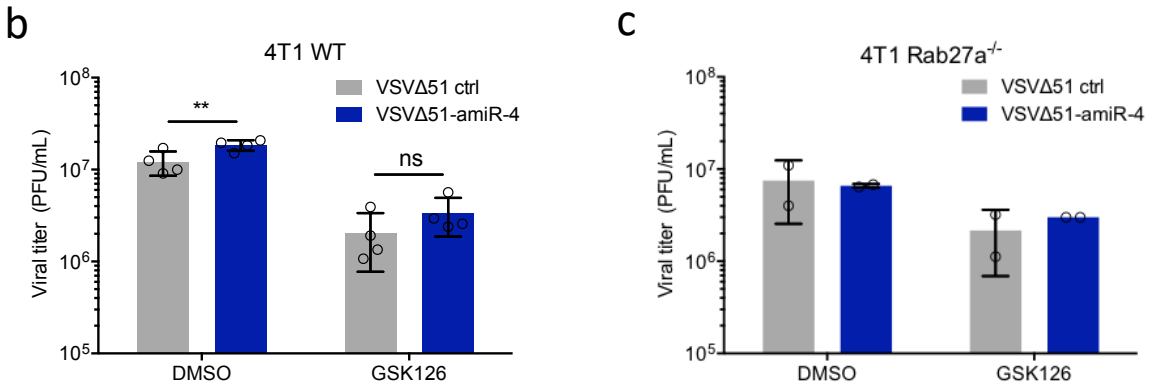
b
4T1 WT
VSVΔ51 ctrl
VSVΔ51-amiR-4
Viral titer (PFU/mL)
**
ns
DMSO
GSK126
c
4T1 Rab27a-/-
VSVΔ51 ctrl
VSVΔ51-amiR-4
Viral titer (PFU/mL)
DMSO
GSK126

BIBLIOGRAPHY

1. Canadian Cancer Society's Advisory Committee on Cancer Statistics. *Canadian Cancer Statistics 2017*. (2017).
2. Bray, F. *et al.* Global cancer statistics 2018: GLOBOCAN estimates of incidence and mortality worldwide for 36 cancers in 185 countries. *CA. Cancer J. Clin.* **68**, 394–424 (2018).
3. Rawla, P., Sunkara, T. & Gaduputi, V. Epidemiology of Pancreatic Cancer: Global Trends, Etiology and Risk Factors. *World J. Oncol.* **10**, 10–27 (2019).
4. Ferlay J EM, Lam F, Colombet M, Mery L, Pineros M, Znaor A, Soerjomataram I, et al. *Global cancer observatory: cancer today*.
5. Rahib, L. *et al.* Projecting Cancer Incidence and Deaths to 2030: The Unexpected Burden of Thyroid, Liver, and Pancreas Cancers in the United States. (2014). doi:10.1158/0008-5472.CAN-14-0155
6. Canadian Cancer Society's Advisory Committee on Cancer Statistics. *Canadian Cancer Statistics 2019*. (2019).
7. Seufferlein, T., Bachet, J. B., Van cutsem, E. & Rougier, P. Pancreatic adenocarcinoma: ESMO-ESDO clinical practice guidelines for diagnosis, treatment and follow-up. *Ann. Oncol.* **23**, (2012).
8. Winter, J. M. *et al.* Survival after resection of pancreatic adenocarcinoma: results from a single institution over three decades. *Ann. Surg. Oncol.* **19**, 169–75 (2012).
9. Zhang, Q. *et al.* Pancreatic Cancer Epidemiology, Detection, and Management. *Gastroenterology Research and Practice* **2016**, (2016).
10. Clancy, T. E. Surgery for Pancreatic Cancer. *Hematol. Oncol. Clin. North Am.* **29**, 701–716 (2015).
11. Strobel, O., Neoptolemos, J., Jäger, D. & Büchler, M. W. Optimizing the outcomes of pancreatic cancer surgery. *Nat. Rev. Clin. Oncol.* **16**, 11–26 (2019).
12. Neoptolemos, J. P. *et al.* A Randomized Trial of Chemoradiotherapy and Chemotherapy after Resection of Pancreatic Cancer. *N. Engl. J. Med.* **350**, 1200–1210 (2004).
13. Neoptolemos, J. P. *et al.* Adjuvant chemotherapy with fluorouracil plus folinic acid vs gemcitabine following pancreatic cancer resection: A randomized controlled trial. *JAMA - J. Am. Med. Assoc.* **304**, 1073–1081 (2010).
14. Oettle, H. *et al.* Adjuvant chemotherapy with gemcitabine and long-term outcomes among patients with resected pancreatic cancer: the CONKO-001 randomized trial. *JAMA* **310**, 1473–81 (2013).
15. Moore, M. J. *et al.* Erlotinib plus gemcitabine compared with gemcitabine alone in patients with advanced pancreatic cancer: a phase III trial of the National Cancer Institute of Canada Clinical Trials Group. *J. Clin. Oncol.* **25**, 1960–6 (2007).
16. Von Hoff, D. D. *et al.* Increased Survival in Pancreatic Cancer with nab-Paclitaxel plus Gemcitabine. *N. Engl. J. Med.* **369**, 1691–1703 (2013).
17. Conroy, T. *et al.* FOLFIRINOX versus Gemcitabine for Metastatic Pancreatic Cancer. *N. Engl. J. Med.* **364**, 1817–1825 (2011).
18. Wang-Gillam, A. *et al.* Nanoliposomal irinotecan with fluorouracil and folinic acid in metastatic pancreatic cancer after previous gemcitabine-based therapy (NAPOLI-1): a global, randomised, open-label, phase 3 trial. *Lancet* **387**, 545–557 (2016).

19. Morris, J. P., Wang, S. C. & Hebrok, M. KRAS, Hedgehog, Wnt and the twisted developmental biology of pancreatic ductal adenocarcinoma. *Nat. Rev. Cancer* **10**, 683–95 (2010).
20. Adamska, A., Domenichini, A. & Falasca, M. Pancreatic Ductal Adenocarcinoma: Current and Evolving Therapies. *Int. J. Mol. Sci.* **18**, (2017).
21. Kleeff, J. *et al.* Pancreatic cancer. *Nat. Rev. Dis. Prim.* **2**, 16022 (2016).
22. Makohon-Moore, A. & Iacobuzio-Donahue, C. A. Pancreatic cancer biology and genetics from an evolutionary perspective. *Nat. Rev. Cancer* **16**, 553–65 (2016).
23. Karanikas, M. *et al.* Pancreatic cancer from molecular pathways to treatment opinion. *Journal of Cancer* **7**, 1328–1339 (2016).
24. Long, J. *et al.* Overcoming drug resistance in pancreatic cancer. *Expert Opin. Ther. Targets* **15**, 817–28 (2011).
25. Gnanamony, M. & Gondi, C. S. Chemoresistance in pancreatic cancer: Emerging concepts. *Oncol. Lett.* **13**, 2507–2513 (2017).
26. Xu, J. *et al.* MiR-497 downregulation contributes to the malignancy of pancreatic cancer and associates with a poor prognosis. *Oncotarget* **5**, 6983–6993 (2014).
27. Liang, C. *et al.* MicroRNA-33a-mediated downregulation of Pim-3 kinase expression renders human pancreatic cancer cells sensitivity to gemcitabine. *Oncotarget* **6**, 14440–14455 (2015).
28. Tréhoux, S. *et al.* Micro-RNAs miR-29a and miR-330-5p function as tumor suppressors by targeting the MUC1 mucin in pancreatic cancer cells. *Biochim. Biophys. Acta* **1853**, 2392–403 (2015).
29. Jacobetz, M. A. *et al.* Hyaluronan impairs vascular function and drug delivery in a mouse model of pancreatic cancer. *Gut* **62**, 112–20 (2013).
30. Prakash, J. Cancer-Associated Fibroblasts: Perspectives in Cancer Therapy. *Trends in cancer* **2**, 277–279 (2016).
31. Karamitopoulou, E. Tumour microenvironment of pancreatic cancer: immune landscape is dictated by molecular and histopathological features. *British Journal of Cancer* **121**, 5–14 (2019).
32. Zhu, Y. *et al.* CSF1/CSF1R blockade reprograms tumor-infiltrating macrophages and improves response to T-cell checkpoint immunotherapy in pancreatic cancer models. *Cancer Res.* **74**, 5057–69 (2014).
33. Zhang, Y. *et al.* Novel agents for pancreatic ductal adenocarcinoma: emerging therapeutics and future directions. *J. Hematol. Oncol.* **11**, 14 (2018).
34. Olive, K. P. *et al.* Chemotherapy in a Mouse Model of Pancreatic Cancer. *Cancer Res.* **324**, 1457–1461 (2010).
35. Provenzano, P. P. *et al.* Enzymatic targeting of the stroma ablates physical barriers to treatment of pancreatic ductal adenocarcinoma. *Cancer Cell* **21**, 418–29 (2012).
36. Feig, C. *et al.* Targeting CXCL12 from FAP-expressing carcinoma-associated fibroblasts synergizes with anti-PD-L1 immunotherapy in pancreatic cancer. *Proc. Natl. Acad. Sci. U. S. A.* **110**, 20212–7 (2013).
37. Hofheinz, R.-D. *et al.* Stromal antigen targeting by a humanised monoclonal antibody: an early phase II trial of sibrotuzumab in patients with metastatic colorectal cancer. *Onkologie* **26**, 44–8 (2003).
38. Narra, K. *et al.* Phase II trial of single agent Val-boroPro (Talabostat) inhibiting Fibroblast Activation Protein in patients with metastatic colorectal cancer. *Cancer Biol. Ther.* **6**, 1691–9 (2007).

39. Erkan, M. *et al.* The role of stroma in pancreatic cancer: diagnostic and therapeutic implications. *Nat. Rev. Gastroenterol. Hepatol.* **9**, 454–67 (2012).
40. Cros, J., Raffenne, J., Couvelard, A. & Poté, N. Tumor Heterogeneity in Pancreatic Adenocarcinoma. *Pathobiology* **85**, 64–71 (2018).
41. Allaway, R. J. *et al.* Genomic characterization of patient-derived xenograft models established from fine needle aspirate biopsies of a primary pancreatic ductal adenocarcinoma and from patient-matched metastatic sites. *Oncotarget* **7**, 17087–17102 (2016).
42. Berry, W. *et al.* Endoscopic ultrasound-guided fine-needle aspirate-derived preclinical pancreatic cancer models reveal panitumumab sensitivity in KRAS wild-type tumors. *Int. J. Cancer* **140**, 2331–2343 (2017).
43. Keller, B. A., Wedge, M.-È., Surendran, A. & Ilkow, C. S. Generating Primary Models of Human Cancer to Aid in the Development of Clinically Relevant Oncolytic Viruses. in 271–284 (2020). doi:10.1007/978-1-4939-9794-7_18
44. Derose, Y. S. *et al.* Tumor grafts derived from women with breast cancer authentically reflect tumor pathology, growth, metastasis and disease outcomes. *Nat. Med.* **17**, 1514–1520 (2011).
45. Peng, S. *et al.* Tumor grafts derived from patients with head and neck squamous carcinoma authentically maintain the molecular and histologic characteristics of human cancers. *J. Transl. Med.* **11**, 198 (2013).
46. Leong, T. L. *et al.* Genomic characterisation of small cell lung cancer patient-derived xenografts generated from endobronchial ultrasound-guided transbronchial needle aspiration specimens. *PLoS One* **9**, (2014).
47. Kelly, E. & Russell, S. J. History of oncolytic viruses: genesis to genetic engineering. *Mol. Ther.* **15**, 651–9 (2007).
48. (1827, G. D.-T. A. J. of the M. S. & 1904, undefined. The influence of complicating diseases upon leukaemia. *search.proquest.com*
49. PELNER, L., FOWLER, G. A. & NAUTS, H. C. Effects of concurrent infections and their toxins on the course of leukemia. *Acta Med. Scand. Suppl.* **338**, 1–47 (1958).
50. Pasquinucci, G. Possible effect of measles on leukaemia. *Lancet (London, England)* **1**, 136 (1971).
51. Gross, S. MEASLES AND LEUKÆMIA. *Lancet* **297**, 397–398 (1971).
52. SOUTHAM, C. M. & MOORE, A. E. Clinical studies of viruses as antineoplastic agents with particular reference to Egypt 101 virus. *Cancer* **5**, 1025–34 (1952).
53. Carter, S. K. IMMUNOTHERAPY OF CANCER IN MAN: CURRENT STATUS AND PROSPECTUS. *Ann. N. Y. Acad. Sci.* **277**, 722–740 (1976).
54. Garber, K. China Approves World's First Oncolytic Virus Therapy For Cancer Treatment. *JNCI J. Natl. Cancer Inst.* **98**, 298–300 (2006).
55. Greig, S. L. Talimogene Laherparepvec: First Global Approval. *Drugs* **76**, 147–154 (2016).
56. Pikor, L. A., Bell, J. C. & Diallo, J. S. Oncolytic Viruses: Exploiting Cancer's Deal with the Devil. *Trends in Cancer* **1**, 266–277 (2015).
57. Stephanie J. DeWitte-Orr and Karen L. Mossman. The antiviral effects of extracellular dsRNA. in *Viruses and Interferon: Current Research* (ed. Mossman, K. L.) 1–18 (Caister Academic Press, 2011).
58. Ebrahimi, S. *et al.* Interferon-Mediated Tumor Resistance to Oncolytic Virotherapy. *J. Cell. Biochem.* **118**, 1994–1999 (2017).

59. Matveeva, O. V & Chumakov, P. M. Defects in interferon pathways as potential biomarkers of sensitivity to oncolytic viruses. *Rev. Med. Virol.* **28**, e2008 (2018).
60. Kaufman, H. L., Kohlhapp, F. J. & Zloza, A. Oncolytic viruses: a new class of immunotherapy drugs. *Nat. Rev. Drug Discov.* **14**, 642–62 (2015).
61. Arulanandam, R. *et al.* VEGF-Mediated Induction of PRD1-BF1/Blimp1 Expression Sensitizes Tumor Vasculature to Oncolytic Virus Infection. *Cancer Cell* **28**, 210–24 (2015).
62. Breitbach, C. J. *et al.* Intravenous delivery of a multi-mechanistic cancer-targeted oncolytic poxvirus in humans. *Nature* **477**, 99–102 (2011).
63. Ilkow, C. S. *et al.* Reciprocal cellular cross-talk within the tumor microenvironment promotes oncolytic virus activity. *Nat. Med.* **21**, 530–6 (2015).
64. Altomonte, J. *et al.* Antifibrotic properties of transarterial oncolytic vsv therapy for hepatocellular carcinoma in rats with thioacetamide-induced liver fibrosis. *Mol. Ther.* **21**, 2032–2042 (2013).
65. Erkan, M. *et al.* How fibrosis influences imaging and surgical decisions in pancreatic cancer. *Front. Physiol.* **3**, 389 (2012).
66. Hammerich, L., Binder, A. & Brody, J. D. In situ vaccination: Cancer immunotherapy both personalized and off-the-shelf. *Molecular Oncology* **9**, 1966–1981 (2015).
67. Hammerich, L., Bhardwaj, N., Kohrt, H. E. & Brody, J. D. In situ vaccination for the treatment of cancer. *Immunotherapy* **8**, 315–330 (2016).
68. Achard, C. *et al.* Lighting a Fire in the Tumor Microenvironment Using Oncolytic Immunotherapy. *EBioMedicine* **31**, 17–24 (2018).
69. Raja, J., Ludwig, J. M., Gettinger, S. N., Schalper, K. A. & Kim, H. S. Oncolytic virus immunotherapy: Future prospects for oncology 11 Medical and Health Sciences 1107 Immunology 11 Medical and Health Sciences 1112 Oncology and Carcinogenesis. *Journal for ImmunoTherapy of Cancer* **6**, (2018).
70. Gujar, S., Pol, J. G. & Kroemer, G. Heating it up: Oncolytic viruses make tumors 'hot' and suitable for checkpoint blockade immunotherapies. *OncoImmunology* **7**, (2018).
71. Andtbacka, R. H. I. *et al.* Talimogene laherparepvec improves durable response rate in patients with advanced melanoma. *J. Clin. Oncol.* **33**, 2780–2788 (2015).
72. Eissa, I. R. *et al.* The Current Status and Future Prospects of Oncolytic Viruses in Clinical Trials against Melanoma, Glioma, Pancreatic, and Breast Cancers. *Cancers (Basel).* **10**, (2018).
73. Keller, B. A. & Bell, J. C. Oncolytic viruses-immunotherapeutics on the rise. *J. Mol. Med. (Berl).* **94**, 979–91 (2016).
74. Hirooka, Y. *et al.* A Phase I clinical trial of EUS-guided intratumoral injection of the oncolytic virus, HF10 for unresectable locally advanced pancreatic cancer. *BMC Cancer* **18**, 596 (2018).
75. Hecht, J. R. *et al.* A phase I/II trial of intratumoral endoscopic ultrasound injection of ONYX-015 with intravenous gemcitabine in unresectable pancreatic carcinoma. *Clin. Cancer Res.* **9**, 555–61 (2003).
76. Mahalingam, D. *et al.* A Phase II Study of Pelareorep (REOLYSIN®) in Combination with Gemcitabine for Patients with Advanced Pancreatic Adenocarcinoma. *Cancers (Basel).* **10**, 160 (2018).
77. Phillips, M. B. *et al.* Current understanding of reovirus oncolysis mechanisms. *Oncolytic Virotherapy* **7**, 53 (2018).
78. Travassos da Rosa, A. P., Tesh, R. B., Travassos da Rosa, J. F., Herve, J. P. & Main,

A. J. Carajas and Maraba viruses, two new vesiculoviruses isolated from phlebotomine sand flies in Brazil. *Am. J. Trop. Med. Hyg.* **33**, 999–1006 (1984).
79. Brun, J. *et al.* Identification of genetically modified Maraba virus as an oncolytic rhabdovirus. *Mol. Ther.* **18**, 1440–9 (2010).
80. Walker, P. J. *et al.* ICTV virus taxonomy profile: Rhabdoviridae. *J. Gen. Virol.* **99**, 447–448 (2018).
81. Finkelshtein, D., Werman, A., Novick, D., Barak, S. & Rubinstein, M. LDL receptor and its family members serve as the cellular receptors for vesicular stomatitis virus. *Proc. Natl. Acad. Sci.* **110**, 7306–7311 (2013).
82. Sun, X., Yau, V. K., Briggs, B. J. & Whittaker, G. R. Role of clathrin-mediated endocytosis during vesicular stomatitis virus entry into host cells. *Virology* **338**, 53–60 (2005).
83. Cureton, D. K., Massol, R. H., Whelan, S. P. J. & Kirchhausen, T. The Length of Vesicular Stomatitis Virus Particles Dictates a Need for Actin Assembly during Clathrin-Dependent Endocytosis. *PLoS Pathog.* **6**, e1001127 (2010).
84. Stanifer, M. L., Cureton, D. K. & Whelan, S. P. J. A recombinant vesicular stomatitis virus bearing a lethal mutation in the glycoprotein gene uncovers a second site suppressor that restores fusion. *J. Virol.* **85**, 8105–15 (2011).
85. Lyles, D. S., Kuzmin, I. V. & Rupprecht, C. E. Rhabdoviridae. in *Fields Virology* 886–922 (Wolters Kluwer Health/Lippincott Williams & Wilkins, 2013). doi:10.1093/cid/ciu346
86. Stojdl, D. F. *et al.* VSV strains with defects in their ability to shutdown innate immunity are potent systemic anti-cancer agents. *Cancer Cell* **4**, 263–275 (2003).
87. Matsuda, T., Karube, H. & Aruga, A. A Comparative Safety Profile Assessment of Oncolytic Virus Therapy Based on Clinical Trials. *Ther. Innov. Regul. Sci.* **52**, 430–437 (2018).
88. Ferguson, M. S., Lemoine, N. R. & Wang, Y. Systemic delivery of oncolytic viruses: hopes and hurdles. *Adv. Virol.* **2012**, 805629 (2012).
89. Filley, A. C. & Dey, M. Immune System, Friend or Foe of Oncolytic Virotherapy? *Front. Oncol.* **7**, 106 (2017).
90. Yokoda, R. *et al.* Oncolytic virus delivery: from nano-pharmacodynamics to enhanced oncolytic effect. *Oncolytic Virotherapy* **Volume 6**, 39–49 (2017).
91. Harrington, K., Freeman, D. J., Kelly, B., Harper, J. & Soria, J.-C. Optimizing oncolytic virotherapy in cancer treatment. *Nat. Rev. Drug Discov.* **18**, 689–706 (2019).
92. Paglino, J. C. & van den Pol, A. N. Vesicular stomatitis virus has extensive oncolytic activity against human sarcomas: rare resistance is overcome by blocking interferon pathways. *J. Virol.* **85**, 9346–58 (2011).
93. Escobar-Zarate, D., Liu, Y.-P., Suksanpaisan, L., Russell, S. J. & Peng, K.-W. Overcoming cancer cell resistance to VSV oncolysis with JAK1/2 inhibitors. *Cancer Gene Ther.* **20**, 582–9 (2013).
94. Moerdyk-Schauwecker, M. *et al.* Resistance of pancreatic cancer cells to oncolytic vesicular stomatitis virus: Role of type I interferon signaling. *Virology* **436**, 221–234 (2013).
95. Diallo, J.-S. *et al.* A high-throughput pharmacoviral approach identifies novel oncolytic virus sensitizers. *Mol. Ther.* **18**, 1123–9 (2010).
96. Arulanandam, R. *et al.* Microtubule disruption synergizes with oncolytic virotherapy by inhibiting interferon translation and potentiating bystander killing. *Nat. Commun.*

6, (2015).
97. McKenzie, B. A. *et al.* In vitro screen of a small molecule inhibitor drug library identifies multiple compounds that synergize with oncolytic myxoma virus against human brain tumor-initiating cells. *Neuro. Oncol.* **17**, 1086–1094 (2015).
98. Sharma, S. & Petsalaki, E. Application of CRISPR-Cas9 based genome-wide screening approaches to study cellular signalling mechanisms. *International Journal of Molecular Sciences* **19**, (2018).
99. Tzelepis, K. *et al.* A CRISPR Dropout Screen Identifies Genetic Vulnerabilities and Therapeutic Targets in Acute Myeloid Leukemia. *Cell Rep.* **17**, 1193–1205 (2016).
100. Rose, E., Bell, J. & Kekre, N. Identifying Mechanisms of Resistance to Oncolytic Virotherapy in Acute Leukemia Through a Genome-wide CRISPR Screen. (Univeristy of Ottawa, 2018). doi:10.20381/ruor-22367
101. Fire, A. *et al.* Potent and specific genetic interference by double-stranded RNA in caenorhabditis elegans. *Nature* **391**, 806–811 (1998).
102. Han, J. *et al.* The Drosha-DGCR8 complex in primary microRNA processing. *Genes Dev.* **18**, 3016–3027 (2004).
103. Okada, C. *et al.* A high-Resolution structure of the pre-microrna nuclear export machinery. *Science (80-.).* **326**, 1275–1279 (2009).
104. Denli, A. M., Tops, B. B. J., Plasterk, R. H. A., Ketting, R. F. & Hannon, G. J. Processing of primary microRNAs by the Microprocessor complex. *Nature* **432**, 231–235 (2004).
105. Meijer, H. A., Smith, E. M. & Bushell, M. Regulation of miRNA strand selection: Follow the leader? in *Biochemical Society Transactions* **42**, 1135–1140 (Portland Press Ltd, 2014).
106. Kobayashi, H. & Tomari, Y. RISC assembly: Coordination between small RNAs and Argonaute proteins. *Biochimica et Biophysica Acta - Gene Regulatory Mechanisms* **1859**, 71–81 (2016).
107. Huntzinger, E. & Izaurralde, E. Gene silencing by microRNAs: Contributions of translational repression and mRNA decay. *Nature Reviews Genetics* **12**, 99–110 (2011).
108. Carthew, R. W. & Sontheimer, E. J. Origins and Mechanisms of miRNAs and siRNAs. *Cell* **136**, 642–655 (2009).
109. Ahmadzada, T., Reid, G. & McKenzie, D. R. Fundamentals of siRNA and miRNA therapeutics and a review of targeted nanoparticle delivery systems in breast cancer. *Biophysical Reviews* **10**, 69–86 (2018).
110. Rovira-Rigau, M. *et al.* Bioselection Reveals miR-99b and miR-485 as Enhancers of Adenoviral Oncolysis in Pancreatic Cancer. *Mol. Ther.* **27**, 230–243 (2019).
111. Varble, A. *et al.* An in vivo RNAi screening approach to identify host determinants of virus Replication. *Cell Host Microbe* **14**, 346–356 (2013).
112. Mahoney, D. J. *et al.* Virus-Tumor Interactome Screen Reveals ER Stress Response Can Reprogram Resistant Cancers for Oncolytic Virus-Triggered Caspase-2 Cell Death. *Cancer Cell* **20**, 443–456 (2011).
113. Workenhe, S. T., Ketela, T., Moffat, J., Cuddington, B. P. & Mossman, K. L. Genome-wide lentiviral shRNA screen identifies serine/arginine-rich splicing factor 2 as a determinant of oncolytic virus activity in breast cancer cells. *Oncogene* **35**, 2465–2474 (2016).
114. de Graaf, J. F., de Vor, L., Fouchier, R. A. M. & van den Hoogen, B. G. Armed

oncolytic viruses: A kick-start for anti-tumor immunity. *Cytokine and Growth Factor Reviews* **41**, 28–39 (2018).
115. Phan, M., Watson, M. F., Alain, T. & Diallo, J.-S. Oncolytic Viruses on Drugs: Achieving Higher Therapeutic Efficacy. *ACS Infect. Dis.* **4**, 1448–1467 (2018).
116. Brachtlova, T. & van Beusechem, V. Unleashing the Full Potential of Oncolytic Adenoviruses against Cancer by Applying RNA Interference: The Force Awakens. *Cells* **7**, 228 (2018).
117. Li, X. *et al.* An Artificially Designed Interfering lncRNA Expressed by Oncolytic Adenovirus Competitively Consumes OncomiRs to Exert Antitumor Efficacy in Hepatocellular Carcinoma. *Mol. Cancer Ther.* **15**, 1436–51 (2016).
118. Hartwell, L. H., Szankasi, P., Roberts, C. J., Murray, A. W. & Friend, S. H. Integrating Genetic Approaches into the Discovery of Anticancer Drugs. *Science (80-.).* **278**, 1064–1068 (1997).
119. Lord, C. J. & Ashworth, A. PARP inhibitors: Synthetic lethality in the clinic. *Science (80-.).* **355**, 1152–1158 (2017).
120. Ning, J., Wakimoto, H., Peters, C., Martuza, R. L. & Rabkin, S. D. Rad51 Degradation: Role in Oncolytic Virus-Poly(ADP-Ribose) Polymerase Inhibitor Combination Therapy in Glioblastoma. *J. Natl. Cancer Inst.* **109**, 1–13 (2017).
121. Théry, C., Zitvogel, L. & Amigorena, S. Exosomes: composition, biogenesis and function. *Nat. Rev. Immunol.* **2**, 569–79 (2002).
122. Valadi, H. *et al.* Exosome-mediated transfer of mRNAs and microRNAs is a novel mechanism of genetic exchange between cells. *Nat. Cell Biol.* **9**, 654–659 (2007).
123. Gould, S. J. & Raposo, G. As we wait: coping with an imperfect nomenclature for extracellular vesicles. *J. Extracell. Vesicles* **2**, 20389 (2013).
124. Abels, E. R. & Breakefield, X. O. Introduction to Extracellular Vesicles: Biogenesis, RNA Cargo Selection, Content, Release, and Uptake. *Cellular and Molecular Neurobiology* **36**, 301–312 (2016).
125. Van Niel, G., D'Angelo, G. & Raposo, G. Shedding light on the cell biology of extracellular vesicles. *Nature Reviews Molecular Cell Biology* **19**, 213–228 (2018).
126. Shapiro, J. A. No genome is an island: toward a 21st century agenda for evolution. *Annals of the New York Academy of Sciences* **1447**, 21–52 (2019).
127. Mathieu, M., Martin-Jaular, L., Lavieu, G. & Théry, C. Specificities of secretion and uptake of exosomes and other extracellular vesicles for cell-to-cell communication. *Nature Cell Biology* **21**, 9–17 (2019).
128. Raposo, G. & Stoorvogel, W. Extracellular vesicles: Exosomes, microvesicles, and friends. *Journal of Cell Biology* **200**, 373–383 (2013).
129. Théry, C. *et al.* Minimal information for studies of extracellular vesicles 2018 (MISEV2018): a position statement of the International Society for Extracellular Vesicles and update of the MISEV2014 guidelines. *J. Extracell. Vesicles* **7**, 1535750 (2018).
130. Ibrahim, A. & Marbán, E. Exosomes: Fundamental Biology and Roles in Cardiovascular Physiology. *Annu. Rev. Physiol.* **78**, 67–83 (2016).
131. Maas, S. L. N., Breakefield, X. O. & Weaver, A. M. Extracellular Vesicles: Unique Intercellular Delivery Vehicles. *Trends in Cell Biology* **27**, 172–188 (2017).
132. Meldolesi, J. Exosomes and Ectosomes in Intercellular Communication. *Current Biology* **28**, R435–R444 (2018).
133. Maacha, S. *et al.* Extracellular vesicles-mediated intercellular communication: Roles

in the tumor microenvironment and anti-cancer drug resistance. *Molecular Cancer* **18**, (2019).
134. Villarroya-Beltri, C., Baixauli, F., Gutiérrez-Vázquez, C., Sánchez-Madrid, F. & Mittelbrunn, M. Sorting it out: regulation of exosome loading. *Semin. Cancer Biol.* **28**, 3–13 (2014).
135. O'Neill, C. P., Gilligan, K. E. & Dwyer, R. M. Role of extracellular vesicles (EVs) in cell stress response and resistance to cancer therapy. *Cancers (Basel)*. **11**, (2019).
136. Han, L., Lam, E. W. F. & Sun, Y. Extracellular vesicles in the tumor microenvironment: Old stories, but new tales. *Molecular Cancer* **18**, (2019).
137. Raab-Traub, N. & Dittmer, D. P. Viral effects on the content and function of extracellular vesicles. *Nature Reviews Microbiology* **15**, 559–572 (2017).
138. Al-Nedawi, K. *et al.* Intercellular transfer of the oncogenic receptor EGFRvIII by microvesicles derived from tumour cells. *Nat. Cell Biol.* **10**, 619–24 (2008).
139. Choi, D. *et al.* The impact of oncogenic egfrviii on the proteome of extracellular vesicles released from glioblastoma cells. *Mol. Cell. Proteomics* **17**, 1948–1964 (2018).
140. Conigliaro, A. & Cicchini, C. Exosome-Mediated Signaling in Epithelial to Mesenchymal Transition and Tumor Progression. *J. Clin. Med.* **8**, 26 (2018).
141. Costa-Silva, B. *et al.* Pancreatic cancer exosomes initiate pre-metastatic niche formation in the liver. *Nat. Cell Biol.* **17**, 816–26 (2015).
142. Hoshino, A. *et al.* Tumour exosome integrins determine organotropic metastasis. *Nature* **527**, 329–35 (2015).
143. Hoen, E. N., Cremer, T., Gallo, R. C. & Margolis, L. B. Extracellular vesicles and viruses: Are they close relatives? *Proceedings of the National Academy of Sciences of the United States of America* **113**, 9155–9161 (2016).
144. Dias, M. V. S., Costa, C. S. & Da Silva, L. L. P. The ambiguous roles of extracellular vesicles in HIV replication and pathogenesis. *Frontiers in Microbiology* **9**, (2018).
145. Khatua, A. K., Taylor, H. E., Hildreth, J. E. K. & Popik, W. Exosomes Packaging APOBEC3G Confer Human Immunodeficiency Virus Resistance to Recipient Cells. *J. Virol.* **83**, 512–521 (2009).
146. Shahabipour, F. *et al.* Exosomes: Nanoparticulate tools for RNA interference and drug delivery. *J. Cell. Physiol.* **232**, 1660–1668 (2017).
147. Johnsen, K. B. *et al.* A comprehensive overview of exosomes as drug delivery vehicles - Endogenous nanocarriers for targeted cancer therapy. *Biochimica et Biophysica Acta - Reviews on Cancer* **1846**, 75–87 (2014).
148. Kojima, R. *et al.* Designer exosomes produced by implanted cells intracerebrally deliver therapeutic cargo for Parkinson's disease treatment. *Nat. Commun.* **9**, 1305 (2018).
149. Shi, X., Cheng, Q. & Zhang, Y. Reprogramming Extracellular Vesicles with Engineered Proteins. *Methods* (2019). doi:10.1016/j.ymeth.2019.09.017
150. Wiklander, O. P. B., Brennan, M. Á., Lötvall, J., Breakefield, X. O. & El Andaloussi, S. Advances in therapeutic applications of extracellular vesicles. *Sci. Transl. Med.* **11**, (2019).
151. Kamerkar, S. *et al.* Exosomes facilitate therapeutic targeting of oncogenic KRAS in pancreatic cancer. *Nature* **546**, 498–503 (2017).
152. Corbett, T. H. *et al.* Induction and chemotherapeutic response of two transplantable ductal adenocarcinomas of the pancreas in C57BL/6 mice. *Cancer Res.* **44**, 717–26

(1984).
153. Sanjana, N. E., Shalem, O. & Zhang, F. Improved vectors and genome-wide libraries for CRISPR screening. *Nature Methods* **11**, 783–784 (2014).
154. Lockwood, W. W. *et al.* Integrative genomic analyses identify BRF2 as a novel lineage-specific oncogene in lung squamous cell carcinoma. *PLoS Med.* **7**, e1000315 (2010).
155. Shen, Y. & Nemunaitis, J. Herpes simplex virus 1 (HSV-1) for cancer treatment. *Cancer Gene Ther.* **13**, 975–92 (2006).
156. Mastrangelo, M. J. *et al.* Intratumoral recombinant GM-CSF-encoding virus as gene therapy in patients with cutaneous melanoma. *Cancer Gene Ther.* **6**, 409–22
157. Bolger, A. M., Lohse, M. & Usadel, B. Trimmomatic: A flexible trimmer for Illumina sequence data. *Bioinformatics* **30**, 2114–2120 (2014).
158. Trapnell, C., Pachter, L. & Salzberg, S. L. TopHat: Discovering splice junctions with RNA-Seq. *Bioinformatics* **25**, 1105–1111 (2009).
159. Trapnell, C. *et al.* Transcript assembly and quantification by RNA-Seq reveals unannotated transcripts and isoform switching during cell differentiation. *Nat. Biotechnol.* **28**, 511–515 (2010).
160. Trapnell, C. *et al.* Differential gene and transcript expression analysis of RNA-seq experiments with TopHat and Cufflinks. *Nat. Protoc.* **7**, 562–578 (2012).
161. Reimand, J., Kull, M., Peterson, H., Hansen, J. & Vilo, J. G:Profiler-a web-based toolset for functional profiling of gene lists from large-scale experiments. *Nucleic Acids Res.* **35**, (2007).
162. Livak, K. J. & Schmittgen, T. D. Analysis of relative gene expression data using real-time quantitative PCR and the 2-ΔΔCT method. *Methods* **25**, 402–408 (2001).
163. Feoktistova, M., Geserick, P. & Leverkus, M. Crystal Violet Assay for Determining Viability of Cultured Cells. *Cold Spring Harb. Protoc.* **2016**, pdb.prot087379 (2016).
164. Jensen, M. M., Jørgensen, J. T., Binderup, T. & Kjaer, A. Tumor volume in subcutaneous mouse xenografts measured by microCT is more accurate and reproducible than determined by 18F-FDG-microPET or external caliper. *BMC Med. Imaging* **8**, 16 (2008).
165. Langlois, R. A., Shapiro, J. S., Pham, A. M. & Tenoever, B. R. In vivo delivery of cytoplasmic RNA virus-derived miRNAs. *Mol. Ther.* **20**, 367–375 (2012).
166. Burkholder, T., Foltz, C., Karlsson, E., Linton, C. G. & Smith, J. M. Health Evaluation of Experimental Laboratory Mice. *Curr. Protoc. Mouse Biol.* **2**, 145–165 (2012).
167. Cody, J. J., Markert, J. M. & Hurst, D. R. Histone deacetylase inhibitors improve the replication of oncolytic herpes simplex virus in breast cancer cells. *PLoS One* **9**, e92919 (2014).
168. Shulak, L. *et al.* Histone Deacetylase Inhibitors Potentiate Vesicular Stomatitis Virus Oncolysis in Prostate Cancer Cells by Modulating NF- B-Dependent Autophagy. *J. Virol.* **88**, 2927–2940 (2014).
169. Chiocca, E. A., Nakashima, H. & Nguyen, T. Combining HDAC inhibitors with oncolytic virotherapy for cancer therapy. *Oncolytic Virotherapy* 183 (2015). doi:10.2147/ov.s66081
170. Kadoch, C. *et al.* Proteomic and bioinformatic analysis of mammalian SWI/SNF complexes identifies extensive roles in human malignancy. *Nat. Genet.* **45**, 592–601 (2013).

171. Waddell, N. *et al.* Whole genomes redefine the mutational landscape of pancreatic cancer. *Nature* **518**, 495–501 (2015).
172. Bitler, B. G. *et al.* Synthetic lethality by targeting EZH2 methyltransferase activity in ARID1A-mutated cancers. *Nat. Med.* **21**, 231–238 (2015).
173. Fu, Y. *et al.* Exosome-mediated miR-146a transfer suppresses type I interferon response and facilitates EV71 infection. *PLoS Pathog.* **13**, (2017).
174. Hurwitz, S. N. *et al.* CD63 Regulates Epstein-Barr Virus LMP1 Exosomal Packaging, Enhancement of Vesicle Production, and Noncanonical NF-κB Signaling. *J. Virol.* **91**, (2017).
175. Ostrowski, M. *et al.* Rab27a and Rab27b control different steps of the exosome secretion pathway. *Nat. Cell Biol.* **12**, 19–30; sup pp 1-13 (2010).
176. Bobrie, A. *et al.* Rab27a supports exosome-dependent and -independent mechanisms that modify the tumor microenvironment and can promote tumor progression. *Cancer Res.* **72**, 4920–30 (2012).
177. Bobrie, A., Colombo, M., Krumeich, S., Raposo, G. & Théry, C. Diverse subpopulations of vesicles secreted by different intracellular mechanisms are present in exosome preparations obtained by differential ultracentrifugation. *J. Extracell. Vesicles* **1**, (2012).
178. Chen, Y., Gao, D. Y. & Huang, L. In vivo delivery of miRNAs for cancer therapy: Challenges and strategies. *Advanced Drug Delivery Reviews* **81**, 128–141 (2015).
179. Balacescu, O. *et al.* MiRNA-Based Therapeutics in Oncology, Realities, and Challenges. in *Antisense Therapy [Working Title]* (IntechOpen, 2018). doi:10.5772/intechopen.81847
180. Shapiro, J. S., Langlois, R. A., Pham, A. M. & Tenoever, B. R. Evidence for a cytoplasmic microprocessor of pri-miRNAs. *RNA* **18**, 1338–1346 (2012).
181. Rouha, H., Thurner, C. & Mandl, C. W. Functional microRNA generated from a cytoplasmic RNA virus. *Nucleic Acids Res.* **38**, 8328–37 (2010).
182. Varble, A. *et al.* Engineered RNA viral synthesis of microRNAs. *Proc. Natl. Acad. Sci. U. S. A.* **107**, 11519–24 (2010).
183. Shapiro, J. S., Varble, A., Pham, A. M. & Tenoever, B. R. Noncanonical cytoplasmic processing of viral microRNAs. *RNA* **16**, 2068–74 (2010).
184. Falkenberg, K. J. & Johnstone, R. W. Histone deacetylases and their inhibitors in cancer, neurological diseases and immune disorders. *Nat. Rev. Drug Discov.* **13**, 673–91 (2014).
185. Forbes, N. E., Abdelbary, H., Lupien, M., Bell, J. C. & Diallo, J. S. Exploiting tumor epigenetics to improve oncolytic virotherapy. *Frontiers in Genetics* **4**, (2013).
186. Marchini, A., Scott, E. M. & Rommelaere, J. Overcoming barriers in oncolytic virotherapy with HDAC inhibitors and immune checkpoint blockade. *Viruses* **8**, (2016).
187. Svitkina, T. M., Verkhovsky, A. B. & Borisy, G. G. Plectin sidearms mediate interaction of intermediate filaments with microtubules and other components of the cytoskeleton. *J. Cell Biol.* **135**, 991–1007 (1996).
188. Burch, T. C., Watson, M. T. & Nyalwidhe, J. O. Variable Metastatic Potentials Correlate with Differential Plectin and Vimentin Expression in Syngeneic Androgen Independent Prostate Cancer Cells. *PLoS One* **8**, (2013).
189. Shin, S. J. *et al.* Unexpected gain of function for the scaffolding protein plectin due to mislocalization in pancreatic cancer. *Proc. Natl. Acad. Sci. U. S. A.* **110**, 19414–19419

(2013).
190. Taylor, M. P., Koyuncu, O. O. & Enquist, L. W. Subversion of the actin cytoskeleton during viral infection. *Nature Reviews Microbiology* **9**, 427–439 (2011).
191. Ding, Y. *et al.* Plectin regulates the signaling and trafficking of the HIV-1 co-receptor CXCR4 and plays a role in HIV-1 infection. *Exp. Cell Res.* **314**, 590–602 (2008).
192. Wolter, J. M., Kotagama, K., Pierre-Bez, A. C., Firago, M. & Mangone, M. 3'LIFE: A functional assay to detect miRNA targets in high-throughput. *Nucleic Acids Res.* **42**, (2014).
193. Clapier, C. R., Iwasa, J., Cairns, B. R. & Peterson, C. L. Mechanisms of action and regulation of ATP-dependent chromatin-remodelling complexes. *Nature Reviews Molecular Cell Biology* **18**, 407–422 (2017).
194. Mathur, R. ARID1A loss in cancer: Towards a mechanistic understanding. *Pharmacology and Therapeutics* **190**, 15–23 (2018).
195. Shain, A. H. & Pollack, J. R. The Spectrum of SWI/SNF Mutations, Ubiquitous in Human Cancers. *PLoS One* **8**, (2013).
196. Yan, Z. *et al.* PBAF chromatin-remodeling complex requires a novel specificity subunit, BAF200, to regulate expression of selective interferon-responsive genes. *Genes Dev.* **19**, 1662–1667 (2005).
197. Weidner, J. M. *et al.* Interferon-Induced Cell Membrane Proteins, IFITM3 and Tetherin, Inhibit Vesicular Stomatitis Virus Infection via Distinct Mechanisms. *J. Virol.* **84**, 12646–12657 (2010).
198. Shen, J. *et al.* ARID1A deficiency promotes mutability and potentiates therapeutic antitumor immunity unleashed by immune checkpoint blockade. *Nat. Med.* **24**, 556–562 (2018).
199. Bitler, B. G. *et al.* ARID1A-mutated ovarian cancers depend on HDAC6 activity. *Nat. Cell Biol.* **19**, 962–973 (2017).
200. Wu, J. N. & Roberts, C. W. M. ARID1A mutations in cancer: Another epigenetic tumor suppressor? *Cancer Discov.* **3**, 35–43 (2013).
201. van Dongen, H. M., Masoumi, N., Witwer, K. W. & Pegtel, D. M. Extracellular Vesicles Exploit Viral Entry Routes for Cargo Delivery. *Microbiol. Mol. Biol. Rev.* **80**, 369–386 (2016).
202. Giachetti, C. & Holland, J. J. Vesicular stomatitis virus and its defective interfering particles exhibit in vitro transcriptional and replicative competition for purified L-NS polymerase molecules. *Virology* **170**, 264–267 (1989).
203. Pardoll, D. M. The blockade of immune checkpoints in cancer immunotherapy. *Nature Reviews Cancer* **12**, 252–264 (2012).
204. Wei, S. C., Duffy, C. R. & Allison, J. P. Fundamental mechanisms of immune checkpoint blockade therapy. *Cancer Discovery* **8**, 1069–1086 (2018).
205. Hellmann, M. D., Friedman, C. F. & Wolchok, J. D. Combinatorial Cancer Immunotherapies. in *Advances in Immunology* **130**, 251–277 (Academic Press Inc., 2016).
206. Twumasi-Boateng, K., Pettigrew, J. L., Kwok, Y. Y. E., Bell, J. C. & Nelson, B. H. Oncolytic viruses as engineering platforms for combination immunotherapy. *Nat. Rev. Cancer* **18**, 419–432 (2018).
207. Chen, C.-Y., Hutzen, B., Wedekind, M. F. & Cripe, T. P. Oncolytic virus and PD-1/PD-L1 blockade combination therapy. *Oncolytic virotherapy* **7**, 65–77 (2018).
208. Zingg, D. *et al.* The Histone Methyltransferase Ezh2 Controls Mechanisms of

Adaptive Resistance to Tumor Immunotherapy. *Cell Rep.* **20**, 854–867 (2017).

CURRICULUM VITAE

EDUCATION

Master of Science - Cellular and Molecular Medicine *2016-2020*
University of Ottawa, Ottawa, ON

Bachelor of Science - Microbiology *2013-2016*
Université Laval, Quebec City, QC

Bachelor of Science - Biochemistry and Medical Laboratory Sciences (not completed)
Université de Moncton, Moncton, NB *2011-2013*

RESEARCH EXPERIENCE

Graduate student – Co-supervisors: Dr. Carolina Ilkow and Dr. John Bell *2016 – 2019*
Department of Cellular and Molecular Medicine, Faculty of Medicine, University of Ottawa
Cancer Therapeutics Program, Centre for Innovative Cancer Research, Ottawa Hospital Research Institute

- Explored the enhanced killing effect of oncolytic or "cancer killing" viruses encoding artificial microRNAs in combination with small molecule therapy on cancer cells and the tumor microenvironment.
- Explored the desmoplastic pancreatic tumor microenvironment and used targeted therapeutic extracellular vesicles for the treatment of pancreatic cancer.

Undergraduate research assistant – Supervisor: Dr. Denis Leclerc *2015 –2016*
Department of Microbiology-Infectiology and Immunology, Faculty of Medicine, Université Laval

- Carried out a research project on the characterization and assembly of plant virus coat proteins into virus-like particles used as influenza vaccine platforms.

Undergraduate research assistant – Supervisor: Dr. Louis Bernier *2014 - 2015*
Department of Forestry, Faculty of Forestry, Geography and Geomatics, Université Laval

- Carried out a research project on the effect of quorum sensing on dimorphism in several fungal Dutch elm disease pathogen strains.

PUBLICATIONS

Journal Articles – Original Research

- **Wedge ME**, Naruzawa ES, Nigg M and Bernier L. 2016. Diversity in dimorphism response of Dutch elm disease pathogens: the inoculum size effect. Can J Microbiol. **62**:525-529. doi:10.1139/cjm-2015-0795
- Keller B, Laight B, Varette O, Broom A, **Wedge ME**, McSweeney B, *et al.* A personalized approach to $BRAF^{K601N}$ melanoma: model development, drug discovery, and clinical correlation. *Manuscript in preparation*
- **Wedge ME,** Jennings VA, Boileau M, Laight B, McKay H, Pikor L, *et al*. Virally programmed extracellular vesicles sensitize cancer cells to oncolytic virus and small molecule therapy. *Manuscript in preparation*

- Chatterjee A, Antonova L, **Wedge ME**, Paramanthanan P, Falls T, Lee R, *et al*. Molecular characterization and xenotransplantation of pancreatic cancer patient samples obtained using EUS-FNA. *Manuscript in preparation*

Journal Articles – Reviews

- Achard C, Surendran A, **Wedge ME**, Ungerechts G, Bell JC and Ilkow CS. 2018. Lighting a fire in the tumor microenvironment using oncolytic immunotherapy. EBioMedicine. **31**:17-24. doi:10.1016/j.ebiom.2018.04.020

Book Chapters

- Keller B, **Wedge ME**, Surendran A and Ilkow CS. 2020. Generating Primary Models of Human Cancer to Aid in the Development of Clinically Relevant Oncolytic Viruses. In: Engeland C. (eds) Oncolytic Viruses. Methods in Molecular Biology, vol 2058. Humana, New York, NY. doi: 10.1007/978-1-4939-9794-7

Published Abstracts

- **Wedge ME** and Ilkow CS. Combining virus-based therapeutics and EV therapy for the treatment of pancreatic cancer [abstract]. Journal of Extracellular Vesicles; 2019 Apr 24-28; Kyoto, Japan. ISEV; 2019. Abstract **OF20.02** doi: 10.1080/20013078.2019.1593587
- **Wedge ME**, Pelin A, Laight B, Bell JC and Ilkow CS. Tailoring oncolytic viruses for the treatment of pancreatic cancer [abstract]. Cancer microenvironment; 2018 Jun 10-14; Lisbon, Portugal. ICMS; 2018. Abstract **O84**. doi: 10.1007/s12307-018-0212-6

PRESENTATIONS

Oral presentations

Combining virus-based therapeutics and EV therapy for the treatment of pancreatic cancer

International Society for Extracellular Vesicles 2019 Annual Meeting – Kyoto, Japan *April 2019*

Tailoring oncolytic viruses for the treatment of pancreatic cancer

Ottawa Hospital Research Institute Research Day – Ottawa, ON *November 2018*

8th International Conference on Tumor Microenvironment – Lisbon, Portugal *June 2018*

1st BMI Symposium of the University of Ottawa – Montebello, QC *May 2018*

Poster presentations

Tailoring oncolytic viruses for the treatment of pancreatic cancer
Biochemistry, Microbiology and Immunology Poster Day (2019), Cellular and Molecular Medicine Research Day (2016-2018), Ottawa Hospital Research Day (2016 and 2017) – Ottawa, ON

Harnessing virus-based therapeutics and exosome targeted therapy for the treatment of pancreatic cancer
Canadian Oncolytic Virus Consortium Terry Fox Research Institute grant renewal site visit and Cellular and Molecular Medicine poster day (2017) – Ottawa, ON

Molecular and Histological Characterization of Pancreatic Cancer Patient-Derived Xenografts
Summit for Cancer Immunotherapy (2016) – Halifax, NS

AWARDS AND SCHOLARSHIPS

Young Investigator Scholarship - ISEV Annual Meeting *2019*
Ontario Graduate Scholarship *2018-2019*
HQP Travel Award - BioCanRx *2018*
Leadership Award - Let's Talk Science Ottawa *June 2018*
National Let's Talk Science Award Finalist *April 2018*
CIHR Frederick Banting and Charles Best Canada Graduate Scholarship *2017-2018*
Ontario Graduate Scholarship - Declined *2017-2018*
Second Prize Winner of the JoVE Film Your Research Contest Jury Choice Award *2017*
Award for Significant Contribution to Science Outreach Let's Talk Science Ottawa *June 2017*
Volunteer of the Month - Let's Talk Science Ottawa *March 2017*
Queen Elizabeth II Graduate Scholarship in Science and Technology *2016-2017*
Excellence Scholarship – University of Ottawa *2016-2019*
Admission Scholarship – University of Ottawa *2016*
NSERC Undergraduate Student Research Award – Université Laval *2014 and 2015*
Dean's List of the Science Faculty – Université de Moncton *2012 and 2013*
Academic Merit Scholarship – Université de Moncton *2011*
Glenwood Kitchen Ltd Scholarship *2011*

VOLUNTEER ACTIVITIES

Ottawa Regional Cancer Foundation - Cancer Champions Breakfast Table Expert *2019*
Health Science Inquiry Journal - Proof reader *2018-2019*
Scholarship writing workshop volunteer – Faculty of Medicine, University of Ottawa *2018*
Canada-wide science fair judge - Ottawa, ON *2018*
Team Leader of the Cancer Education Program - Let's Talk Science Ottawa *2017-2018*
University of Calgary's Cybermentor program *2017-2019*
Judge for the Connecting Young Minds Undergraduate Conference *2017*
OHRI volunteer at the 9th Annual Biotechnology Symposium at La Cité Collégiale *2017*
Science Outreach Volunteer - Let's Talk Science *2016-2019*
Health Science Inquiry Journal - Reviewer *2016-2018*
Member of the COVCo fundraising committee for the annual Terry Fox Runs *2016-2018*
Volunteer at the Third Life Sciences Research Day – Université Laval *2016*
Symbiose used book sale Volunteer – Université de Moncton *2012 - 2013*
Volunteer on a humanitarian trip to Honduras - Global Medical Brigade *2012*